Ph.D. Thesis

Daniel Gram

Minimizing side effects for pediatric patients treated with craniospinal irradiation

TITLE: Minimizing side effects for pediatric patients
                    treated with craniospinal irradiation

AUTHOR: Daniel Gram

DEPARTMENTS: Department of Oncology
                    Section of Radiotherapy
                    Rigshospitalet
                    Copenhagen, Denmark

                    Niels Bohr Institute
                    University of Copenhagen
                    Copenhagen, Denmark

PRINCIPAL   Per Munck af Rosenschöld, Ph.D.
SUPERVISOR: Niels Bohr Institute
                    University of Copenhagen
                    Copenhagen, Denmark &
                    Radiation Physics - Department of Hematology,
                    Oncology and Radiation Physics
                    Skåne University Hospital
                    Lund, Sweden

CO-SUPERVISORS: Thomas Björk-Eriksson, MD., Ph.D.
                    Department of Oncology
                    Institute of Clinical Sciences
                    Sahlgrenska Academy at the
                    University of Gothenburg &
                    Regional Cancer Centre West
                    Gothenburg, Sweden

                    Patrik Brodin, Ph.D.
                    Institute for Onco-Physics
                    Albert Einstein College of Medicine &
                    Montefiore Medical Center
                    Bronx, NY, USA

                    Karsten Nysom, MD., Ph.D.
                    Department of Paediatrics and Adolescent Medicine
                    The Juliane Marie Center
                    Rigshospitalet
                    Copenhagen, Denmark

"Don't underestimate the value of doing nothing, of just going along, listening to all the things you can't hear, and not bothering."

— Winnie the Pooh

Contents

Abstract

Second only to leukemia, primary tumors in the central nervous system (CNS) are the most commonly occurring malignancies in children, with medulloblastoma being the most prevalent. The standard-of-care for medulloblastoma consists of a combination of surgery, chemotherapy and craniospinal irradiation (CSI) and is usually administered to children above 3-5 years of age. Pediatric CNS tumors, although rare, have a devastating impact on patients and their families both due to the disease and the severe treatment related side effects. Most long-term survivors of malignant pediatric CNS tumors treated with CSI have significant late effects, such as perturbed growth, hearing or vision loss, cardiovascular events, lung toxicity and neurocognitive impairment, and patients irradiated at a younger age tend to have worse outcomes. Since the frequency and severity of late side effects generally increase with time, they are especially debilitating for pediatric cancer survivors as they mature into adulthood.

The purpose of this PhD project was to investigate different possibilities of reducing side effects to organs-at-risk (OARs) for pediatric patients with CNS malignancies treated with CSI. We investigated setup errors and uncertainties to evaluate margins and robustness perturbations needed for CSI treatments. These results were used to create realistic hippocampal-sparing proton therapy treatment plans aimed at reducing neurocognitive impairment. The results from that study demonstrated that it is possible to reduce the risk of neurocognitive impairment with only a minimal impact on target coverage and without reducing the estimated tumor control. We further investigated the effects of linear energy transfer (LET) and how it impacts the radiobiologically weighted dose distribution generally and how these results affect the sparing of the hippocampi specifically. We found that areas of where the proton beam stops can be highly affected depending on the tissue specific parameters assigned to the tumor and OARs. This field of study needs further investigation before biologically weighted doses can be used clinically, especially in the setting of hippocampal-sparing (HS) CSI. We also created mathematical models for predicting OAR doses from spinal irradiation treatments delivered in the era before 3D treatment planning and volumetric dose reporting. The aim of this was to be able to link OAR doses with long-term follow-up data for an increased understanding of dose-response relationships in cohorts of pediatric cancer survivors, which could further reduce the side effects to this patient group.

The work conducted and results presented in this thesis show that there are actionable opportunities for minimizing side effects of pediatric patients with CNS malignancies treated with CSI.

Dansk Resumé

Næst efter leukæmi, er tumorer i det centrale nervesystem (CNS) den hyppigste type kræft hos børn. Medulloblastom er den hyppigste ondartede hjernetumor hos børn. Oftest behandles medulloblastom med en kombination af kirurgi, kemoterapi og stråleterapi af det craniospinale (CSI) område og gives til patienter fra 3-5 års alder. Selv om pædiatriske CNS-tumoer er relativt sjældne, har de en altoverskyggende indvirkning på patienter og deres familier på grund af selve kræftsygdommen men også på grund af de mange, svære bivirkninger. Langt de fleste af de langtidsoverlevende børn der har fået denne meget aggressive behandling, har mange og svære bivirkninger så som vækstforstyrrelse, høretab og tab af syn, kardiovaskulære begivenheder, lungetoksicitet samt neurokognitiv skade og jo yngre patienterne var ved behandlingen, desto sværere bivirkninger får de. Eftersom hyppighed og sværhedsgrad af disse bivirkninger generelt øges med tiden, er de delvis invaliderende for børnene der har overlevet deres kræft imens de vokser op.

Hovedformålet med dette PhD projekt var at undersøge muligheder for at mindske strålingen til risikoorganer og dermed også mindske nogle af de mange sene bivirkninger der rammer børn med CNS-tumorer der har fået CSI behandling. Vi undersøgte fejl og usikkerheder ved patientlejring og evaluerede hvilke marginaler og robusthedsparametre der krævedes for CSI behandling. Resultaterne brugte vi derefter til at generere realistiske hippocampus skånende stråleplaner med protoner for at reducere de neurokognitive senfølger. Disse resultater viser at det er muligt at mindske risikoen for neurokognitive senfølger med kun et minimalt tab i stråledækning af behandlingsområdet og uden nogen påvirkning af tumor kontrol. Vi undersøgte også effekterne af lineær energioverførsel og hvordan de påvirker radiobiologiske dosisfordelinger generelt, samt hvordan de påvirker hippocampus specifikt. Vi fandt ud af at områder hvor protonstrålen stoppes kan blive stærkt påvirket afhængigt af hvilke bløddelsvæv-værdier der antages at gælde for tumoren og det raske væv. Dette forskningsområde kræver flere studier før disse radiobiologiske dosisfordelinger kan blive brugt i klinikken, især for hippocampus skånende behandlinger med proton stråleterapi. Vi udviklede også matematiske modeller for at kunne forudsige hvilke doser risikoorganer modtager ved CSI behandlinger der er givet i en tid før 3D planlægning og rapportering af volumetrisk dosis. Formålet med dette var at give mulighed for at sammenholde doser til risiko organer med langtids opfølgningsdata for at øge forståelsen omkring dosis-respons forholdet i kohorter af kræftoverlevende børn, for på længere sigt at mindske bivirkningerne hos patientgruppen.

Arbejdet som er blevet gennemført i dette PhD projekt viser at der findes muligheder for at minimere bivirkningerne hos børn der modtager strålebehandling med CSI for deres CNS-tumorer.

Publications

This thesis contains the following three manuscripts, based on research carried out at Copenhagen University Hospital, Rigshospitalet and The Skandion Clinic between 2017 and 2020

STUDY I **DANIEL GRAM**, ANDRÉ HARALDSSON, N. PATRIK BRODIN, KARSTEN NYSOM, THOMAS BJÖRK-ERIKSSON, PER MUNCK AF ROSENSCHÖLD. Residual positioning errors and uncertainties for pediatric craniospinal irradiation and the impact of image guidance. *Accepted for publication in Radiation Oncology*

STUDY II **DANIEL GRAM**, N. PATRIK BRODIN, THOMAS BJÖRK-ERIKSSON, KARSTEN NYSOM, PER MUNCK AF ROSENSCHÖLD. The risk of radiation-induced neurocognitive impairment and the impact of sparing the hippocampus during pediatric proton cranial irradiation. *Submitted to Radiotherapy and Oncology*

STUDY III **DANIEL GASIC**[‡], PER MUNCK AF ROSENSCHÖLD, IVAN R. VOGELIUS, MAJA V. MARALDO, MARIANNCE C. AZNAR, KARSTEN NYSOM, THOMAS BJÖRK-ERIKSSON, SØREN M. BENTZEN, N. PATRIK BRODIN. Retrospective estimation of heart and lung doses in pediatric patients treated with spinal irradiation. *Radiotherapy and Oncology*, 128(2):209-213, 2018

[‡]Daniel Gasic changed his name to Daniel Gram in August 2019

Related publications not included in this thesis

Listed below are publications based on research carried out between 2017 and 2020 that are related to this thesis, however, not included

1. ABDOSSALAM M. MADKHALI, **DANIEL GRAM**, CAMILLA HANQUIST STOKKEVÅG, KATHERINE VALLIS, PER MUNCK AF ROSENSCHÖLD, MARK HILL. The Effect of Spatial Dose Averaging on Predicting Malignant Induction Probability and Secondary Cancer Risk. *Under submission to Acta Oncologica*

Proceedings

Listed below are presentations made at international conferences between 2017 and 2020

List of conference contributions related to my thesis:

1. **DANIEL GASIC**[‡]. "Exploring the potential for clinical introduction of hippocampal-sparing intensity modulated proton therapy of pediatric medulloblastoma." Invited speaker at the *Third Nordic Symposium in Pediatric Proton Radiotherapy* in Uppsala, Sweden, 10-11 September 2018

2. **DANIEL GASIC**[‡], ANDRÉ HARALDSSON, N. PATRIK BRODIN, KARSTEN NYSOM, THOMAS BJÖRK-ERIKSSON, PER MUNCK AS ROSENSCHÖLD. "Positioning uncertainties for pediatric craniospinal irradiation and the impact of image guidance." Abstract and poster presentation at *The European Society for Radiotherapy and Oncology - ESTRO 38* in Milan, Italy, 26-30 April 2019

List of related conference contributions but not included in the thesis:

1. ABDOSSALAM M. MADKHALI **DANIEL GASIC**[‡], PER MUNCK AF ROSENSCHÖLD. "Effect of mean dose or voxel-wise calculation in prediction of radiation-induced secondary cancers." Abstract and poster presentation at *57ᵗʰ Particle Therapy Co-Operative Group - PTCOG* in Cincinnati, OH., USA, 21-26 May 2018

2. LYKKE K. JOHANSEN, VANJA R. GRAM, **DANIEL GASIC**[‡]. "Daily Image guided radiotherapy - the relevance for patients with metastatic spinal cord compression." Abstract and poster presentation at *The European Society for Radiotherapy and Oncology - ESTRO 38* in Milan, Italy, 26-30 April 2019

3. ABDOSSALAM M. MADKHALI, **DANIEL GASIC**[‡], F. VAN DEN HEUVEL, MARK HILL, PER MUNCK AF ROSENSCHÖLD, KATHERINE VALLIS. "Effect of radiotherapy boost on secondary cancer for paediatric medulloblastoma patients". Abstract and poster presentation at *58ᵗʰ Particle Therapy Co-Operative Group - PTCOG* in Manchester, United Kingdom, 10-15 June 2019

[‡]Daniel Gasic changed his name to Daniel Gram in August 2019

"We don't have the key. We can't open whatever it is we don't have that it unlocks. So what purpose would be served in finding whatever need be unlocked, which we don't have, without first having found the key what unlocks it?"

— Captain Jack Sparrow

Acknowledgements

I was very fortunate to have retained the support of some truly amazing people throughout the course of my PhD studies – supervisors, co-authors, colleagues, co-workers, fellow students, friends and family without whom this thesis would have been impossible. I have truly been standing on the shoulders of giants.

I would first like to thank my supervisors for guiding me along through this journey, for your valuable criticism, for making this project possible and for memorable Skype meetings. Thank you to my primary supervisor Per Munck af Rosenschöld for long and fruitful discussions, for your guidance and for keeping me on track when my mind wandered off and for always pushing me to go further. At times, all the extra work could be frustrating, but it yielded a great improvement. Thank you, Thomas Björk-Eriksson, for all your encouragement, both personal and professional advices and your boundless optimism. You always see the potential in others. Thank you for helping me to achieve mine. Also, an extra thank you for getting me home when I risked becoming stranded in Milan. Thank you, Patrik Brodin, for suffering through my stupidity, your incredible commitment, for all the help with statistics, mathematics and programming and also for your friendship. Your attention to details is unparalleled and if it wasn't for you, I would probably still be manually exporting and importing data. I would also like to thank Karsten Nysom for being my anchor, for taking on the various extra roles and responsibilities needed and for being my local "team of supervisors". This thesis would not have been possible without you.

Thank you to my other co-authors; Ivan Vogelius, Maja Maraldo, Marianne Aznar, Søren Bentzen and André Haraldsson for all your contributions and valuable input to the manuscripts in this thesis. I am very grateful that you undertook this endeavor with me. Thank you Abdossalam Madkhali for a rewarding collaboration.

I would also like to express my gratitude to all my colleagues at the Skandion Clinic in Uppsala, Sweden for the proton therapy knowledge I gained during my time there and for making my four months at your department a great experience. Especially thank you to Håkan Nyström and Alexandru Dasu for giving me this opportunity.

Thanks to Ivan Vogelius, Lena Specht and Christoffer Johansen for creating a great research setting for us to work in and for maintaining it during these isolated pandemic days. To all my fellow graduate students and other past and present members of the interdisciplinary research group at the Department of Oncology. To Michael Lundemann and Jonas Scherman for the help with MATLAB® and LaTeX templates. To Isak Wahlstedt for C# debugging. To all my co-workers at the Section of Radiotherapy for some memorable coffee breaks from time to time. To Nikolaj Jensen for providing clinical depth dose data and to Bob Smulders for general discussions and brainstorming idéas about CSI. Thank you, Thomas Carlslund, Torben Gøth and Andreas Dähnhardt for providing valuable technical support. To Tobias Pommer for valuable input to my first study and to Laura Rechner for persuading me to sign up for the hardest course of my life, Survival Analysis, and for the help to get through it.

Special thanks to Johan Sjöberg and Marcus Krantz for proof-reading.

On a personal note, I would like to thank my family including my parents and my brother David for your support and for always believing in me.

I owe my biggest thanks to my wife Vanja and my daughter Alva, you have given my life new meaning. Thank you for all your love and for always being there for me. This would not have been possible without you.

Abbreviations

α/β tissue specific parameters or fractionation sensitivity

^{60}**Co** Cobalt-60

2D two-dimensional

3D three-dimensional

3D-CRT 3D-conformal radiotherapy

AL action level

AP anterior-posterior

BMI body mass index

CBCT cone-beam computed tomography

CERR computational environment for radiotherapy research

CI confidence interval

CNS central nervous system

CSF cerebrospinal fluid

CSI craniospinal irradiation

CT computed tomography

CTV clinical target volume

DNA deoxyribonucleic acid

DoF degrees of freedom

DVH dose-volume histogram

EFS event-free survival

EPID electronic portal imaging device

GTV gross tumor volume

Gy gray

Gy$_{\text{RBE}}$ gray for protons

HI homogeneity index

HS hippocampal-sparing

IGRT image-guided radiotherapy

IMPT intensity modulated proton therapy

IMRT intensity modulated radiotherapy

kg kilogram

kV kilovoltage

LET linear energy transfer

Linac linear accelerator

LOO leave-one-out

M memory

MB medulloblastoma

MeV megaelectron volt

ML medial-lateral

MLC multileaf collimator

MRI magnetic resonance imaging

MV megavoltage

NAL no action level

nj narrow field junction

NTCP normal tissue complication probability

O organization

OAR organ(s)-at-risk

OBI on-board imaging

OR odds ratio

PBC pencil beam convolution

PD prescribed dose

PDDC percentage depth dose curve

PTV planning target volume

RBE relative biological effect

RMSD root-mean-square deviation

RU random uncertainty

SD standard deviation

SE systematic error

SI superior-inferior

SOBP spread-out Bragg peak

SU systematic uncertainty

TCP tumor control probability

TE task efficiency

TPS treatment planning system

VMAT volumetric modulated arc therapy

wj wide field junction

List of Tables

List of Figures

List of Equations

"The important thing in science is not so much to obtain new facts as to discover new ways of thinking about them"

— William Lawrence Bragg

1

Introduction

1.1   Outline

This thesis is based on three manuscripts and parts of this work have been presented at various conferences and meetings (see Proceedings list). In the first two chapters the introduction, background and motivation are presented. Chapter three and four include methodological considerations and findings for the investigations conducted. Together with the findings, some implications are presented and discussed. Final remarks, outlook, conclusions and future perspectives are given in chapters five through seven. The manuscripts are included at the end of this thesis (see Papers).

1.2   Improving quality of life

This thesis is a stand-alone part of a series of works and studies conducted by the same research group in order to reduce radiation toxicity and improve quality of life for pediatric patients receiving treatment for malignancies of the central nervous system (CNS). To achieve this, part of the focus was to investigate the feasibility and possible clinical implementation of sparing the hippocampus from higher doses of radiation when treating the CNS with craniospinal irradiation (CSI) for these pediatric patients. The research is being conducted by a multidisciplinary group involving researchers from the Niels Bohr Institute, University of Copenhagen and Rigshospitalet in Denmark, Skåne University Hospital, Lund University, Sahlgrenska University Hospital and Regional Cancer Centre West in Sweden and the Albert Einstein College of Medicine and Montefiore Medical Center in New York in the United States. The aims and studies included are summarized in Aims and table 1.1.

1.3   Funding

Table 1.1: Overview of the studies included

Patients and methods	Highlights
STUDY I	
38 pediatric patients included where setup images were registered offline in order to evaluate imaging protocols and treatment margins	• The current study can be used for improving margin calculations and/or robust optimization of radiotherapy for pediatric medulloblastoma • The wide field junction protocol is the preferred protocol studied since it allows for correction in the superior-inferior direction • Longer field lengths are associated with larger uncertainties, suggesting that the youngest patients might benefit from narrower margins
STUDY II	
24 pediatric patients included where multiple plans were created for each patient using different positioning uncertainties, hippocampus doses and robust optimization in order to evaluate the TCP and NTCP for CNS and hippocampi when sparing the hippocampus by lowering its received radiation dose	• Hippocampal-sparing HS IMPT for medulloblastoma patients can be constructed using realistic positioning uncertainty estimates and robust treatment planning methods • We provide estimates of potential benefit of clinically realistic and robust HS IMPT regarding neurocognitive impairment as compared to standard radiotherapy • In this simulation study, HS IMPT considerably reduced predicted neurocognitive adverse effects with marginal effect to target coverage while maintaining and estimated tumor control probability
STUDY III	
21 pediatric patients included where CT scans and treatment plans were evaluated in order to develop multivariable linear regression models for retrospective estimation of doses to the heart and lungs	• This study provides a simple recipe for retrospective heart and lung dose evaluation • The current study can be used for analyzing heart and lung dose effect relationships on historical cohorts in long-term pediatric cancer survivors • Accurate models linking organ dose to late toxicity can aid in the decision making when competing radiation techniques are considered and could also help to identify patients in need of close post-treatment surveillance for late adverse effects

1.4   Aims

The overall aim of this PhD project was to minimize side effects to pediatric CNS patients treated with CSI. This thesis addresses these problems by creating tools to aid researchers in analyzing dose effect relationships as well as studying the effects of uncertainties and errors for different dose levels to the hippocampus, all in order to investigate the potential and possible clinical implementation of hippocampal-sparing radiotherapy treatments. The work in this thesis is divided into four interim aims:

1. Determine the systematic and random components of uncertainties related to patient positioning for pediatric craniospinal irradiation treatments (STUDY I).

2. Explore the estimated risk of neurocognitive impairment and tumor control probability from hippocampal-sparing proton therapy (STUDY II).

3. To create a mathematical model to act as a simple tool for analyzing dose effect relationships when retrospectively studying late effects in long-term pediatric cancer survivors (STUDY III).

4. Explore the effects of linear energy transfer and radiobiological effectiveness for hippocampal-sparing treatments (unpublished data).

Three studies were set up in order to address these interim aims and they are summarized in table 1.1.

1.5   Notes

Throughout this thesis all referrals to hippocampus relates to both the left and right hippocampi as one common structure unless it is indicated which one is described. A multi-energetic pencil beam scanning technique is used when referring to intensity modulated proton therapy (IMPT). The unit of gray (Gy) is used for describing photon absorbed dose while gray for protons (Gy_{RBE}) is used to describe proton biological dose. Assuming a relative biological effect (RBE) of 1.1, the nominal prescription dose for pediatric patients of 1.8 Gy and Gy_{RBE} is therefore 1.64 Gy for protons.

*"So perhaps the best thing to do is to stop writing introductions
and get on with the book"*

— Winnie the Pooh

2

Background

This chapter provides an overview and brief explanation on some of the topics related to this work. The section is divided into four main parts; section 2.1 explains the different types of radiotherapy techniques and modalities used, section 2.2 provides brief explanations on the radiobiology aspects of this thesis, section 2.3 contain a brief summary of the diseases and anatomy of organs important to the understanding and section 2.4 which describes the craniospinal treatment as well as some aspects of hippocampal avoidance.

2.1   Radiotherapy

External beam radiotherapy is a well-established cancer treatment option and is currently applied in roughly 50% of all cancer treatments [1]. In some cases, it is used as a stand-alone treatment modality and in other cases in combination with chemotherapy and/or surgery or immunotherapy [2]. Historically, x-rays (photons) and high energy electrons using linear accelerators (Linacs) have been the proffered choice for radiotherapy [3]. In recent past, proton radiotherapy has emerged as a prominent alternative even though they were proposed as an alternative already in 1946 [4].

Treatment techniques

The most common modality in external radiotherapy is the use of Linacs that are able to rotate around the patient and produce the ionizing radiation needed for treatment. Most Linacs can deliver photons and electrons. The energy of photons and electrons is deposited as a function of depth and while photons (Figure 2.1) are the most widely used type, electrons are sometimes used for superficial tumors. The deposited energy is measured in absorbed dose and quantified in Gy where one Gy is defined as the absorption of one joule of radiation energy per kilogram (kg) of tissue by the international system of units (SI-units).

In today's radiotherapy practice a clear majority of all plans are optimized based on images acquired with computed tomography (CT) scans. The position that the patient is scanned in composes the reference image with which the setup images are compared to at the treatment unit. This position must be repeated as accurately as possible since radiotherapy does not differentiate between tissues, which means that all deviations, large or small, translational or rotational, will result in a different dose distribution inside the patient and as dose distributions increases conformality they may become more sensitive to setup errors. There is a wide variety of different techniques of delivering photon radiation; 3D-conformal radiotherapy (3D-CRT), intensity modulated radiotherapy (IMRT), volumetric modulated arc therapy (VMAT), (helical) tomotherapy [5] and several others. In 3D-CRT the dose is delivered by adjusting the shape of individual radiation beams using a multileaf collimator
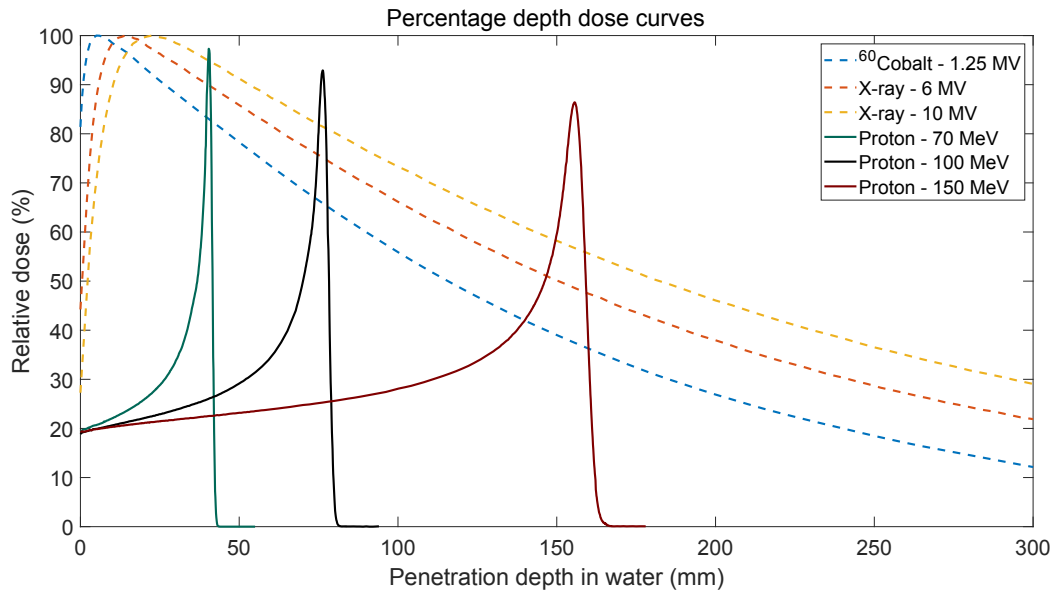
Figure 2.1: Percentage depth dose curve (PDDC) for three different photon energies including ^{60}Co used in STUDY III together with three different proton energies. The 6 MV and 10 MV photon energies are measured depth doses performed at the Department of Oncology, Section of Radiotherapy, Rigshospitalet. The ^{60}Co photon energy is a simulated depth dose curve from a Siemens Gammatron-3 treatment unit and the proton depth doses are simulated beam energies from The Skandion Clinic, Gantry 1 (GTR1).

(MLC). To achieve the desired dose to the tumor a number of these beams are used with different gantry, collimator and couch angles together with relative field weights. This way, a rather uniform dose distribution can be achieved while still obtaining a modest sparing of the organ(s)-at-risk (OAR)s [6]. If the MLC instead of shaping the beam to the tumor is used to modulate (block and open certain areas within the radiation beam) the technique is usually called IMRT [7]. It is generally possible to achieve a comparable or even a more uniform dose distribution with IMRT compared to 3D-CRT, however, there could be an increase in radiation induced second malignancies due to a larger volume being irradiated to lower doses [8–10]. The VMAT technique involves the gantry rotating around the patient during continuous irradiation and a simplified explanation is that it is basically a rotational IMRT [11]. This rotational technique is capable of delivering similar dose distributions as IMRT with one or more arcs, allowing for a faster treatment compared to IMRT. In addition, the beam output and gantry rotation speed can further be modified with the possibility of an even more conformal dose distribution [11]. Tomotherapy visually resembles a CT system and essentially is very similar to a rotating IMRT/VMAT treatment. During treatment, the immobilized patient is positioned on a couch that continuously moves through the rotating gantry while irradiating [12].

A less modern technique is the use of teletherapy machines that delivers a different radiation beam quality, namely the isotope Cobalt-60 (^{60}Co). This machine acts as a housing for the ^{60}Co pellets. The ^{60}Co is a radioactive element that constantly undergo nuclear decay producing the x-rays needed for treatment [13, 14]. The decay produces stable, dichromatic beams of 1.17 megaelectron volt (MeV) and 1.33 MeV which results in an average beam energy of 1.25 MeV (Figure 2.1). Due to the constant decay (half-life = 5.3 years) it affects the treatment time. An older pellet requires a longer treatment time to give the same dose as a newer source with shorter treatment time. Most ^{60}Co teletherapy machines have been replaced by Linacs in developed countries and are today mostly used for sterilization of foods, implants and other devices [14, 15]. The use of ^{60}Co still has modern applications in the form of the gamma knife [16, 17]

The interesting nature, characteristics and physical properties of protons and possible advantages for cancer treatments was first reported by Wilson [4] and the first clinical treatments in the world were performed with research accelerators at Lawrence Berkeley National Laboratory (California, United States) in 1954 [18], and at The Svedberg Laboratory (Uppsala, Sweden) in 1957 [19]. The use of protons instead of photons is scarcely

novel [18], however, most treatments were conducted at research centers and the first hospital-based proton treatment was recorded in 1990 [20]. Due to considerable technological difficulties, the first commercially produced systems were not available until 2001 [21].

One of the main hurdles for the slow adoption of proton therapy centers is the high cost of building and maintaining these centers [22]. However, the number of patients treated at proton therapy centers have unquestionably exploded from around 876 patients treated in 1990 [23] to roughly 14,500 patients treated in 2014 and is expected to be over 300,000 patients in 2030 [24]. As of April 2020 there are 90 proton facilities in operation and another 32 under construction worldwide [25].

Protons are accelerated to the treatment energy (typically in the range of 70-230 MeV) using either a cyclotron or a synchrotron. The, very thin, proton beams (usually called "beamlets") are then transported to the gantry for patient delivery. The beamlets are then spread during treatment delivery using magnetic scanning to ensure correct volume irradiation. The main difference to photons is that protons continuously lose a small amount of their energy as they travel through tissue but at the end of the proton's penetration range the deposited dose is increased manyfold (Figure 2.1) and this part is commonly known as the Bragg peak [26]. The depth is predefined according to tumor position and can be changed by varying the protons' initial energy. Due to proton range straggling (not all protons of the same energy have the same range) and to widen the otherwise very narrow treatment depth (i.e. to provide uniform dose within the tumor volume), there is usually a need for multiple proton energies (Bragg peaks) and the technique of utilizing multiple Bragg peaks is generally referred to as the spread-out Bragg peak (SOBP) [27, 28].

The typical physical characteristic of protons allows for lower integral dose surrounding the tumor [29–31]. This is a great advantage over photon radiation due to the ability of reducing the risk of treatment induced secondary cancers [32–36]. There is, however, disadvantages with protons as well. The field penumbra is slightly wider for protons compared to photons, by typically a few millimeters [37, 38]. Proton treatments are also more sensitive to setup errors due to the misalignment of the beams and density heterogeneities [39, 40]. Further, there are studies showing a different linear energy transfer (LET) for protons which can yield a widely different RBE in contrast to earlier experiences from photons (see Biological optimization) and also that it might not be a constant as previously assumed [41–43].

Errors and uncertainties

Within the field of radiotherapy, one usually refers to errors and uncertainties of different types [44]. First, errors are usually defined as the difference in shift between actual and intended position at treatment. This position is usually verified with an x-ray image (see Setup verification imaging). For uncertainties, it is important to keep in mind that there are mainly two different components to uncertainties, both with its own set of sources. The random component (Figure 2.2) is the inter-fractionation part and stem from positioning of the patient based on external markers on either the patient's skin or immobilization device (e.g. mask). The random component can also stem from internal motion relative to these markers. Thus, random uncertainties are different for each treatment fraction and causes a blurring in the precision of the dose delivery.

The second type of uncertainty is the systematic component which stems from changes over the course of the treatment. Examples of the systematic component (Figure 2.2) could be that the patient's anatomy changes for a longer period of time or it could be due to mechanical mismatches between the CT simulation and imaging device on the Linac or treatment machine. Thus, systematic uncertainties occur in the same way at each of the patient's treatments and usually causes deviation in the precision of the dose delivery.

These errors and uncertainties can cause major changes to the dose to the patient and should always be accounted for according to international recommendations [45–47]. In radiotherapy using photons the most common method is to expand the clinical target volume (CTV) by a margin either uniform or non-uniform depending on tumor type and location resulting in the geometrical concept of planning target volume (PTV). The size of the expanded volume should be large enough to account for the above stated uncertainties. However, since this expansion is encompassing healthy tissue it also needs to be minimized to spare this tissue and reduce the general irradiated volume inside the patient and potentially avoiding unintentional irradiation of OARs.
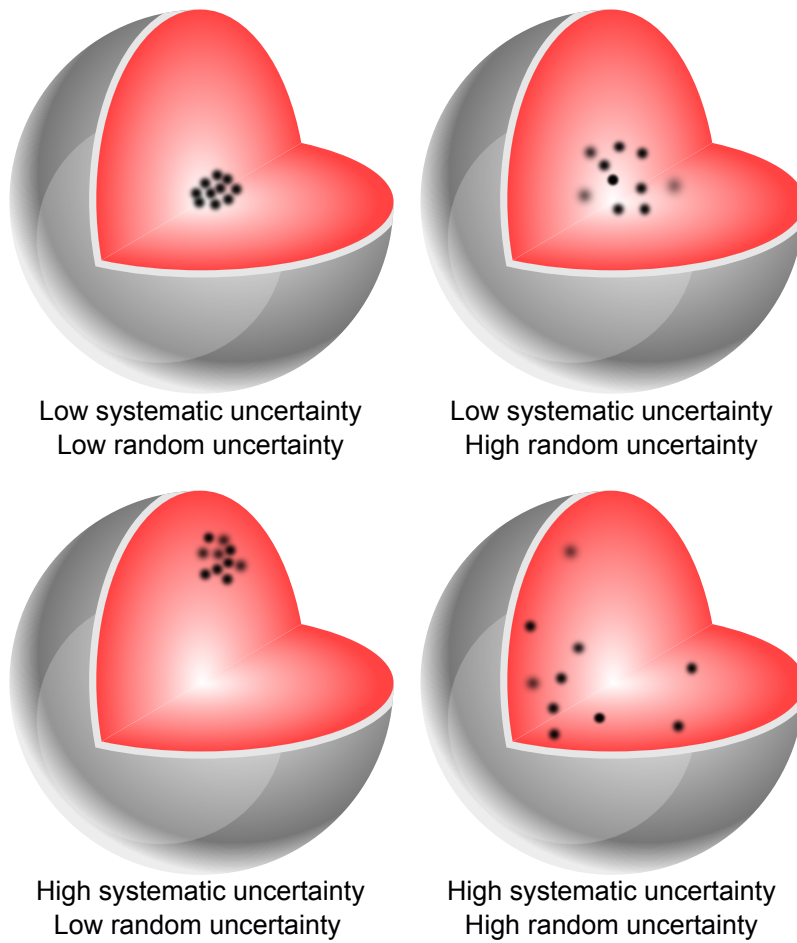
Figure 2.2: Systematic and random uncertainties. The red volume represents the CTV and the black circles represent the isocenter at treatment. Ideally the isocenter should be in the middle of the tumor.

When it comes to radiotherapy using protons, the PTV is flawed by definition since it does not take into account the proton beam's range uncertainty [39, 48, 49]. For this reason, the robust optimization [50] technique using different perturbations has been developed. Instead of creating an expanded volume around the target, the system takes into account, user defined, range uncertainties and setup uncertainties by shifting the isocenter and addresses multiple uncertainty scenarios simultaneously. Additionally, the plans should also be evaluated robustly using dose-volume histogram (DVH) and other tools available [39, 49, 51–53]. There are also quite considerable biological uncertainties in proton therapy (see Biological optimization) presented later in this chapter.

Setup verification imaging

Historically, it has not been standard of care to daily verify the patient's position with an x-ray image before treatment. However, imaging of patient positioning has been an essential part of radiotherapy since the introduction of the CT scanner [54, 55]. The patient is positioned using wall-mounted lasers in relation to markers on the patient's skin, mask or other immobilization device [56]. The most common practice today is image-guided radiotherapy (IGRT) which means that the patients setup position is verified to correct for random setup uncertainties and most centers perform this daily [57–62]. Daily IGRT has been standard practice at Rigshospitalet since late 2009.

Patients can be positioned using many different types of imaging systems. The two simplest ways to take an image of the patient is to use either the electronic portal imaging device (EPID) using megavoltage (MV) x-rays or the on-board imaging (OBI) device using kilovoltage (kV) x-rays [63, 64]. These techniques result in two planar, two-dimensional (2D) images. In terms of matching on bony anatomy these two systems are comparable, however, a reduced image contrast can be expected for the MV energy system [65]. The OBI can also be used to scan the patient three-dimensional (3D), using cone-beam computed tomography (CBCT), first introduced by Jaffray et al. [66]. During a continuous gantry rotation, the system acquires multiple 2D projections that are later reconstructed into a 3D volume set. This set of images are then used for matching on either bony anatomy or soft tissue areas, such as OARs, in relation to their target area [67]. Tomotherapy utilizes a similar system but with MV-energy instead of kV-energy [68]. With daily imaging some setup uncertainties can be considerably reduced since they are thus automatically accounted for [63, 67].

Most proton accelerators are equipped with imaging systems, many of which have CBCT capability. Imaging in proton therapy is essential to be able to reduce some of the margins used due to uncertainties [69].

2.2 Radiobiology

Radiation damages both tumor cells and surrounding healthy tissue. Damage to organs and other healthy tissue can cause both acute and late adverse effects which means that patients with tumors closer to OARs are at a higher risk of side effects [70, 71]. Pediatric patients are at an even greater risk due to their normal tissues being under constant development and longer life expectancy [34, 72–77]. In radiotherapy, the radiation interacts with atoms in the body and facilitates generation of free radicals through indirect ionization. Free radicals are highly reactive ions that damages cells generally and deoxyribonucleic acid (DNA) specifically [78]. Damage to the DNA primarily consists of single strand breaks and double strand breaks where the latter is the more important part since it usually leads to cell apoptosis [79].

The deposited energy is measured in absorbed dose and quantified in Gy. However for protons, the quantification unit Gy_{RBE} (see Notes) is often used. The very high energy in proton therapy induces reactions that can produce secondary protons, deuterons, tritons, ^{3}He, ^{4}He, other ions and neutrons. Especially neutrons constitute for a high risk of unintentional irradiation to the patient since the production is extensive and the shielding of neutrons is not trivial [80]. Neutrons are very penetrating, and their biological effectiveness is up to 20 times higher than that of a proton, depending on the energy of the neutrons [81]. Neutron exposure therefore increases the risk of late adverse effects and secondary cancers [82, 83].

Tumor control probability and normal tissue complication probability

The main objective in radiotherapy is to obtain local tumor control by giving the tumor sufficient dose to accomplish this. At the same time, it is highly important to spare the surrounding healthy tissue from severe complications by keeping the dose as low as possible. Trying to achieve both aims at the same time is intuitive but conflicting. Increased dose to the tumor yields increased tumor control probability (TCP) but it could also increase the normal tissue complication probability (NTCP) due to the increased absorbed dose. The NTCP is in most cases the limiting factor. The irradiated volume is often an important parameter included in normal tissue dose respogammnse curves (Figure 2.3) since there is extensive evidence that the response depends on the volume of normal tissue irradiated [70, 75, 84–89]. It is important to keep in mind that for some normal tissue toxicities there is no lower dose limit tolerance at which the complication rate is zero. An endpoint is a specific circumstance that either has transpired or not. In clinical situations, the data for dose-response curves is attained in terms of incidence rates for any selected endpoint for multiple dose levels [90].

Tumor cells are, in general, less likely to repair damage from ionizing radiation compared to the surrounding healthy tissue and this generates one of the fundamental conditions of radiotherapy; the therapeutic window or ratio (Figure 2.3) which is the region between the two curves. In radiotherapy, there are also a set of tools available that widens this ratio (e.g. fractionation schedules) and increases the potential benefit from radiotherapy [91, 92].
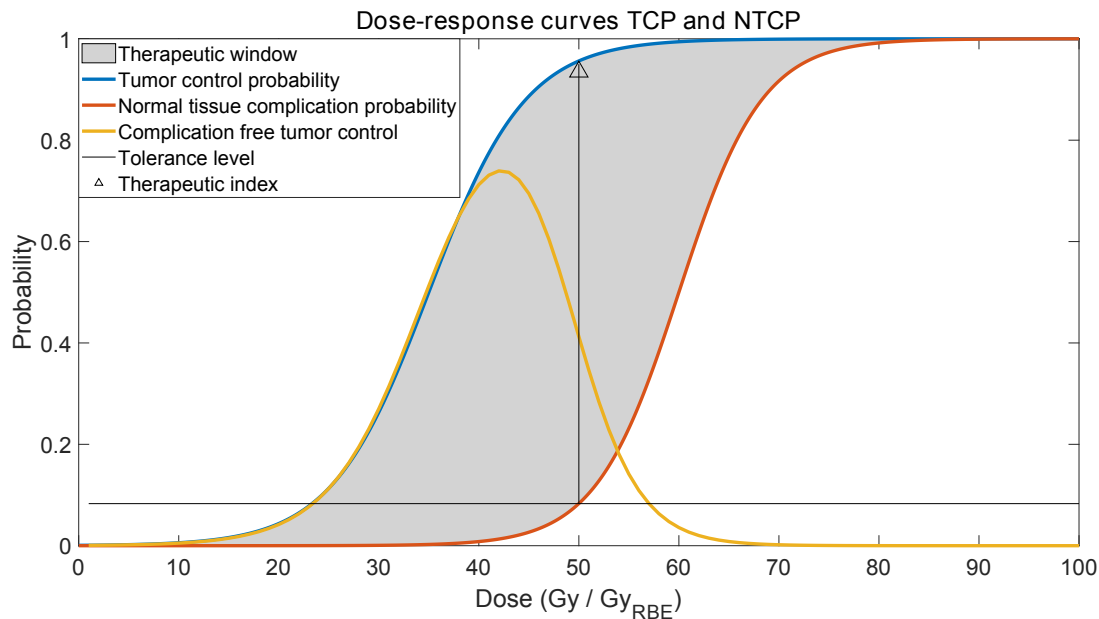
Figure 2.3: Dose-response curves for tumor control probability (TCP) and normal tissue complication probability (NTCP) and the relationship between them. The therapeutic window or therapeutic ratio is the difference in absorbed dose between the curves (gray area). The maximum probability for tumor control without normal tissue complications is presented in yellow and is described as $TCP(1 - NTCP)$. Therapeutic index is the ratio of the expected TCP to NTCP at a clinically assigned maximum tolerance (in this case, 8%). The curves have been computer generated using simulated values and the mathematical models of dose-response relationships are derived from Bentzen and Tucker 1997 [93].

The circumstances for TCP and NTCP models are very complicated since the tissue response rate is influenced by multiple dynamical factors, factors that are influenced by the co-movement of other factors. For example, the radiosensitivity of tissue strongly depend on oxygenation, angiogenesis, cell cycle interphase, rate of repopulation and other dynamically changing factors and these conditions can be rather different for different parts of the tumor. The NTCP models aim to describe the complication probability of healthy tissue for a certain endpoint as there is comprehensive evidence that the radiation response for normal tissue strongly depends on the irradiated volume [84, 85, 87–89]. The improved understanding of the volume dependence of healthy tissue response can

be credited the clinical applications of TCP and NTCP models. This is especially true for the tolerance data and fit parameters provided by Emami et al [84] and Burman et al [85]. More recently, advances in outcomes and research priorities have been extensively reviewed in the QUANTEC initiative [70].

Biological optimization

The treatment planning process is usually based on prescription dose to the target and certain dose constraints to the different OARs in the near vicinity of the target volume. In many cases, instead of dosmetric surrogates, it might be preferable to optimize on endpoints or outcomes such as TCP and NTCP which are more clinically relevant parameters as they claim to predict the radiation response in patients [94–98]. Instead, the differences in biological effect needs to be considered. The biologic effectiveness of protons has been assumed to have a generic fixed value of 1.1 relative to photons and is currently being employed at proton facilities [47, 99–101]. This RBE pertains to the dose in the SOBP for all types of tissues and thus, does not differentiate between e.g. lung and muscle tissue. Despite large amounts of data there are still considerable uncertainties in proton RBE. Several studies suggest that the RBE value actually is variable across the SOBP [41–43, 100, 102–108]. The RBE increases with increased LET and thus, depth and is suggested to range from approximately 1.1 in the entrance, 1.15 in the center, 1.35 at the distal edge up to roughly 1.7 in the distal fall-off. The biological uncertainties are very complex, and it depends on complex functions of LET, fraction dose, type of tissue, cell type, endpoint(s) and more [100]. This suggests that the RBE is variable and increases as a function of depth (Figure 2.4), with increased dose and with decreased tissue specific parameters or fractionation sensitivity (α/β) (e.g. the RBE increases more with lower values for α/β). The α/β values are given through studies conducting comprehensive research in NTCP dose-response models and organ specific outcome data and are used to describe the shape of the fractionation response [70, 71, 84, 109]. In general, this ratio is low (0.5-6 Gy) for late reacting tissue and somewhat higher (7-20 Gy) for early reacting tissue and tumors [91]. Typically values of 2-3 Gy and 10 Gy are used clinically for late reacting tissue and tumor tissue, respectively [78, 110].
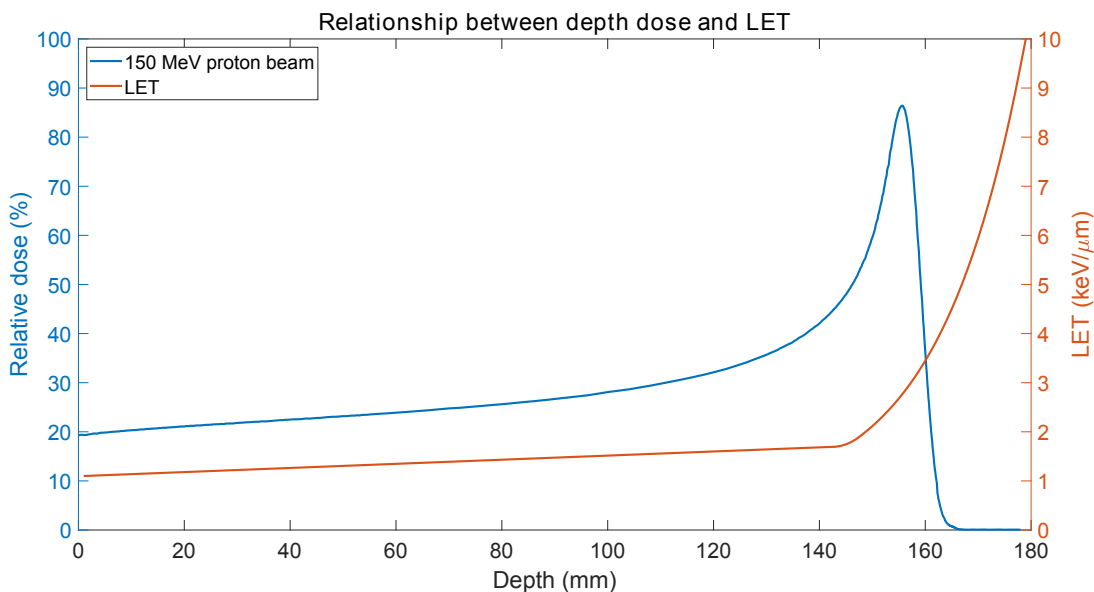
Figure 2.4: The relationship between a proton depth dose curve and the linear energy transfer (LET). The proton depth dose curve for 150 MeV is a simulated beam energy from The Skandion Clinic, Gantry 1 (GTR1) and the LET is computer generated using random numbers. Please observe that the two curves correspond to the y-axis of the same color.

It is actually quite unlikely that the distal edge would conform to the target shape in multifield IMPT since multiple beams converge on each other inside the target and many of the small beamlets delivers dose throughout the volume. This means that the LET can be very different resulting in rather different RBE values, compared

to the ones stated above, throughout the target. This could further confound the use of biological optimization for protons due to additional uncertainties.

2.3   Diseases and anatomy

Second only to leukemia, neoplasms in the CNS are the most common types of malignancies in children [111]. It is, however, the leading cause of cancer related childhood death [112]. Fortunately, cancer in children and adolescents is generally uncommon (Figure 2.5) and in contrast to adults, a majority of pediatric CNS tumors are infratentorial (i.e. they originate in the lower, back part of the brain). The most common pediatric brain tumors are medulloblastoma (MB), astrocytoma, germinoma and ependymoma. The treatment of these and other CNS tumors can be quite different depending on patient diagnosis, age and tumor-related risk factors, such as residual tumor volume, M-stage, histology and molecular subgroups including various genetic mutations [113]. Furthermore, anatomy has a role in determination of treatment and prognosis. For example, a tumor in the cerebellum is more often safely resected whereas tumors appending the brainstem usually are not. For some types of tumors, the cerebrospinal fluid (CSF) is an important route for tumor dissemination. Metastatic dissemination implicates a treatment challenge and cause of death in patients with some CNS tumors (e.g. MB) [114]. Some pediatric CNS tumors are treated with focal irradiation while others are treated with CSI and focal boost which leads to very different toxicity profiles. Even though the treatment has become somewhat more stratified over the last decade, it has remained rather consistent. Most long-term survivors of malignant pediatric CNS tumors treated with CSI have significant neurocognitive late effects (see Treatment related side effects), and patients treated at a younger age tend to have worse outcomes [115, 116].
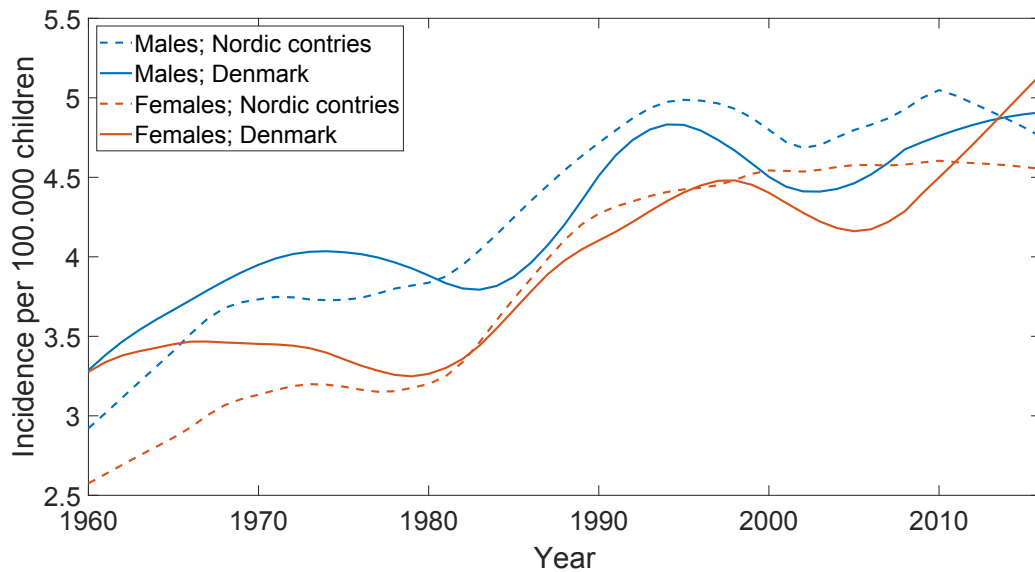
Figure 2.5: Cancer incidence per 100.000 children (0-19 years old) with brain and CNS tumors in Denmark (solid lines) and the the nordic contries (dashed line; including Sweden, Denmark, Finland, Norway, Iceland, Faroe Islands and Greenland) between 1960 and 2016 for males (blue lines) and females (red lines). The data stem from the NORDCAN project [117].

The hippocampus

The hippocampus is a small part of the temporal lobes of the brain (Figure 2.6), with a shape of a curved tube that closely resembles a seahorse and it is a part of the limbic system in the human brain [118]. It consists of five combined parts (two main parts) called cornu Ammonis (CA1-CA4) and the dentae gyrus in an interlocking

"U" composition. Humans have two hippocampus located along the border of the medial temporal lobe, one in each hemisphere. The hippocampus plays an important role in the neurogenesis, memory encoding and mood regulation [119, 120], even during sleep [121]. It has also been associated with learning abilities and emotions [120]. It is not believed that memory is stored there, more that it works as a memory retriever. The hippocampus is therefore very important in connection of how scents and emotions can trigger a strong memory.
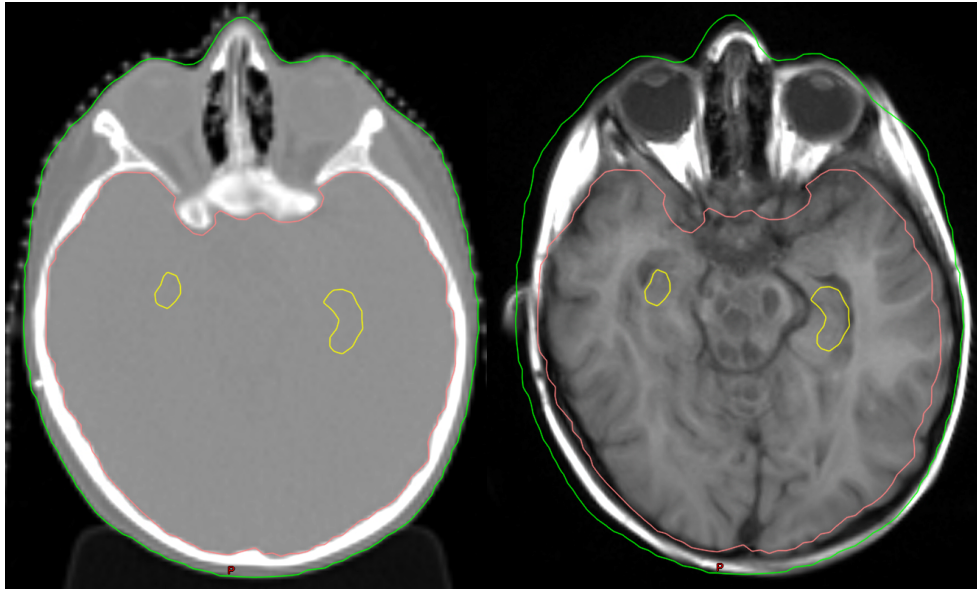
Figure 2.6: Transversal view of a computed tomography (CT) and T_1-weighted magnetic resonance imaging (MRI) showing the central location of the hippocampus (yellow contour) and the cranial clinical target volume (CTV) (light red).

Damage to the hippocampus

When the hippocampus is damaged it can seriously affect its function and have long-term impact on these patients and the damage can occur from various sources (e.g. irradiation). The hippocampus are sensitive to radiation [122–124] and it has been shown that the neurogenesis occurs in the hippocampus [119] and that radiation damages hippocampal stem cell differentiation [125]. Sparing the hippocampus has been correlated with improved memory preservation [126, 127], although the exact repercussion of the damage can be somewhat different depending on the affected hippocampus in relation to the patient's brain location of language. Studies suggest that damage to the left hippocampus can affect verbal quotient while complications with visual information and spatial memory as a result after damage to the right hippocampus [128–131].

2.4 Craniospinal treatment

A combination of surgery, chemotherapy and CSI is the most used treatment combination for MB, however, for other primary tumors in the CNS it can vary considerable depending on patient diagnosis, age and tumor-related risk factors. For example, surgical resection of the tumor can be carried out either before or after one or more cycles of chemotherapy. The neurosurgeon always has to weigh the benefit of removing as much as possible of the tumor against the risk of impairing vital components in the brain. A complete microscopic removal of the tumor is not possible thus, surgery is many times followed by both radiotherapy and multiple cycles of chemotherapy. There is a wide variety of different chemotherapy types used for CNS treatments; vincristine, cisplatin, carboplatin, cyclophosphamide, vinblastine, methotrexate and on rare occasions also etoposide and doxorubicin. Additionally, alkylating antineoplastic agents such as lomustine and temozolomide and the MEK inhibitor trametinib are often used along with the chemotherapy. For example, a MB patient at our institution
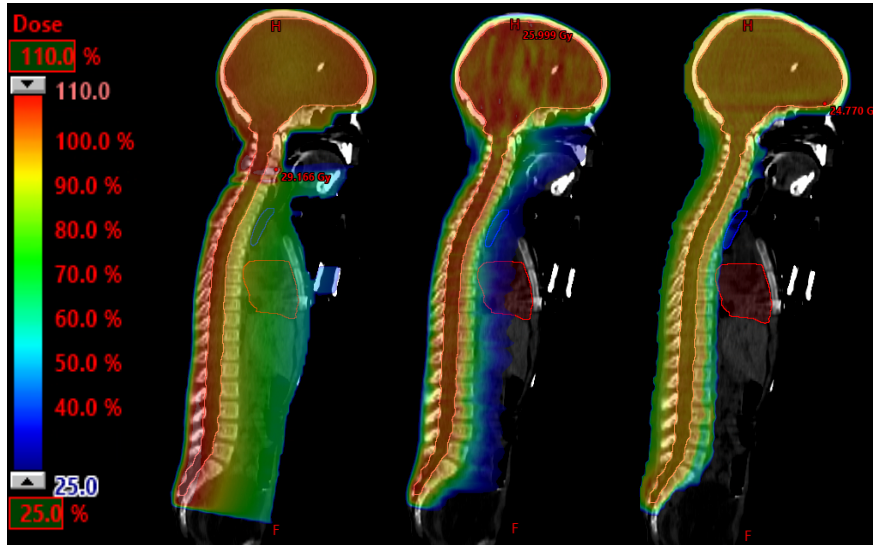
Figure 2.7: Dose distribution in a sagital orientation for 3D-CRT (left), IMRT (middle) and IMPT (right) craniospinal irradiation techniques.

often receives the "Packer-protocol" which consists of weekly vincristine followed by 8 cycles of cisplatin, lomustine and vincristine [132]. This is also consistent with other institutions prescription [133]. External beam radiotherapy is one of the most effective types of treatments for malignant CNS tumors and while CSI is one of the cornerstones in MB treatments, it is rarely used for low grade tumors (e.g. low grade glioma, LGG) where a surgical resection is the main type of treatment.

The treatment volume for CSI includes the entire CNS subarachnoid space and the inferior border is extended below S2 to include the thecal sac. Combining the cranial and spinal parts of the treatment requires careful technical planning and depends greatly on the choice of treatment modality and technique. Most patients are prescribed a dose of either 23.4 or 36 Gy to the entire brain and spinal axis in a risk-adapted dose prescription, subsequently each prescription regimen being followed by a boost treatment to the original or residual tumor bed to a total dose of 54-55.8 Gy [134, 135].

Historically, both electrons and photons have been used for CSI treatments and recently protons have emerged as a contender to the conventional treatments by offering the possibility of greatly reducing the integral dose, which is of predominant importance for pediatric patients because of late carcinogenic effects [29, 73, 136–138]. Especially compelling is the lack of exit dose for the spinal part of the CSI treatment where the heart and lungs can be considerably spared (Figure 2.7). The use of protons has also generated the possibility of greatly sparing the hippocampus [139–142], which can be compared to advanced, modern photon therapy techniques that are able to spare the hippocampus to some extent [122, 127, 143–145].

Treatment related side effects

Many patients surviving their treatment for a CNS tumor in childhood suffer from late side effects [75, 76, 146–149]. First and foremost, secondary malignances are a late adverse event as a large portion of the patient's body is being irradiated [150]. Since the elective part of the cranial target covers the entire brain there are many OARs in the vicinity. Radiation to eyes, optic nerves and/or chiasm can result in loss of vision or blindness and as the ears are in the direct path of the radiotherapy beams many patients also suffer from hearing loss or deafness. Neurocognitive impairment (see Avoiding the hippocampus) is a side effect arising from irradiation of the brain, where irradiation of the hippocampus (Figure 2.6) has been suggested to contribute substantially to this impairment in the brain [126, 127, 144].

Since the whole spinal axis is also irradiated, other side effects are possible such as perturbed growth, cardiac events such as congestive heart failure and myocardial infarction and lung toxicity are also frequent. The most

common causes of death among pediatric cancer survivors are relapse of primary cancer, secondary cancer and cardiovascular disease [151–157]. Other potentially fatal, side effects arises from pulmonary toxicity [158–160]. Late side effects such as loss of vision, hearing loss, growth impairment, gonadal dysfunction, other endocrine disorders and neurocognitive impairment are usually non-fatal, however, they affect the patient's quality of life after treatment. Nausea, vomiting, headache, skin reactions and infections are other types of acute side-effects that can occur from this treatment [161].

There are various laudable efforts of collecting long-term follow-up data of large pediatric cancer patient cohorts [162–168], some containing data dating back several decades. These databases comprise the cornerstone in many retrospective dose-effect relationship studies. These databases could, together with mathematical models, aid the process of linking doses with the documented long-term effects [169].

Avoiding the hippocampus

Pediatric cancer survivors comprise a rapidly growing group of young adults [72]. However, a longer survival is associated with long-term morbidity and mortality [152, 170]. Craniospinal treatment is a quite aggressive type of CNS treatment (see Craniospinal treatment) which is very effective but it is also associated with a substantial risk of late adverse effects. One of the most severe, non-fatal, and also most common side effects is neurocognitive impairment and/or decline [171], unfortunately, a younger age at treatment is correlated with worse cognitive deficits [115, 116]. There are multiple studies that have reported a relationship between ionizing radiation dose to the brain and cognitive impairment for pediatric patients [146, 172–175] where dose to the hippocampus and cognitive outcome is one of them [146, 176]. Recently, in order to improve treatment related, neurocognitive side effects, several studies investigating hippocampal-sparing (HS) treatments has begun to emerge [122, 127, 139–145, 177].

Consequently, it is important to try to spare the hippocampus when treating adult patients and it is highly likely that it is even more important to spare when treating pediatric patients [126, 146, 178] especially in terms of neurocognitive impairment but also in terms of quality of life [127, 148].

3

Methodological considerations

This section provides a description of the patients and some of their characteristics included in the three studies. It also contains a brief summary of the methods and elaborates on some of the methods chosen. A total of 38, 24 and 21 pediatric patients where used in STUDY I, STUDY II and STUDY III, respectively. Further details regarding additional comparisons are available in the appendix.

3.1 STUDY I

Purpose: Investigate the setup errors for pediatric CSI and explore how daily IGRT has impacted positioning uncertainty.

Motivation: To allow for informed margin calculation and robust optimization of treatments.

This was a multicenter study with pediatric patients from both Rigshospitalet and Skåne University Hospital where we simulated different treatment imaging protocols to allow for more informed margin calculation and robust optimization for different clinics treating pediatric CSI patients regardless of the imaging protocol employed at these clinics. The imaging protocols included were skin-marker based setup, action level (AL), no action level (NAL), IGRT for narrow field junction (nj) ($IGRT_{nj}$) and IGRT for wide field junction (wj) ($IGRT_{wj}$). We refer to $IGRT_{nj}$ as a treatment protocol with narrow field junctions and sharp dose gradients, i.e. where the field positions cannot be altered in the cranio-caudal direction without the risk of considerable changes in the dose distribution. The $IGRT_{wj}$ refers to a treatment protocol where wide field junctions and flat dose gradients are optimized to be overlapping, thus, dosimetric consequences of uncertainties in the cranio-caudal directions will be very small.

The patients in this study had been treated with CSI on either a Linac or tomotherapy unit. A 3- and 6-degrees of freedom (DoF) offline match was performed, respectively, in all cardinal directions; superior-inferior (SI), anterior-posterior (AP), medial-lateral (ML), yaw (rotation around the AP axis), pitch (rotation around the ML axis) and roll (rotation around the SI axis). These notations and the corresponding rotations are illustrated in Figure 3.1.

There are essentially two approaches to handle uncertainties related to the treatment within the field of radiotherapy; reducing and/or accounting for them. Both are important and it is unrealistic to assume that it is possible to eliminate them all together. There are also studies that have developed widely used algorithms for calculating margins [179–183] and with these algorithms standardized or personalized margins can be calculated

using our data. We also present results for both narrow- and wide field junction irradiation techniques (nj and wj) since some centers that use conformal techniques do not apply imaging-based shifts in the SI-axes after treating the first isocenter due to narrow field junctions and steep dose gradients. The wide field junctions are usually associated with proton treatments, but they are also possible to achieve using more modern photon therapy techniques such as IMRT and VMAT.

One of the patient characteristics being evaluated in this study was the patient's body mass index (BMI). Since BMI of children and adolescents varies considerably with both sex and age, it is exceptionally challenging to use the BMI for analysis. Therefore, the BMI was expressed as Z-scores [184] and calculated according to previously published methods [185, 186] prior to analysis.
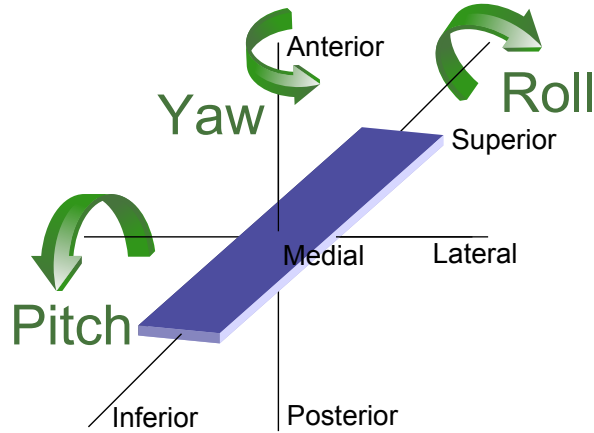
Figure 3.1: Schematic of the anatomical notations and their corresponding rotations.

The systematic error (SE) was calculated by taking the average mean residual setup error for all patients over their entire treatment. The SE should thus be close to zero since a higher number would indicate a systematic deviation affecting the procedure (e.g. misaligned lasers, miscalibration of radiation isocenter, improper settings on the immobilization device or similar). The systematic uncertainty (SU) is defined as the standard deviation (SD) of the mean errors for all patients over their entire treatment while the random uncertainty (RU) is defined as the root-mean-square deviation (RMSD)* for all patients, again over the entire treatment. All data were collected for each cardinal direction (Figure 3.2) according to van Herk [44] and Kutcher et al. [187]. In figure 3.2, each of the circular shaped markers represent the patient's setup discrepancy between actual and planned/ideal position. For clarity, the registrations are presented in a 2D-plane. The corresponding vectors represents the SE. The difference between the vector and each of the image registrations is the random error distribution.

Positioning uncertainties for all included imaging protocols were evaluated against the pre-treatment setup images and univariate linear regression models were fitted for the various positioning uncertainties and residual errors using all covariates. The positioning uncertainties and residual errors where quantified by means of Spearman's rank correlation coefficients or Wilcoxon's rank-sum tests for continuous and categorical variables, respectively. The variance of each isocenter for all cardinal directions is assumed to be the same. This assumption is tested with a two-sample F-test and based on the results. The F-test did not reject the null hypothesis that the samples comes from normal distributions with the same variance ($p = 0.054 - 0.799$). Therefore, this data is pooled to increase the statistical power of the comparisons.

The complex margin formula (equation 3.1) proposed by van Herk et al. [179] was applied to calculate the PTV margin required for pediatric CSI at our institution to provide 95% dose coverage to 90% of the patients. The PTV margin (m_{PTV}) is given by

$$m_{PTV} = 2.5 \sum + 1.64\sqrt{\sigma^2 + \sigma_p^2} - 1.64\sigma_p \qquad (3.1)$$

---

*The RMSD is the square root of the average of the squared errors.

where $\sum$ is the systematic uncertainty, the random uncertainty is described by σ and σ_p represents the penumbra. Margin calculations are designed to take delineation uncertainty into account [179]. Although this has been identified to be the largest source of uncertainty [188, 189] there are many institutions that do not include it. Therefore, we show margin calculations based on three different delineation uncertainties; 0, 2 and 4 mm.
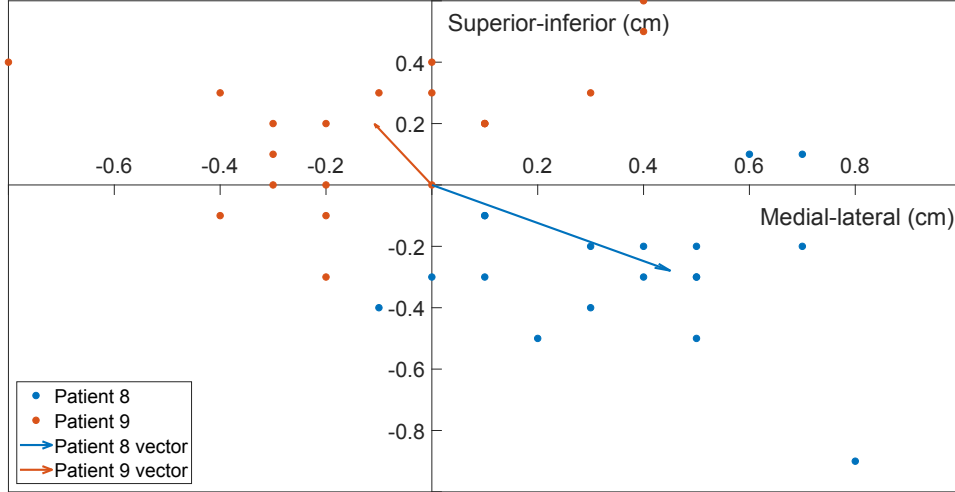
Figure 3.2: Schematic representation regarding positioning uncertainty evaluation for patient 8 and patient 9 (randomly chosen from our dataset). It is presented in 2D for simplicity. The image shows a head-first supine position with a top viewing and values are presented in cm. Adapted from Kutcher et al. [187].

3.2 STUDY II

Purpose: Investigate the risk of neurocognitive impairment for HS IMPT

Motivation: Estimating the benefit of reducing the risk of neurocognitive adverse effects without reducing the probability for tumor control

The pediatric patients in this study were re-planned and a total of 504 HS IMPT plans were generated; 432 plans for the elective volume and 72 boost plans. Only the cranial part of the target was considered for the purpose of this study. In accordance with treatments of standard risk medulloblastoma at Rigshospitalet, plans were prescribed 23.4 Gy$_{\text{RBE}}$ + 30.6 Gy$_{\text{RBE}}$ in 1.8 Gy$_{\text{RBE}}$ fractions to the elective and boost target volumes, respectively. The hippocampal dose objectives were defined in relation to five different levels of avoidance; 5, 7, 9, 12 and 15 Gy$_{\text{RBE}}$ with the intent of studying how much of the hippocampus are able to be spared without compromising the clinical objectives to the target. These levels of avoidance were chosen based on previously published data regarding hippocampal sparing treatments and also to cover a wide range of dose levels due to the possibility of interpolating data between the points. Plans optimized without dose restrictions to any of the hippocampal objectives (denoted standard CSI plan) were used for comparisons. There is a broad variety of different definitions for homogeneity index (HI). The HI (equation 3.2) used in this study is

$$\text{HI} = \left(\frac{Target\ volume_{107\%} - Target\ volume_{95\%}}{Target\ volume} \right) \cdot 100\% \tag{3.2}$$

defined as the relative target volume receiving $V_{95\%}$ - $V_{107\%}$ of the prescription dose where a HI score of 100% constitutes a completely homogeneous plan. When evaluating treatment plans, we also used the dose to 0.03 cm^3 of the volume ($D_{0.03\,\text{cm}^3}$) instead of using the maximum dose to individual voxels. A highly modulated IMPT plan tends to have some hot-spot effects on single voxels, especially in areas of considerable density changes (e.g. when the beam is entering an air-filled ventricle from bony anatomy). The plans were deemed clinically acceptable if the following conditions were met: $V_{95\%} \geq 95\%$ of the prescribed dose (PD), $D_{0.03\,\text{cm}^3} \leq 110\%$ of PD, $D_{0.03\,\text{cm}^3} \leq 107\%$ of the PD to the brainstem, dose to the chiasm ≤ 50 Gy$_{\text{RBE}}$ and a HI for CTV$_{\text{elective}}$ of ≥ 95.

We explored the difference in hippocampal dose for the different plans by investigating patient characteristics such as gross tumor volume (GTV) size, hippocampal size and the distance between CTV$_{\text{boost}}$ and the hippocampus, defined as the center of the hippocampus to the closest point of CTV$_{\text{boost}}$.

We analyzed the plans by considering the estimated clinical benefit of sparing the hippocampus and how the difference in hippocampal dose would affect the TCP and NTCP in the form of estimated risk of neurocognitive impairment using previously published models [139, 146, 190]. The TCP dose-response model (equation 3.3) presented by Brodin et al. [190] has been evaluated against recently published data [191] to test its applicability and updated for use in this study. The TCP is estimated as the product, j, for each included target volume

$$\text{TCP} = \prod_{j=1}^{R} \text{TCP}_j = \prod_{j=1}^{R} \left\{ \frac{1 - P_{0,\,j}}{1 + \left(\dfrac{D_{50,\,j}}{D_j}\right)^{4\gamma_{50,\,j}}} + P_{0,\,j} \right\} \tag{3.3}$$

where P_0 is the TCP without irradiation and γ_{50} is the normalized dose-response inclination at the 50% control level. $D_{50,\,j}$ represents the dose that is required to obtain an event-free survival (EFS) of $\frac{1 + P_{0,\,j}}{2}$. The derived logistic NTCP dose-response functions, presented by Blomstrand et al. [139], are based on odds ratios from Armstrong et al. [146] and the following model (equation 3.4)

$$\left.\begin{array}{l} \text{OR}_D = \dfrac{\left(\frac{p_D}{1 - p_D}\right)}{\left(\frac{p_0}{1 - p_0}\right)} \\[2ex] \text{OR}_D = \text{OR}_{10}^{\frac{D}{10\,\text{Gy}_{\text{RBE}}}} \end{array}\right\} \Rightarrow p_D = \frac{\text{OR}_{10}^{\frac{D}{10\,\text{Gy}_{\text{RBE}}}}}{\left(\frac{1}{p_0} - 1\right) + \text{OR}_{10}^{\frac{D}{10\,\text{Gy}_{\text{RBE}}}}} \tag{3.4}$$

where D is the total dose (in Gy$_{\text{RBE}}$), OR10 is the corresponding OR per 10 Gy$_{\text{RBE}}$ dose increase, p_0 is the baseline risk of impairment without irradiation and p_D is the risk of impairment at the total dose D. The updated dose-response parameters (employed in equation 3.3) and ORs (employed in equation 3.4) used in the models are presented in table 3.1.

Table 3.1: TCP and NTCP dose-response model parameters

Parameters	TCP	NTCP$_{\text{TE}}$	NTCP$_{\text{O}}$	NTCP$_{\text{M}}$
Elective γ_{50}	0.36			
Elective P_0	0.695			
Elective D_{50}	17.0 Gy$_{\text{RBE}}$			
Boost γ_{50}	0.36			
Boost P_0	0.716			
Boost D_{50}	40.36 Gy$_{\text{RBE}}$			
Baseline		0.24	0.123	0.246
Odds ratio (OR)		2.95	2.21	1.45

Abbreviations: TCP = Tumor control Probability, NTCP = Normal tissue complication probability, TE = Task efficiency, O = Organization and M = Memory

Important to note is that the confidence interval (CI) for the NTCP model parameters are reasonably wide as the models used are subject to limitations and uncertainties and the TCP dose-response model's uncertainties increase for lower doses where no clinical data is available. These models are not stratified based on different molecular subgroups or patient's performance status which can further confound use.

3.3 STUDY III

Purpose: Investigate whether treatment information from older medical records can be used to retrospectively estimate doses to heart and lungs.

Motivation: Creating mathematical models that could facilitate studies in long-term adverse effects.

We reviewed our clinical database for all pediatric patients treated with spinal irradiation and had medical records describing age at radiation exposure (the patients age at treatment), how the patient was positioned on the Linac couch and the gender of the patient. The radiation plan information such as the field length and field width were also collected. We also needed volumetric imaging information such as the CT images to reconstruct the dose distribution. We tried to use as many explanatory predictors as possible since the volumetric data is often not available from historical cohorts where the patients were treated in an era before CT based dose planning. For example, using the patients' age at treatment as a surrogate for organ volume since the size of the organ usually grows as the child does. This is crucial in order to avoid attributing correlations to characteristics e.g. to associate the correlation between age at exposure and risk of cardiac toxicity to age, when it may in fact be the heart dose that drives the association.

We found 21 eligible patients that had been treated with 6 MV 3D-CRT. Only the spinal target was considered for this study. The full analysis was performed in MATLAB® release 2014b (The MathWorks, Inc., Natick, MA, USA) using a computational environment for radiotherapy research (CERR) [192] after export from our treatment planning system (TPS) (Eclipse™ v. 13.7 (Varian Medical Systems, Palo Alto, CA, USA). For the purposes of this thesis and to confirm the validity of our models, five randomly selected plans were re-calculated using our updated TPS (Eclipse™ v. 15.1 (Varian Medical Systems, Palo Alto, CA, USA). No differences were found.

Another important aspect is that this model may be applied to patient plans previously delivered using ^{60}Co teletherapy machines (see Treatment techniques), which is why all plans were re-calculated using a Siemens Gammatron-3. Since the ^{60}Co Gammatron-3 required the dose to be calculated using a pencil beam convolution (PBC) algorithm, all Linac plans were also calculated using the same PBC algorithm (STUDY III - SUPPLEMENTARY MATERIAL) to assure there were no algorithm related confounds with our model.

Multiple linear regression, that was used in this study, is a function that allows for predictions about a known variable against an unknown [193–195]. In other words, the techniques use explanatory variables to predict the outcome of a response variable. The multiple linear regression (equation 3.5) attempts to model the relationship between the explanatory and response variables by fitting a linear equation to all the observed data available. Multivariable linear regressions are usually described:

$$y = \beta_0 + x_1\beta_1 + x_2\beta_2 + \ldots + x_n\beta_n \qquad (3.5)$$

were y is the continuous dependent variable (e.g. estimated dose), x describes the explanatory variables for each predictor, β_0 is the intercept term (a constant) and β_n being the slope for each explanatory variable. The model's coefficient of determination (i.e. how much the variation in outcome is explained) is given by an R^2-value and a leave-one-out (LOO) analysis was performed to assess the predictive performance of the model.

The LOO analysis was used to validate the models internally. A LOO analysis is a cross validation resampling method (also known as iterated k-fold cross validation) that measures the generalization performance of a

model, typically with low bias and variance. The number of folds is equal to the number of patients in the data set and the learning algorithm is applied once for each patient where all the other patients are used to train the model that is subsequently used as a test set for each specific patient [196–199].

3.4 Unpublished data

Purpose: Assess how the LET and RBE affect the dose distribution

Motivation: Investigate how the dose distribution is altered when trying the stop the beam in the middle of the brain closely in front of the hippocampus.

Since the LET is known to increase as the proton deposits its energy this could potentially play a vital role in the sparing of the hippocampus. The central placement of the hippocampus possesses a great challenge since regardless of the beam's direction the beam will have to stop in front of the hippocampus. This means that the greatest increase in LET is expected close to the edge of the organ proposed to be avoided.

In order to calculate the RBE-weighted dose distribution, a linear quadratic-based RBE model based on several studies [106, 200–203] is used. This model takes into account the dependence of RBE on the dose averaged LET, the tissue specific parameters and the dose delivered. There are multiple phenomenological models [106, 204–211] available for calculating the RBE as well as Monte Carlo based systems for tracking dose averaged LET [212, 213]. A dose averaged LET map is created from the IMPT plans, subsequently, the RBE-weighted dose distribution is calculated based on the tissue specific parameter chosen for each of the organs and tumor. We simulated the response from both early and late responding tissues as well as the tumors, multiple α/β values ranging from two to ten where used [71, 110]. Herein the main problem is presented. The elective target for CSI is the whole brain and the spinal cord partly due to the CSF. It is, however, impossible to delineate the CSF or tumor cells alone which means that the entire brain is assigned the same tissue specific parameter regardless of cell type since an α/β value can only be assigned to a contoured organ or structure. The difference of assigning a low vs a high tissue specific parameter results in immensely different RBE-weighted dose distributions and this effect is multiplied in areas of high LET, such as the distal edge of the proton beam. Preliminary results are presented in the next chapter.

4

Findings and implications

This chapter summarizes and highlights the results obtained in STUDY I, STUDY II and STUDY III. It also contains results previously unpublished and it elaborates on some of the results and observations made, including findings not included in the manuscripts. Some details regarding additional un-pooled data and more comprehensive and detailed results from the different studies are available in Appendix A.

4.1 STUDY I - Residual positioning errors in pediatric CSI

These results are based on 492 fractions across 38 patients. Each fraction had 1-3 isocenters and both 3-DoF and 6-DoF un-pooled and pooled with six cardinal directions data making available a total of 13,572 data points for each of the simulated imaging protocols. Since there are a wide variety of treatment and imaging units, many with different inherent uncertainties, this study mainly focuses on providing uncertainties that stem from setup images. These results could hopefully aid clinics providing pediatric CSI in personalizing the treatment margins regardless of imaging protocol and number of isocenters.

Large inter-fractional deviations occurred when correcting the shifts according to any of the imaging protocols. This was especially notable for rotational deviations with a larger uncertainty for larger deviations (the uncertainties presented in table 4.1 and figures 4.1 and 4.2 illustrates the tendencies mentioned). Rotational uncertainties are generally larger and more noticeable than translational uncertainties (Table 4.1 and Figure 4.1 and 4.2) mostly due to increase in change further away from the isocenter. The effect of rotational uncertainty peaks farthest away from the isocenter and then decreases closer to it and is minimal at the matching point of the isocenter. Generally, the largest uncertainties were found in the SI direction or around the SI direction (roll) for patients treated on a Linac while tomotherapy inherently perfectly maintain the junction geometry.

The residual errors should only include rotational deviation since translational errors were corrected at treatment. However, rotational errors can affect the translational deviation as well (table A.1-A.5). Translational positioning deviations greater than 1 cm occurred in 6% of all fractions and 33% of the patients had at least one such correction. Rotational deviations greater than 1° occurred in 34% of all fractions and 80% of the patients had at least one such correction. Each patient investigated in this study had at least one deviation larger than the PTV margin and these deviations therefore would comprise a geometric miss for patients treated without a daily IGRT-protocol. The lumbar isocenter generally had more residual setup errors compared to the other isocenters.

Moderate to strong correlations between total field length and residual setup errors were found. This means that a longer total field length is correlated with a larger residual setup error. It also indicates that larger margins might be warranted for longer field lengths due to prohibited movement in the SI direction after the first isocenter(s) has been treated. However, For Linac-based multiple isocenter treatments this presents an issue

Table 4.1: SU and RU for all included imaging protocols presenting both 3- and 6- DoF and all isocenters pooled (Units: cm and °). The numbers displayed in bold indicate a statistically significant difference compared to skin-mark based setup.

3-DoF	SI		AP		ML	
	SU	RU	SU	RU	SU	RU
Translational						
- IGRT (nj)	0.18	0.26	**0.03**	**0.05**	**0.03**	**0.05**
- IGRT (wj)	**0.02**	**0.05**	**0.03**	**0.05**	**0.03**	**0.05**
- Skin	0.20	0.27	0.18	0.27	0.12	0.23
- AL	0.20	0.26	0.13	0.22	0.07	0.20
- NAL	0.18	0.32	0.09	0.28	0.07	0.24

6-DoF	SI/Roll		AP/Yaw		ML/Pitch	
	SU	RU	SU	RU	SU	RU
Translational						
- IGRT (nj)	0.15	0.26	**0.02**	**0.05**	**0.02**	**0.05**
- IGRT (wj)	**0.02**	**0.05**	**0.02**	**0.05**	**0.02**	**0.05**
- Skin	0.20	0.26	0.19	0.31	0.14	0.27
- AL	0.15	0.26	0.14	0.26	0.09	0.24
- NAL	0.13	0.31	0.11	0.32	0.09	0.29
Rotational						
- IGRT (nj)	**0.02**	**0.12**	0.22	0.66	**0.04**	**0.14**
- IGRT (wj)	**0.02**	**0.12**	**0.02**	**0.05**	**0.04**	**0.14**
- Skin	0.39	0.91	0.27	0.67	0.42	0.86
- AL	0.37	0.87	0.25	0.66	0.39	0.79
- NAL	0.31	1.10	0.22	0.74	0.38	0.88

Abbreviations: DoF = Degrees of freedom, SI = Superior-inferior, AP = Anteroposterior, ML = Medial-lateral, SU = Systematic uncertainty, RU = Random uncertainty, IGRT = Image-guided radiotherapy, nj = Narrow field junction, wj = Wide field junction, AL = Action level, NAL = Non-action level

for standardizing margins where corrections in the SI direction cannot be applied as the irradiation of the first isocenter defines the position of the next only in a certain couch shift. By focusing on IGRT for each isocenter, variations of the distance between isocenters and therefore in the dosimetrical properties of the junction can occur as the anatomical length of the spinal column is varying and adapted margins might not be able to address this issue.

The IGRT$_{nj}$ protocol eliminated the correlations in all directions except SI and yaw while the IGRT$_{wj}$ protocol eliminated all significant correlations and relationships, as these were adjusted based on daily setup images.

Unsurprisingly, applying any type of imaging protocol reduces the uncertainties and residual setup errors compared to aligning the patient using skin-marks alone. An interesting time-trend found was that patients treated in the earlier years were more accurately positioned to the skin-marks compared to the patients treated later in the cohort. This difference might originate from less time being spent on patient alignment when a verification image is pending.

By using the uncertainties found in this study with the margin calculation proposed by van Herk et al. [179], the difference in margins depending on delineation uncertainties was investigated. We have previously assessed an uncertainty budget of 2.41 mm for the uncertainties that stem from the treatment couch, gantry, imaging vs.

radiation isocenter and image registrations. A standard deviation of the penumbra width of 3.2 mm [179] was assumed for these calculations. Since these calculations are related to the PTV margin, the results are rendered obsolete for IMPT centers. However, the uncertainties could be used to determine perturbations for robust optimizations.

Table 4.2: The PTV margin (calculated from the CTV) for pediatric CNS patients being treated with CSI for the spinal target using daily IGRT for three different contouring uncertainties only accounting for translational uncertainties (Units: mm).

Delineation uncertainty	SI	AP	ML
0 mm	6.9	7.1	7.1
2 mm	11.9	12.1	12.1
4 mm	16.9	17.1	17.1

Abbreviations: SI = Superior-inferior, AP = Anterior-posterior, ML = Medial-lateral

The results vary notably depending on the assumed delineation uncertainty (table 4.2). An important note is that these margin calculations only accounts for translational uncertainties (3-DoF) thus, ignoring errors that stem from rotational uncertainties. This means that the resulting margins should be considered as a lower limit since the effect of rotational uncertainties might increase these results. Even though the delineation uncertainty has been identified to be the largest source of uncertainty [188, 189] there is a well-defined grayscale between soft tissue and bony anatomy both when contouring and performing setup alignment at the craniospinal axis for these patients. Therefore, the delineation uncertainty should be rather low for these patients (disregarding delineation of the tumor bed).
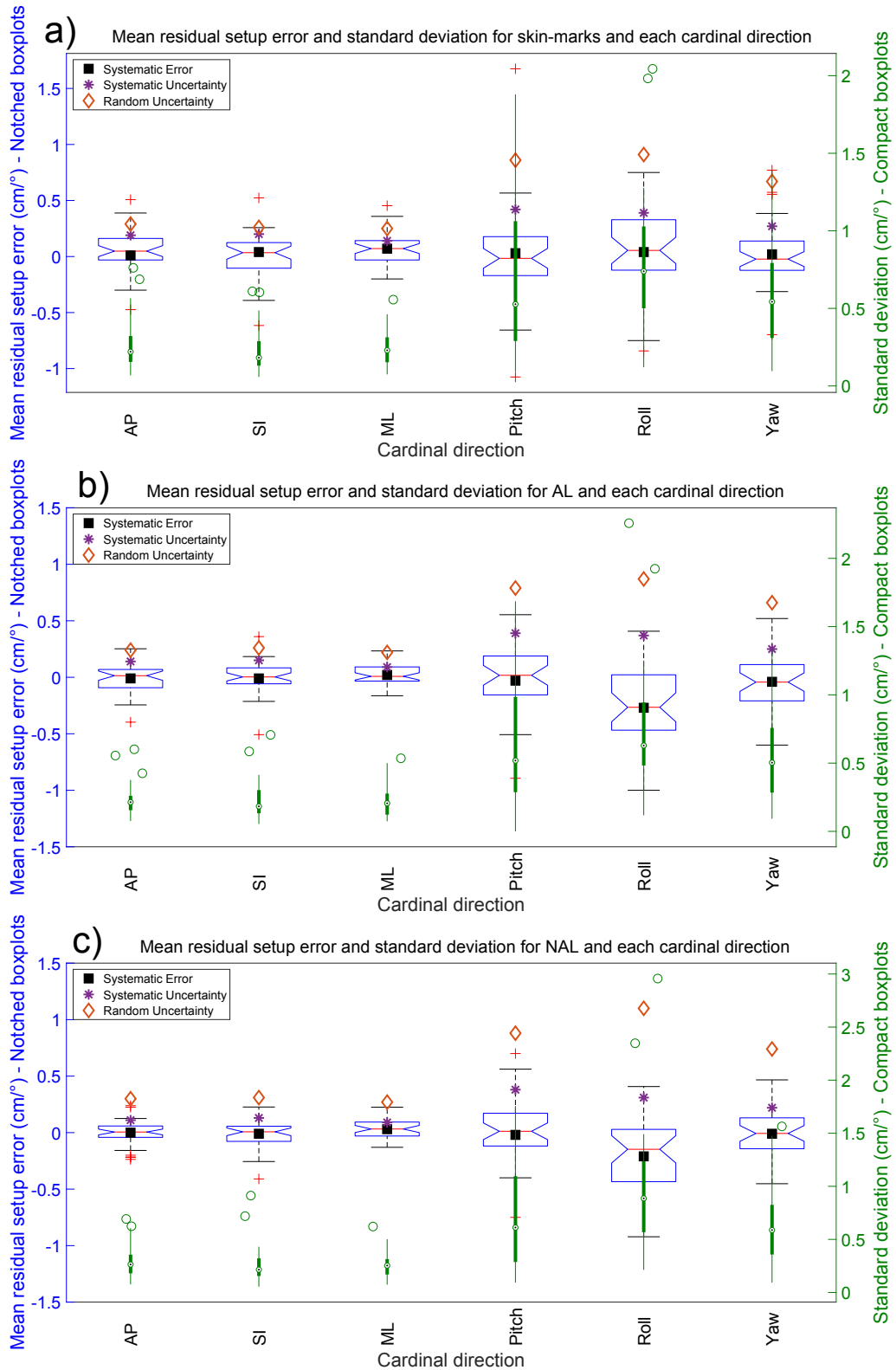
Figure 4.1: Mean setup error (mm) displayed with blue notched boxplots (left blue y-axis) and their standard deviation (mm) displayed with green compact filled boxplots (right green y-axis) for **a)** skin-marks, **b)** AL-protocol and **c)** NAL-protocol for all six cardinal directions examined given as the median (central red line / white circle), 25th and 75th percentile (blue notched box / green filled box) and range (black dashed / green solid line). The individually plotted markers (red plus signs / green circles) indicate the outliers. For all errors and uncertainties, the left blue y-axis is used. Please note that there are two different dimensions (cm and °).
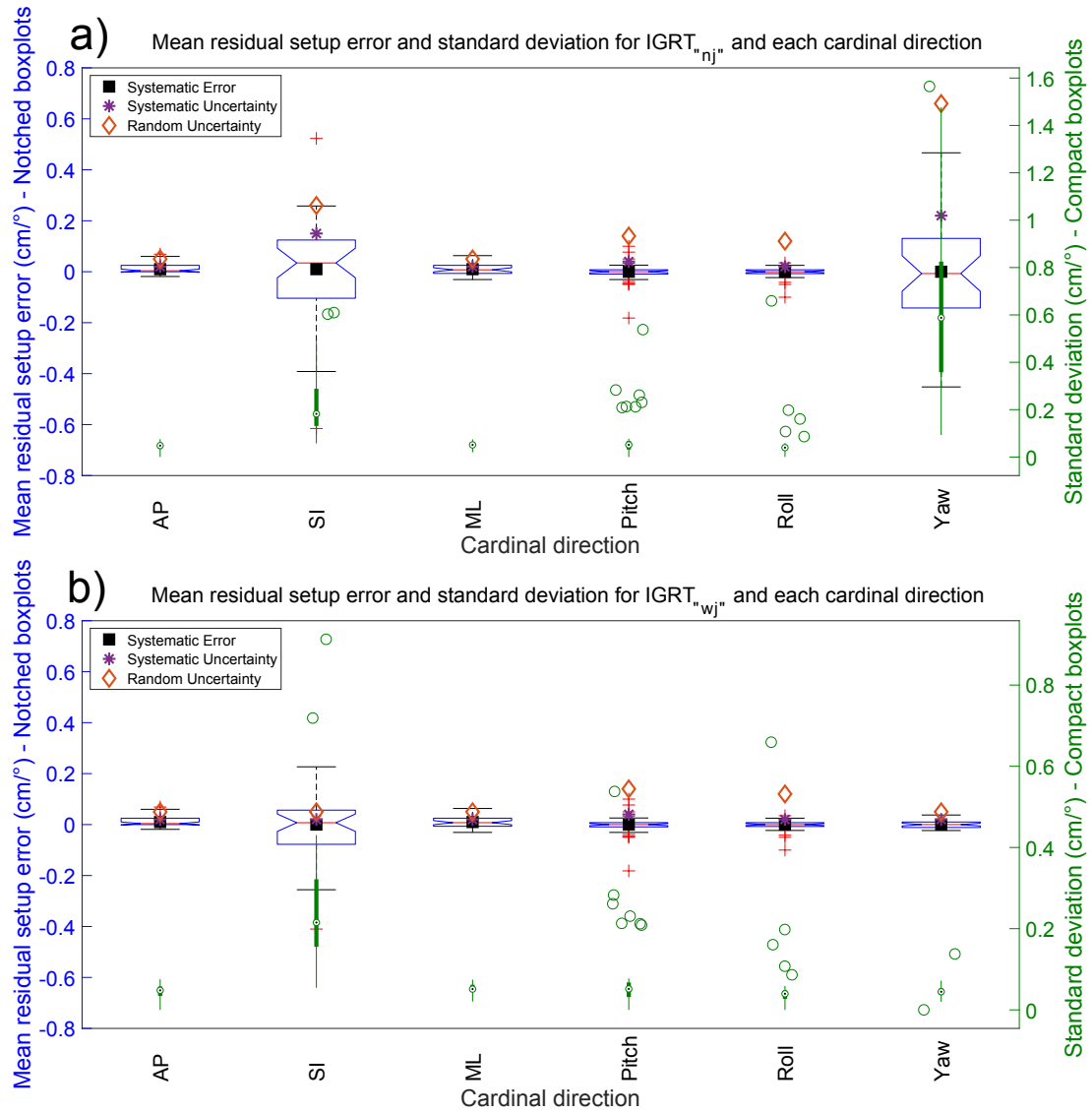
Figure 4.2: Mean setup error(mm) displayed with blue notched boxplots (left blue y-axis) and their standard deviation (mm) displayed with green compact filled boxplots (right green y-axis) for **a)** IGRT$_{nj}$-protocol and **b)** IGRT$_{wj}$-protocol for all six cardinal directions examined given as the median (central red line / white circle), 25th and 75th percentile (blue notched box / green filled box) and range (black dashed / green solid line). The individually plotted markers (red plus signs / green circles) indicate the outliers. For all errors and uncertainties, the left blue y-axis is used. Please note that there are two different dimensions (cm and °).

4.2 STUDY II - Risk of neurocognitive impairment in pediatric CSI

It is feasible to reduce the dose to the hippocampus considerably with minimal dose reduction to the target. However, a lower dose constraint to the hippocampus is related to a higher risk of failure to meet one or more target criteria for what constitutes a clinically acceptable plan (Figure 4.3). The robust optimization with perturbations of 2% / 2 mm resulted in the fewest number of failed plans while both 3.5% / 3 mm and 1% / 1 mm resulted in another three and four clinically unacceptable plans, respectively, for the lowest dose constraint (Supplementary Figures A.1 and A.2 in Appendix A). There is a wide variation on how clinics set their robustness perturbations and what uncertainties they utilize [214, 215]. We choose to investigate these results based on 2% / 2 mm uncertainty since this study only covers the cranial part of the CSI treatment where the patient is securely positioned in a mask, omitting the spinal part where larger uncertainties might be necessary.
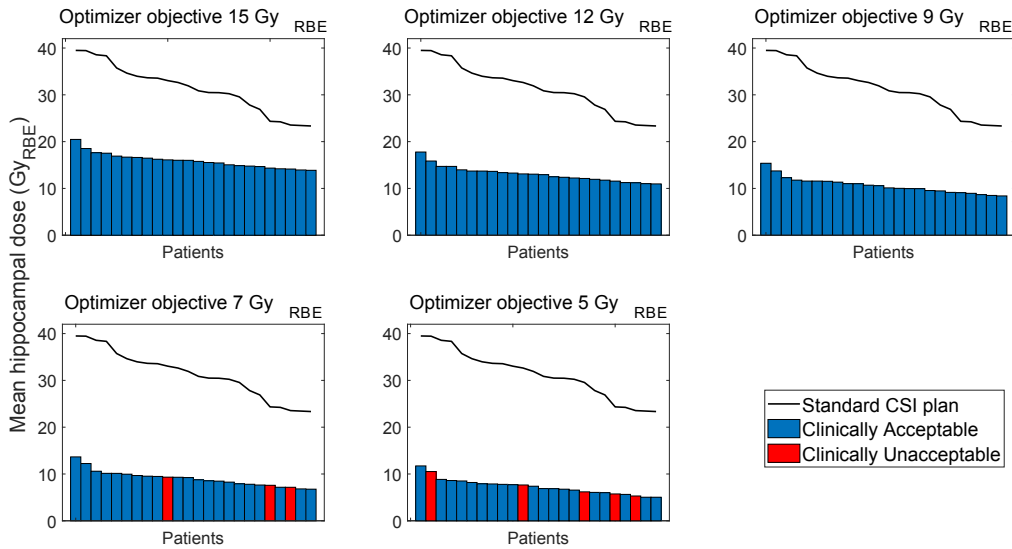
Figure 4.3: Mean hippocampus dose (Gy$_{RBE}$) for all patients optimized with 2% / 2 mm. The blue bars indicate a clinically acceptable plan and the red bars indicate a plan that has been deemed unacceptable according to the parameters described in the chapter covering Methodological considerations for STUDY II. The black line is the mean hippocampus dose (Gy$_{RBE}$) for the standard CSI plans and corresponds to each of the patients.

There is a clear correlation between hippocampus dose and distance between the hippocampus and CTV$_{boost}$ where a longer distance is associated with lower dose to hippocampus (Figure 4.4a). When comparing GTV and hippocampal size to the hippocampus doses there are similar trends to lower doses with smaller sizes (Figure 4.4b and 4.4c). As expected, the largest differences occur for the standard CSI plans even though there are some minor differences for the HS plans as well. If we use 9 Gy$_{RBE}$ (yellow line) as an example; the hippocampus dose is reduced with approximately 4.7 Gy$_{RBE}$ and 1.3 Gy$_{RBE}$ per cm distance between the hippocampus and CTV$_{boost}$ for standard CSI plan and 9 Gy$_{RBE}$ optimized plan, respectively. Similarly, the hippocampus dose is increased by 0.04 Gy$_{RBE}$ and 0.01 Gy$_{RBE}$ per cm^3 GTV size and the corresponding values for hippocampus size are an increase in dose with 0.5 Gy$_{RBE}$ and 0.2 Gy$_{RBE}$ per cm^3, respectively.

The TCP was relatively consistent at 78.5-80.5% 5-year EFS (Figure 4.5) for all plans and patients and it compares well to the current multimodality treatment [216]. The limited difference in TCP estimates is explained by the small hippocampus volume which only constitutes for roughly 1% of the total irradiated volume. The NTCP was calculated for both the median mean estimated risk of cognitive impairment (table 4.3) and the average mean reduced estimated risk of cognitive impairment (table 4.3) which constitutes of three subsections; task efficiency, organization and memory.

Table 4.3: NTCP calculations for median mean estimated risk of impairment and average mean reduced estimated risk of impairment for task efficiency, organization and memory, with corresponding range or standard deviation. All of the results given below are statistically significant compared to their closest higher neighboring value (p<0.001), based on a stepwise comparison of paired t-tests.

	TE	(Range)	O	(Range)	M	(Range)
Risk of impairment						
- 5 Gy$_{RBE}$	40.6%	(35.3 – 52.9%)	19.8%	(17.3 – 26.2%)	29.8%	(28.2 – 33.5%)
- 7 Gy$_{RBE}$	45.5%	(39.6 – 58.0%)	22.3%	(19.3 – 29.3%)	31.3%	(29.5 – 35.1%)
- 9 Gy$_{RBE}$	49.2%	(43.9 – 62.5%)	24.2%	(21.4 – 32.2%)	32.4%	(30.8 – 36.6%)
- 12 Gy$_{RBE}$	56.3%	(50.8 – 68.4%)	28.2%	(25.1 – 36.5%)	34.6%	(32.9 – 38.7%)
- 15 Gy$_{RBE}$	63.8%	(58.6 – 74.3%)	33.1%	(29.6 – 41.6%)	37.1%	(35.3 – 41.1%)
- Standard CSI plan	90.4%	(79.8 – 95.8)	62.8%	(47.2 – 76.3%)	51.2%	(43.7 – 58.6%)
	TE	**SD**	**O**	**SD**	**M**	**SD**
Reduced risk of impairment compared to standard CSI plans						
- 5 Gy$_{RBE}$	48.2%	3.1	42.1%	7.7	21.1%	3.7
- 7 Gy$_{RBE}$	43.7%	3.1	39.8%	7.6	19.7%	3.7
- 9 Gy$_{RBE}$	39.4%	3.1	37.5%	7.4	18.4%	3.6
- 12 Gy$_{RBE}$	32.9%	2.9	33.8%	7.3	16.4%	3.6
- 15 Gy$_{RBE}$	25.4%	2.8	29.0%	7.1	13.9%	3.6

Abbreviations: TE = task efficiency, O = organization, M = memory, SD = standard deviation, CSI = craniospinal irradiation
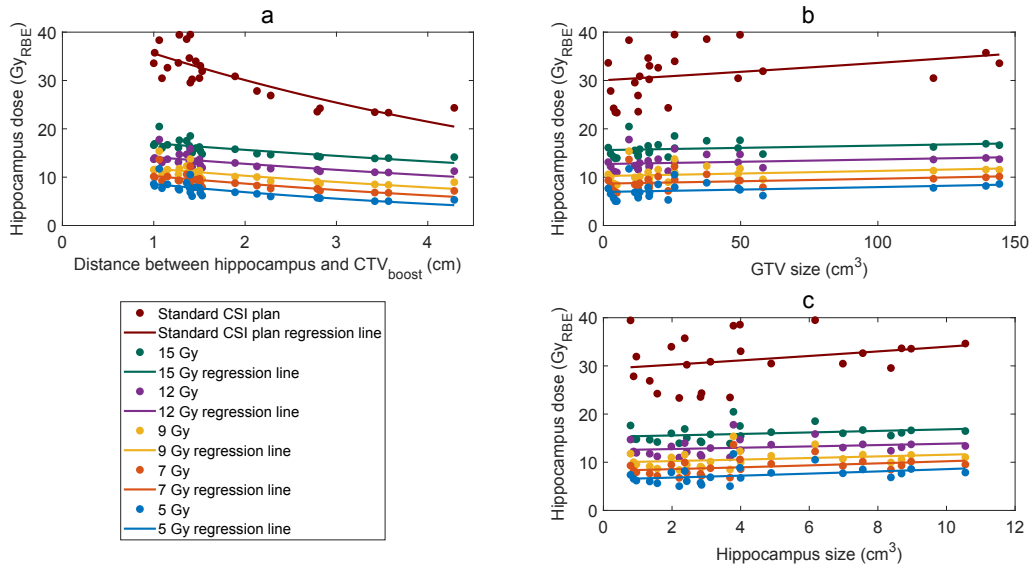
Figure 4.4: The included patients hippocampus doses (Gy$_{RBE}$) plotted against **a)** the distance between the center of hippocampus and the closest point of CTV$_{boost}$ volume **b)** GTV size and **c)** hippocampus size including corresponding regression lines.
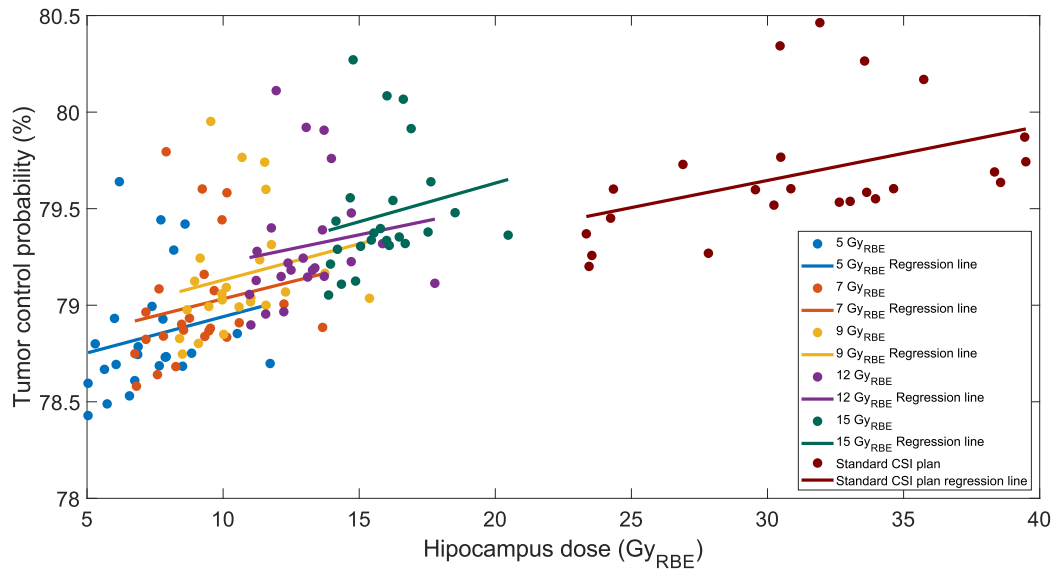
Figure 4.5: Scatter plot displaying the tumor control probability for 5-year EFS for all patients against the hippocampus doses (Gy$_{RBE}$) and their corresponding regression lines.

4.3 STUDY III - Pediatric retrospective dosimetry

The spinal irradiation field width showed strong associations with both mean heart dose and mean lung dose. The field width (Figure 4.6b) was, found to be a statistically significant dose predictor of both the heart and lung dose, but not field length, likely as the heart and lungs were fully covered by the field in the superior-inferior direction leaving changes at the ends insignificant. Age (Figure 4.6a) was also found to be a significant predictor of mean heart and lung doses which supports the general assumption that age is a good surrogate for heart and lung volume.
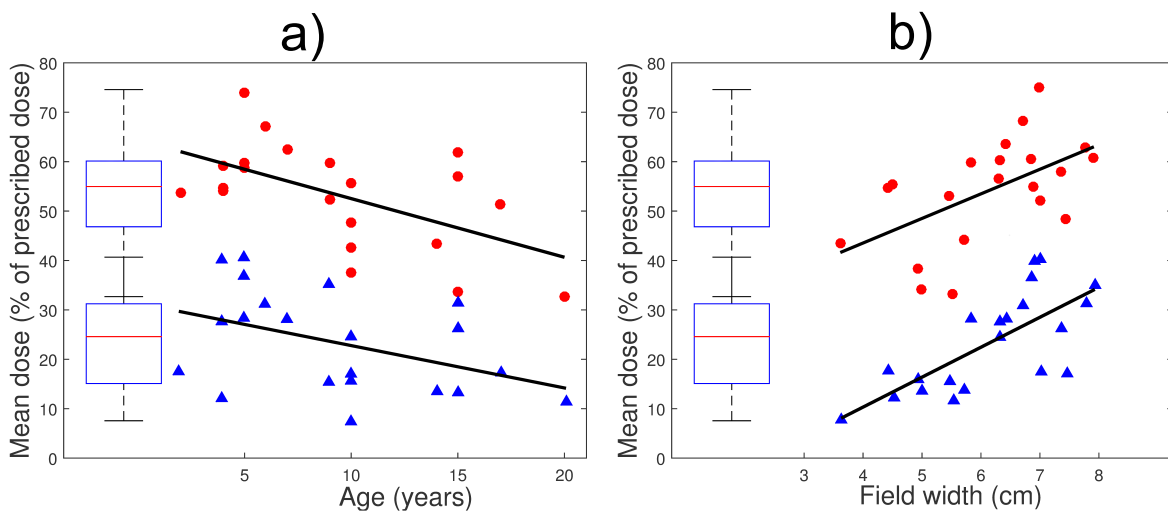
Figure 4.6: Multivariable linear regression models for mean heart (red circles) and lung (blue triangles) doses versus **a)** patient age at treatment and **b)** spinal field width with boxplots representing the mean heart and lung dose distribution for all 21 included pediatric patients given as mean, 25th – 75th percentile and range covering 99.3% of the data points (there are no outliers). Please note that the range of the boxplots overlap.

The models based on age and spinal field width showed excellent predictive performance (table 4.4) with almost 70% and 80% of the variance in mean heart and lung dose, respectively, explained by the model for Linac plans.

Table 4.4: The final multivariable linear regression models for mean heart and mean lung dose for both Linacs and ^{60}Co plans. Model performance is given by R^2 and RMSD for the leave-one-out (LOO) validation ($RMSD_{LOO}$).

Predictor variable Linac	β	95% CI
Mean heart dose ($R^2 = 0.70$, $RMSD_{LOO} = 6.7\%$)		
Age (y)	-1.37	(-1.95 , -0.78)
Field width (cm)	5.68	(3.17 , 8.18)
Constant	31.4	
Mean lungs dose ($R^2 = 0.79$, $RMSD_{LOO} = 5.2\%$)		
Age (y)	-1.05	(-1.51 , -0.59)
Field width (cm)	6.69	(4.73 , 8.64)
Constant	-7.90	
Predictor variable ^{60}Co	β	**95% CI**
Mean heart dose ($R^2 = 0.58$, $RMSD_{LOO} = 7.6\%$)		
Age (y)	-1.17	(-1.82 , -0.51)
Field width (cm)	5.85	(2.54 , 9.17)
Constant	34.4	
Mean lungs dose ($R^2 = 0.78$, $RMSD_{LOO} = 4.9\%$)		
Age (y)	-0.88	(-1.31 , -0.45)
Field width (cm)	7.64	(5.45 , 9.84)
Constant	-6.37	

Abbreviations: R^2 = The model's coefficient of determination, $RMSD_{LOO}$ = The root-mean-square deviation for the leave-one-out cross validation, β = Slope for the explanatory variable (regression coefficient), CI = Confidence interval, y = years

Further, the association between organ volume and mean heart and lung dose was investigated to demonstrate if age indeed performs as a surrogate variable for this association. Heart volume suggests to well predict mean heart dose ($R^2 = 50.5\%$ in univariable linear regression). Conversely, lung volume does not appear to function as a particularly good univariable predictor for mean lung dose ($R^2 = 5.6\%$) and it actually appears to be the combination of age and spinal field width ($R^2 = 78.9\%$) that provides a suitable surrogate measure for the proportion of lungs receiving incident irradiation. This measure was arbitrarily defined as the proportion receiving >10% of prescription dose for clarification, $R^2 = 98.8\%$). The LOO analysis performed demonstrates that the final models with age and spinal field width performs well and, when compared to the excluded patients, presents accurate estimates of heart and lung doses.

Together with laudable efforts of managing large databases with long-term follow-up of large pediatric cancer patient cohorts with data collected during several decades [162–168], these models will serve as effective means of retrospectively estimating heart and lung doses in pediatric patients treated with spinal irradiation in an era without 3D dose data from CT/TPS. Due to relatively large inter-patient variation in heart and lung dose, other prospective studies validating these derived models are warranted.

4.4 Unpublished data - LET and RBE

These preliminary findings are based on a small sample of only five patients, which is also the reason as to why statistical tests have been omitted. The figure samples shown in this section are all taken from the same patient, one included in all three studies (patient 12 in STUDY I, patient 8 in STUDY II and patient 1 in STUDY III) presented in this thesis.
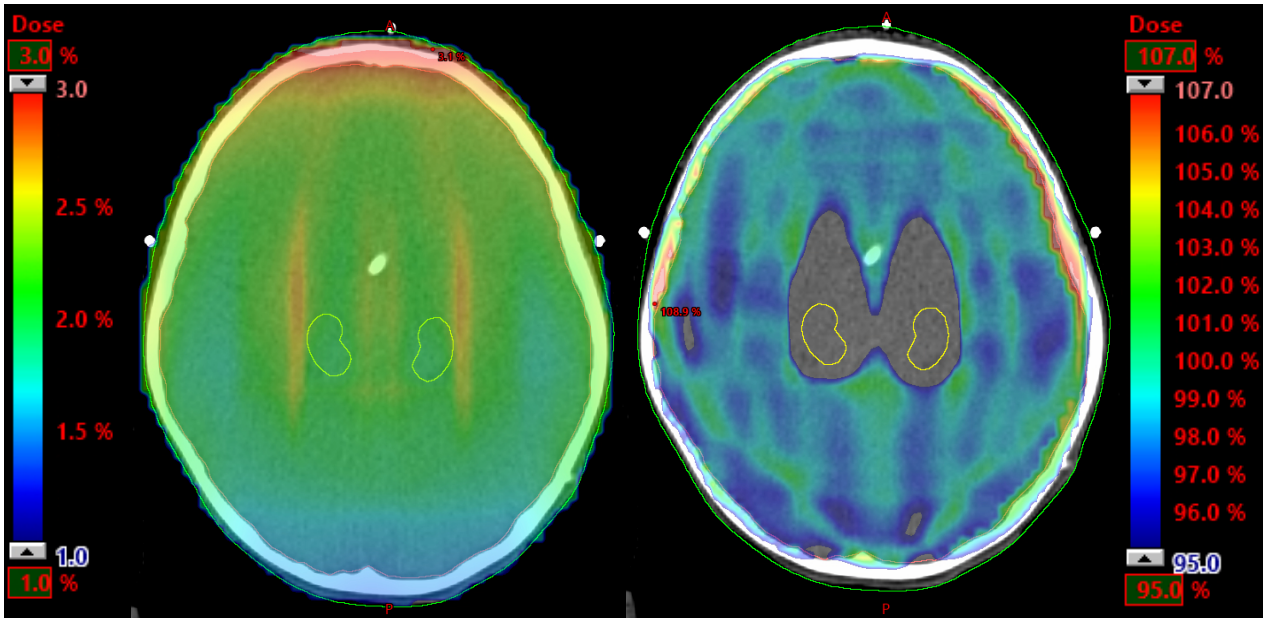

Figure 4.7: The dose averaged LET map (left) and RBE-weighted dose distribution (right) for a HS IMPT plan when using a tissue specific parameter of 10 to the whole brain (elective target), including the hippocampus. D_{max} = 112.8% of prescribed dose

The tissue specific parameters chosen in these examples were set to either 2 (healthy tissue) or 10 (tumor tissue). The considerable difference between figure 4.7 and 4.8 illustrates how the choice of tissue specific parameter impacts the resulting RBE-weighted dose distribution. RBE-weighted doses ranges from 90 – 140.3% of the prescribed dose (based on the first five patients) and are always higher for lower tissue specific parameters in accordance with measurements and other empirical models. The greatest increase in dose occurs in areas where the beam stops (Figure 4.8) with a beam setup of 0°, 90° and 270° in a head-first-supine position . Even though the LET tends to decrease as the number of fields increases this effect is negated with a smeared-out effect generally increasing the areas of higher RBE-weighted dose. This is, however, very dependent on the tissue specific parameters assigned. When assessing the effect of the dose averaged LET and RBE-weighted dose for a standard CSI plan (no dose constraint to the hippocampus) there were only minor changes to the dose distribution which should not be of any clinical concern. This suggest that the extra distal-edges of the beam mid target would constitute the parameters that have the largest impact on the RBE-weighted dose.

Similar effects are observed for the boost plans and here, the effect of tissue specific parameters is even more noticeable (Figure 4.9). There is a clear visible boundary between the tumor volume (α/β = 10) and the brainstem (α/β = 2).

When assigning the elective target (CTV$_{elective}$) a tissue specific parameter of 10 this means that the entire brain is assumed to be the target, which is current standard of practice. If this assumption was valid, there would not be any large deviations when LET is considered for standard CSI plans (Figure 4.10). There are only small differences and reassuringly, a recent study found no increase in CNS injury and no correlation with RBE from proton treatments compared to photon treatments [217]. Further verification studies of the models are necessary and these results should be compared with clinical data, similar to the analysis conducted by Peeler et al. [107]. They found a correlation between increased LET for pediatric ependymoma treatments and MRI

Figure 4.8: The dose averaged LET map (left) and RBE-weighted dose distribution (right) for a HS IMPT plan when using a tissue specific parameter of 10 to the whole brain (elective target), excluding the hippocampus which were assigned $\alpha/\beta = 2$. $D_{max} = 135.6\%$ of prescribed dose.

Figure 4.9: The dose averaged LET map (left) and RBE-weighted dose distribution (right) for a boost plan when using a tissue specific parameter of 10 to the tumor bed (boost target). The brainstem was assigned a tissue specific parameter of 2 (for late responding tissue). $D_{max} = 140.3\%$ of prescribed dose.

image changes post radiation indicating increased biological dose effectiveness. Such results may improve these phenomenological models, since verified reactions such as normal tissue damage to the brain can provide further insight regarding RBE knowledge.
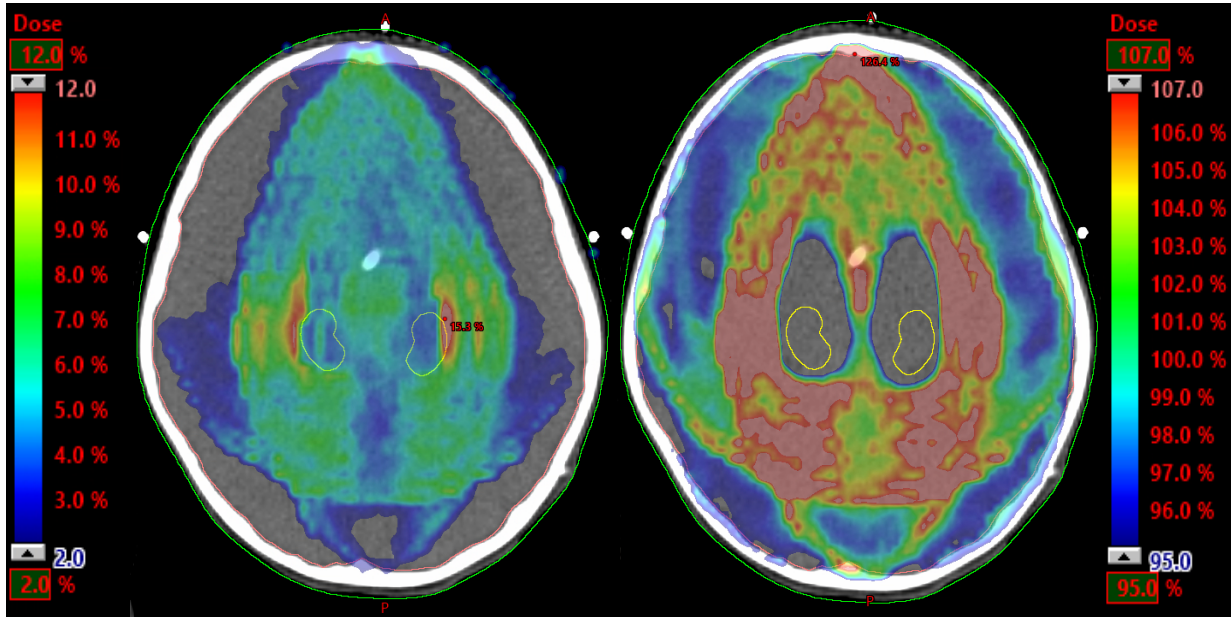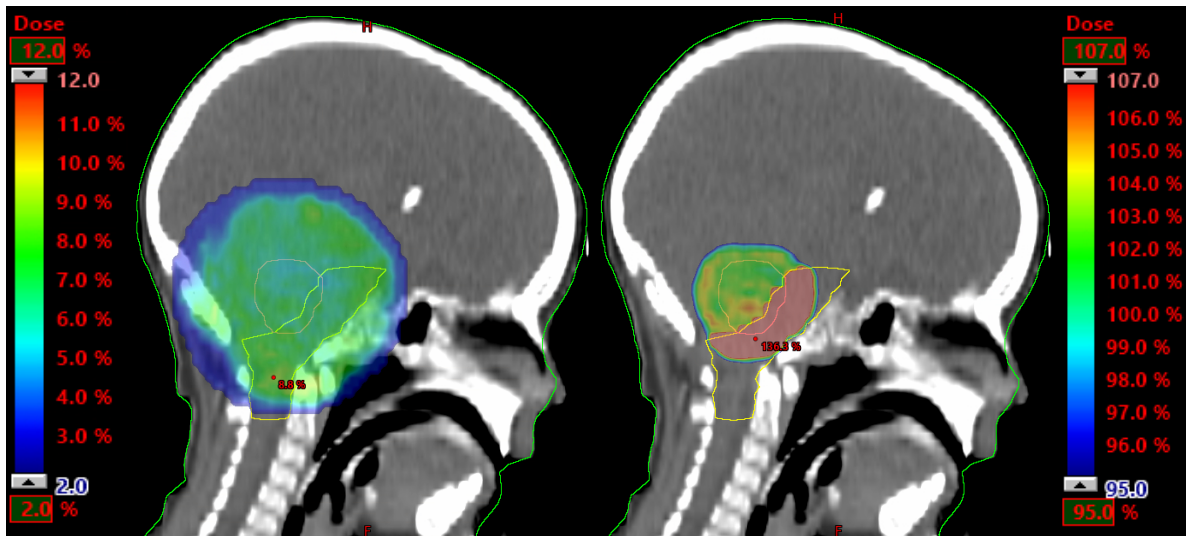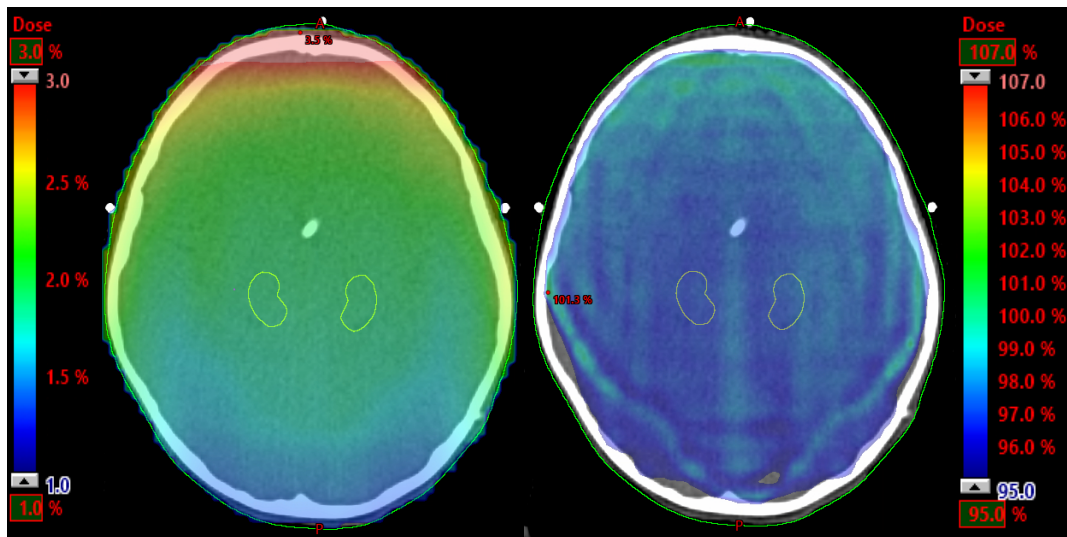
Figure 4.10: The dose averaged LET map (left) and RBE-weighted dose distribution (right) for the standard CSI-plan when using a tissue specific parameter of 10 to the whole brain (elective target), including the hippocampus. D_{max} = 104.1% of prescribed dose.

"Think it over, think it under"

— Winne the Pooh

5

Final remarks and outlook

This chapter provides an overview of the strengths and limitations of the studies in this thesis. It also gives a brief commentary of how these results could affect future treatments and studies.

5.1   Strengths and limitations

STUDY I

The ideal patient image registration in STUDY I is based on two different registration tools with automatic matching capabilities on bony anatomy with a manual tweak if needed. There are a vast number of algorithms and registration tools available for image matching and there is no attestation that the ones used here are ideal for craniospinal registration of CNS patients. Since the region of interest were set for each registration this could also affect the ability of the registration tools. The fact that this was a multicenter study provides some important generalizability to this study.

STUDY II

In STUDY II, models for both TCP and NTCP estimations were applied and these models are of course subject to limitations and uncertainties. The TCP model used is supported by new clinical data [191] although some assumptions had to be made due to missing patterns of failure data when updating the model parameters. The TCP model used is not stratified based on different molecular subgroups or patient's performance status and represents standard-risk MB. The largest limitation in the NTCP models used to estimate neurocognitive impairment are the odds ratio estimates taken from Armstrong et al. [146]. Despite these limitations the results presented in this study are put into a more clinical context since instead of only presenting doses to the tumor and OARs, estimates of the risk of cognitive impairment are demonstrated together with estimates of the tumor control probability.

STUDY III

When developing mathematical models to help facilitate retrospective studies (as in STUDY III) there will generally be a difference between the models depending on where they were created. Meaning that the patient data, from which the models are derived, can be substantially different depending on patient fixations and dose planning strategies as well as the number of patients in the study. Therefore, validation of models like the ones presented here are always warranted, preferably by prospective studies. Even though 24 pediatric CNS patients

generally might be considered as an appropriate number of patients in this setting, it is still a very limited number of patients. One of the key advantages is the comparison to both older types of calculation algorithms and treatment units. Many of the patients in a large cohort followed for decades have very likely been treated with machines not easily available today, thus rendering many models created on modern algorithms and linear accelerators less accurate.

Unpublished data

There are several models for calculating the LET- and RBE-weighted doses, each resulting in different dose distributions [211]. This conclusion highlights uncertainties related to this field of study and gives rise to questions regarding which one should be utilized and why. The model utilized for the unpublished data [106, 200–203] in this thesis does in no way provides worst-case scenarios [211]. To be able to calculate the dose averaged LET, the included fields in the plan must be without a range shifter. This can in many ways affect the plan quality of the original plan, especially for shallow reaching targets. There are however large uncertainties due to tissue specific parameters related to this. Other, limitations related to these uncertainties are additionally problematic in this setting considering whether the hippocampus should be defined as part of the target or as an OAR. The use of RBE-weighted dose distributions could, furthermore, be influenced by the indication that some CNS tumors might have a higher tissue specific parameter than previously considered, e.g. different MB cell lines measured in vitro having α/β-values ranging from 14 – 82 Gy [218], which is far greater than the general assumption of using α/β=10 for tumor tissue. Encouragingly, a recent study found no increase in CNS injury and no correlation with RBE from proton treatment for MB compared to photon treatments [217]. However, Peeler et al. [107] found a correlation between increased LET and post treatment MRI-verified soft tissue changes indicating that there could be an increased biological dose effectiveness.

5.2   Improved quality of life for pediatric patients with CNS malignancies?

As many of the children surviving their CNS treatment suffer from late side effects [75, 76, 146–149] great steps should be taken to improve sparing the OARs from incident radiation.

There are multiple studies that have reported a relationship between ionizing radiation dose to the brain and cognitive impairment for pediatric patients [146, 172–175]. Undoubtedly, higher prescription doses, delivered to OARs including the hippocampus, causes neurocognitive impairment [216, 219, 220] that can affect quality of life [127, 221]. Since many of the pediatric patients are long-term survivors this indicates the importance of these types of studies for improving quality of life [126].

It is important to keep in mind that the hippocampus is, apart from OAR, a target as it contains cerebrospinal fluid and reduced dose might carry an increased risk of recurrences. Therefore, the primary priority of HS-CSI is still tumor control and it might not be appropriate to spare the hippocampus for high-risk MB [222] or other types of high-risk CNS diagnoses. Since a considerable amount of the brain volume is being irradiated to an excess of 54 Gy/Gy$_{RBE}$ a recurrence would likely be fatal as there are limited salvage options after receiving full dose CSI [223].

Given that one of the most common causes of death among pediatric cancer survivors is cardiovascular disease [151] and that other potentially fatal, side effects include pulmonary fibrosis, acute pulmonary toxicity and restrictive lung disease [158–160] the heart and lungs are important OARs that should, be avoided. Retrospective studies of long-term follow-up data can improve the dose-response and tolerance knowledge of these organs.

5.3   Commentary

This thesis could impact clinical practice of the CSI treatments at Rigshospitalet in several ways. For example, the PTV margins being utilized today could be compared and/or validated to the margins calculated in STUDY I. In addition, aims 2 and 4 provided valuable insight into the benefits of hippocampal-sparing CSI and the effects of the complexities around LET- and RBE-based dose calculation. The next step for establishing the benefits

estimated in STUDY II would be a prospective clinical trial of HS CSI for pediatric CNS patients. However, some of the findings reported in this thesis and other similar *in silico* studies should be verified first. We hope that the results presented in this thesis are able to inspire and inform such a clinical trial.

"Think, think, think"

— Winne the Pooh

6
Conclusion

The work conducted and results presented in this thesis show that there are further possibilities of minimizing side effects to pediatric CNS patients treated with CSI.

Daily IGRT substantially reduces setup uncertainties for pediatric CSI patients and should be the preferred choice of imaging protocol if possible, especially when all cardinal directions are available for corrections based on the pre-treatment verification images (**aim 1**). There are situations were a daily IGRT does not guarantee satisfactory alignment and thus should elicit a re-positioning of the patients to ensure accurate alignment throughout the patients' course of radiotherapy. For treatment centers that are unable to perform IGRT this thesis (STUDY I) present results that could improve and facilitate margin and uncertainty calculations to improve the treatment accuracy. The results could also be used to improve robust optimization perturbations at IMPT centers where PTV margins are uncommon. With the help of margin calculation formulas, personalized margins could help improve late adverse effects e.g. by using correct margins in the anteroposterior directions to minimize incident radiation to the heart and lungs, particularly if doses linked to long-term follow up toxicity could be applied (**aim 3**). The models developed in STUDY III could also facilitate linking organ dose to late toxicity which in turn could aid in the clinical decision making and could help identify patients in need of closer post-treatment surveillance for late adverse events.

With improved perturbations for IMPT robust optimization it is possible to e.g. estimate the clinical benefit in neurocognitive impairment by sparing the hippocampus with added accuracy. According to STUDY II, it is possible to reduce the risk of cognitive impairment from roughly 90%, 60% and 50% to 50%, 40% and 20% for task efficiency, organization and memory impairment, respectively (**aim 2**). This considerable reduction in neurocognitive adverse effects is possible with only a minimal compromise of the target coverage while maintaining, tumor control.

When calculating the RBE-weighted dose distribution for proton beams from dose averaged LET there is an evident difference compared to the dose distribution calculated by the TPS, demonstrated by the unpublished data (**aim 4**). However, additional studies investigating the role and values of tissue specific parameters and how to define certain organs are warranted before these strategies would be clinically applicable.

Considering all evidence, it seems feasible to reduce side effects, e.g. by preserving hippocampus functions based on accurate margins, for pediatric CNS patients treated with CSI with a maintained tumor control.

7

Denouement and future perspectives

In this thesis we have focused on techniques and models that could potentially minimize side effects substantially, particularly neurocognitive impairment. The treatment for medulloblastoma and other types of malignant CNS tumors is rather aggressive, and the current multimodality treatment yields a 5-year progression free survival of 75-80% for standard-risk patients [224]. Most children therefore survive to adulthood [72] and side effects should thus be minimized since longer survival is associated with long-term morbidity and mortality [152, 170]. Proton therapy conveys the impression of being very suitable for pediatric CSI [30–32, 225], however, there are still some ambiguity regarding variable RBE modeling [226, 227] especially regarding clinical implementation of radiobiological optimization for proton therapy treatment planning and the supporting clinical data which need further investigation [228, 229]. Many of the RBE models could also be used for treatment plan evaluation in their present form, however, this is very time consuming and they require compability improvements to many of the existing TPSs for this to become a feasible alternative. Additionally, the hippocampus needs detailed and comprehensive investigations in order to evaluate appropriate tissue specific parameters. Verification studies of the phenomenological models are warranted and the results from these studies should be compared with clinical data similar to the analysis conducted by Peeler et al. [107]. Such results may improve these phenomenological models, since MRI-verified reactions such as normal tissue damage to the brain can provide further insight into the RBE knowledge.

The models demonstrated in this thesis [169] and used for retrospectively analyzing heart and lung doses warrant validation before using them for linking organ doses to late toxicity for analyzing side effects with documented long-term follow-up. Similar models could also be developed, but instead of using the standardized method of mean doses, they would rely on voxel-based dose calculations which take into account the spatial dose distribution and the impact of dose heterogeneities (see Related publications not included in this thesis). The dose is very rarely uniform across any organ and therefore, it is likely difficult to develop acceptable models of the response of an organ based solely on the mean dose.

There are studies that have shown the benefits and advantages of protons for pediatric CSI treatments [29, 32, 230] and the expected reduction in life years lost as a result [231] and it is therefore considered a promising alternative for pediatric patients [232]. However, additional clinical evidence is needed as the current evidence is scarce due to small cohorts and short follow-up [233]. Prediction models based on the risk of neurocognitive impairment data from STUDY II at certain doses to the hippocampus could be developed to anticipate individual risks, pretreatment, to facilitate treatment plan evaluation for pediatric patients considered for a HS treatment. Furtheremore, refined versions of such models might be capable of treatment plan optimizations based on these risks and future versions might also be able to employ RBE-weighted dose optimizations. Systems developed for assessing plan robustness and dosimetric accuracy for HS IMPT could perform as a type of pretreatment

quality assurance.

No clinical trials of hippocampal sparing in children with CNS tumors have been undertaken but part of the aim of this thesis is to provide preliminary data to prepare for a possible clinical trial. The most compelling evidences to date comes from the randomized phase III trial NRG Oncology CC001 that showed significantly lower risk of cognitive impairment for hippocampal-sparing whole-brain irradiation for adult patients [144]. The hippocampus doses determined in this thesis require verification from dosimetric experiments. Subsequently, a well-designed clinical trial of sparing the hippocampus in pediatric CSI patients may commence.

Bibliography

[1] G. Delaney, S. Jacob, C. Featherstone, and M. Barton, "The role of radiotherapy in cancer treatment: estimating optimal utilization from a review of evidence-based clinical guidelines," *Cancer: Interdisciplinary International Journal of the American Cancer Society*, vol. 104, no. 6, pp. 1129–1137, 2005. 5

[2] R. Serre, S. Benzekry, L. Padovani, C. Meille, N. André, J. Ciccolini, F. Barlesi, X. Muracciole, and D. Barbolosi, "Mathematical modeling of cancer immunotherapy and its synergy with radiotherapy," *Cancer research*, vol. 76, no. 17, pp. 4931–4940, 2016. 5

[3] N. C. Daw and A. Mahajan, "Photons or Protons for Non-Central Nervous System Solid Malignancies in Children: A Historical Perspective and Important Highlights," *American Society of Clinical Oncology Educational Book*, vol. 33, no. 1, pp. e354–e359, 2013. 5

[4] R. R. Wilson, "Radiological use of fast protons," *Radiology*, vol. 47, no. 5, pp. 487–491, 1946. 5, 6

[5] J. S. Welsh, R. R. Patel, M. A. Ritter, P. M. Harari, T. R. Mackie, and M. P. Mehta, "Helical tomotherapy: an innovative technology and approach to radiation therapy," *Technology in cancer research & treatment*, vol. 1, no. 4, pp. 311–316, 2002. 5

[6] K. L. Baglan, M. B. Sharpe, D. Jaffray, R. C. Frazier, J. Fayad, L. L. Kestin, V. Remouchamps, A. A. Martinez, J. Wong, and F. A. Vicini, "Accelerated partial breast irradiation using 3D conformal radiation therapy (3D-CRT)," *International Journal of Radiation Oncology* Biology* Physics*, vol. 55, no. 2, pp. 302–311, 2003. 6

[7] A. Brahme, J.-E. Roos, and I. Lax, "Solution of an integral equation encountered in rotation therapy," *Physics in Medicine & Biology*, vol. 27, no. 10, p. 1221, 1982. 6

[8] T. Gupta, J. Agarwal, S. Jain, R. Phurailatpam, S. Kannan, S. Ghosh-Laskar, V. Murthy, A. Budrukkar, K. Dinshaw, K. Prabhash, *et al.*, "Three-dimensional conformal radiotherapy (3D-CRT) versus intensity modulated radiation therapy (IMRT) in squamous cell carcinoma of the head and neck: a randomized controlled trial," *Radiotherapy and Oncology*, vol. 104, no. 3, pp. 343–348, 2012. 6

[9] E. J. Hall and C.-S. Wuu, "Radiation-induced second cancers: the impact of 3D-CRT and IMRT," *International Journal of Radiation Oncology* Biology* Physics*, vol. 56, no. 1, pp. 83–88, 2003.

[10] D. Followill, P. Geis, and A. Boyer, "Estimates of whole-body dose equivalent produced by beam intensity modulated conformal therapy.," *International journal of radiation oncology* biology* physics*, vol. 38, no. 3, pp. 667–672, 1997. 6

[11] K. Otto, "Volumetric modulated arc therapy: IMRT in a single gantry arc," *Medical physics*, vol. 35, no. 1, pp. 310–317, 2008. 6

[12] T. R. Mackie, J. Balog, K. Ruchala, D. Shepard, S. Aldridge, E. Fitchard, P. Reckwerdt, G. Olivera, T. McNutt, and M. Mehta, "Tomotherapy," in *Seminars in Radiation Oncology*, vol. 9, pp. 108–117, WB SAUNDERS COMPANY, 1999. 6

[13] B. Healy, D. van der Merwe, K. Christaki, and A. Meghzifene, "Cobalt-60 machines and medical linear accelerators: competing technologies for external beam radiotherapy," *Clinical Oncology*, vol. 29, no. 2, pp. 110–115, 2017. 6

[14] B. Lambert and J. Martin, "Sterilization of implants and devices," in *Biomaterials Science*, pp. 1339–1353, Elsevier, 2013. 6

[15] B. Caballero, L. C. Trugo, and P. M. Finglas, *Encyclopedia of food sciences and nutrition*. Academic, 2003. 6

[16] A. Wu, G. Lindner, A. Maitz, A. Kalend, L. Lunsford, J. Flickinger, and W. Bloomer, "Physics of gamma knife approach on convergent beams in stereotactic radiosurgery," *International Journal of Radiation Oncology* Biology* Physics*, vol. 18, no. 4, pp. 941–949, 1990. 6

[17] C. Lindquist, L. Kihlström, and E. Hellstrand, "Functional neurosurgery-a future for the gamma knife?," *Stereotactic and functional neurosurgery*, vol. 57, no. 1-2, pp. 72–81, 1991. 6

[18] C. Tobias, J. Lawrence, J. Born, R. McCombs, J. Roberts, H. Anger, B. Low-Beer, and C. Huggins, "Pituitary irradiation with high-energy proton beams a preliminary report," *Cancer research*, vol. 18, no. 2, pp. 121–134, 1958. 6, 7

[19] M. Jermann, "Particle therapy statistics in 2014," *International Journal of Particle Therapy*, vol. 2, no. 1, pp. 50–54, 2015. 6

[20] J. M. Slater, J. O. Archambeau, D. W. Miller, M. I. Notarus, W. Preston, and J. D. Slater, "The proton treatment center at loma linda university medical center: rationale for and description of its development," *International Journal of Radiation Oncology* Biology* Physics*, vol. 22, no. 2, pp. 383–389, 1992. 7

[21] W. D. Newhauser and R. Zhang, "The physics of proton therapy," *Physics in Medicine & Biology*, vol. 60, no. 8, p. R155, 2015. 7

[22] M. Goitein and M. Jermann, "The relative costs of proton and X-ray radiation therapy," *Clinical Oncology*, vol. 15, no. 1, pp. S37–S50, 2003. 7

[23] J. Sisterson, "World wide proton therapy experience in 1997," in AIP C*onference* P*roceedings*, vol. 475, pp. 959–962, American Institute of Physics, 1999. 7

[24] P. Goethals and R. Zimmerman, "Proton Therapy World Market Report," vol. May, pp. 1–250, MEDrays intell, 2015. 7

[25] "PTCOG: Particle therapy co-operative group website." Available online from https://www.ptcog.ch/, last accessed 2020-04-05. 7

[26] W. H. Bragg and R. Kleeman, "XXXIX. on the α particles of radium, and their loss of range in passing through various atoms and molecules," *The London, Edinburgh, and Dublin Philosophical Magazine and Journal of Science*, vol. 10, no. 57, pp. 318–340, 1905. 7

[27] D. Jette and W. Chen, "Creating a spread-out Bragg peak in proton beams," *Physics in Medicine & Biology*, vol. 56, no. 11, p. N131, 2011. 7

[28] H.-M. Lu and H. Kooy, "Optimization of current modulation function for proton spread-out bragg peak fields," *Medical physics*, vol. 33, no. 5, pp. 1281–1287, 2006. 7

[29] W. S. Clair, J. Adams, M. Bues, B. Fullerton, S. La Shell, H. Kooy, J. Loeffler, and N. Tarbell, "Advantage of protons compared to conventional X-ray or IMRT in the treatment of a pediatric patient with medulloblastoma," *International Journal of Radiation Oncology* Biology* Physics*, vol. 58, no. 3, pp. 727–734, 2004. 7, 14, 41

[30] G. E. Yuh, L. N. Loredo, L. T. Yonemoto, D. A. Bush, K. Shahnazi, W. Preston, J. M. Slater, and J. D. Slater, "Reducing toxicity from craniospinal irradiation: using proton beams to treat medulloblastoma in young children," *The Cancer Journal*, vol. 10, no. 6, pp. 386–390, 2004. 41

[31] M. Yoon, D. H. Shin, J. Kim, J. W. Kim, D. W. Kim, S. Y. Park, S. B. Lee, J. Y. Kim, H.-J. Park, B. Park, *et al.*, "Craniospinal irradiation techniques: a dosimetric comparison of proton beams with standard and advanced photon radiotherapy," *International Journal of Radiation Oncology* Biology* Physics*, vol. 81, no. 3, pp. 637–646, 2011. 7

[32] R. Miralbell, A. Lomax, L. Cella, and U. Schneider, "Potential reduction of the incidence of radiation-induced second cancers by using proton beams in the treatment of pediatric tumors," *International Journal of Radiation Oncology* Biology* Physics*, vol. 54, no. 3, pp. 824–829, 2002. 7, 41

[33] R. Epstein, I. Hanham, and R. Dale, "Radiotherapy-induced second cancers: are we doing enough to protect young patients?," *European Journal of Cancer*, vol. 33, no. 4, pp. 526–530, 1997.

[34] U. Schneider, A. Lomax, and B. Timmermann, "Second cancers in children treated with modern radiotherapy techniques," *Radiotherapy and Oncology*, vol. 89, no. 2, pp. 135–140, 2008. 9

[35] M. Yoon, S. H. Ahn, J. Kim, D. H. Shin, S. Y. Park, S. B. Lee, K. H. Shin, and K. H. Cho, "Radiation-induced cancers from modern radiotherapy techniques: intensity-modulated radiotherapy versus proton therapy," *International Journal of Radiation Oncology* Biology* Physics*, vol. 77, no. 5, pp. 1477–1485, 2010.

[36] M. Xiang, D. T. Chang, and E. L. Pollom, "Second cancer risk after primary cancer treatment with three-dimensional conformal, intensity-modulated, or proton beam radiation therapy," *Cancer*, 2020. 7

[37] T. A. van de Water, A. J. Lomax, H. P. Bijl, M. E. de Jong, C. Schilstra, E. B. Hug, and J. A. Langendijk, "Potential benefits of scanned intensity-modulated proton therapy versus advanced photon therapy with regard to sparing of the salivary glands in oropharyngeal cancer," *International Journal of Radiation Oncology* Biology* Physics*, vol. 79, no. 4, pp. 1216–1224, 2011. 7

[38] D. E. Hyer, P. M. Hill, D. Wang, B. R. Smith, and R. T. Flynn, "Effects of spot size and spot spacing on lateral penumbra reduction when using a dynamic collimation system for spot scanning proton therapy," *Physics in Medicine & Biology*, vol. 59, no. 22, p. N187, 2014. 7

[39] A. Lomax, "Intensity modulated proton therapy and its sensitivity to treatment uncertainties 2: the potential effects of inter-fraction and inter-field motions," *Physics in Medicine & Biology*, vol. 53, no. 4, p. 1043, 2008. 7, 9

[40] A. J. Lomax, E. Pedroni, H. P. Rutz, and G. Goitein, "The clinical potential of intensity modulated proton therapy," *Zeitschrift für Medizinische Physik*, vol. 14, no. 3, pp. 147–152, 2004. 7

[41] D. Belli, P. Bettega, F. Calzolari, R. Cera, M. Cherubini, M. Dalla Vecchia, S. Durante, G. Favaretto, G. Gialanella, and M. Grossi, "Inactivation of human normal and tumour cells irradiated with low energy protons," *International journal of radiation biology*, vol. 76, no. 6, pp. 831–839, 2000. 7, 11

[42] R. A. Britten, V. Nazaryan, L. K. Davis, S. B. Klein, D. Nichiporov, M. S. Mendonca, M. Wolanski, X. Nie, J. George, and C. Keppel, "Variations in the RBE for cell killing along the depth-dose profile of a modulated proton therapy beam," *Radiation research*, vol. 179, no. 1, pp. 21–28, 2013.

[43] M. Aoki-Nakano, Y. Furusawa, A. Uzawa, Y. Matsumoto, R. Hirayama, C. Tsuruoka, T. Ogino, T. Nishio, K. Kagawa, M. Murakami, *et al.*, "Relative biological effectiveness of therapeutic proton beams for HSG cells at japanese proton therapy facilities," *Journal of radiation research*, vol. 55, no. 4, pp. 812–815, 2014. 7, 11

[44] M. Van Herk, "Errors and margins in radiotherapy," in *Seminars in radiation oncology*, vol. 14, pp. 52–64, Elsevier, 2004. 7, 18

[45] ICRU-50, "Prescribing, recording and reporting photon beam therapy," in *International Comission on Radiation Units and Measurements*, Oxford University Press, 1993. 7

[46] ICRU-62, "Prescribing, recording and reporting photon beam therapy (supplement to ICRU report 50)," in *International Comission on Radiation Units and Measurements*, Oxford University Press, 1999.

[47] ICRU-78, "Prescribing, recording and reporting proton-beam therapy," in *International Comission on Radiation Units and Measurements*, Oxford University Press, 2007. 7, 11

[48] M. Engelsman, M. Schwarz, and L. Dong, "Physics controversies in proton therapy," in *Seminars in radiation oncology*, vol. 23, pp. 88–96, Elsevier, 2013. 9

[49] J. Unkelbach, T. C. Chan, and T. Bortfeld, "Accounting for range uncertainties in the optimization of intensity modulated proton therapy," *Physics in Medicine & Biology*, vol. 52, no. 10, p. 2755, 2007. 9

[50] W. Liu, X. Zhang, Y. Li, and R. Mohan, "Robust optimization of intensity modulated proton therapy," *Medical physics*, vol. 39, no. 2, pp. 1079–1091, 2012. 9

[51] A. Lomax, "Intensity modulated proton therapy and its sensitivity to treatment uncertainties 1: the potential effects of calculational uncertainties," *Physics in Medicine & Biology*, vol. 53, no. 4, p. 1027, 2008. 9

[52] P. C. Park, J. P. Cheung, X. R. Zhu, A. K. Lee, N. Sahoo, S. L. Tucker, W. Liu, H. Li, R. Mohan, L. E. Court, *et al.*, "Statistical assessment of proton treatment plans under setup and range uncertainties," *International Journal of Radiation Oncology* Biology* Physics*, vol. 86, no. 5, pp. 1007–1013, 2013.

[53] D. Pflugfelder, J. Wilkens, and U. Oelfke, "Worst case optimization: a method to account for uncertainties in the optimization of intensity modulated proton therapy," *Physics in Medicine & Biology*, vol. 53, no. 6, p. 1689, 2008. 9

[54] G. N. Hounsfield, "Computerized transverse axial scanning (tomography): Part 1. Description of system," *The British journal of radiology*, vol. 46, no. 552, pp. 1016–1022, 1973. 9

[55] J. Ambrose, "Computerized transverse axial scanning (tomography): Part 2. Clinical application," *The British journal of radiology*, vol. 46, no. 552, pp. 1023–1047, 1973. 9

[56] L. J. Verhey, M. Goitein, P. McNulty, J. E. Munzenrider, and H. D. Suit, "Precise positioning of patients for radiation therapy," *International Journal of Radiation Oncology* Biology* Physics*, vol. 8, no. 2, pp. 289–294, 1982. 9

[57] D. Verellen, M. De Ridder, N. Linthout, K. Tournel, G. Soete, and G. Storme, "Innovations in image-guided radiotherapy," *Nature Reviews Cancer*, vol. 7, no. 12, pp. 949–960, 2007. 9

[58] L. A. Dawson and M. B. Sharpe, "Image-guided radiotherapy: rationale, benefits, and limitations," *The lancet oncology*, vol. 7, no. 10, pp. 848–858, 2006.

[59] D. Jaffray, P. Kupelian, T. Djemil, and R. M. Macklis, "Review of image-guided radiation therapy," *Expert review of anticancer therapy*, vol. 7, no. 1, pp. 89–103, 2007.

[60] D. Verellen, M. De Ridder, and G. Storme, "A (short) history of image-guided radiotherapy," *Radiotherapy and Oncology*, vol. 86, no. 1, pp. 4–13, 2008.

[61] A. Bujold, T. Craig, D. Jaffray, and L. A. Dawson, "Image-guided radiotherapy: has it influenced patient outcomes?," in *Seminars in Radiation Oncology*, vol. 22, pp. 50–61, Elsevier, 2012.

[62] J. L. Guerra, I. Marrone, J. Jaen, M. Bruna, C. Sole, A. Sanchez-Reyes, E. Rivin, M. Ortiz, F. Calvo, and R. Matute, "Outcome and toxicity using helical tomotherapy for craniospinal irradiation in pediatric medulloblastoma," *Clinical and Translational Oncology*, vol. 16, no. 1, pp. 96–101, 2014. 9

[63] K. A. Langmack, "Portal imaging," *The British journal of radiology*, vol. 74, no. 885, pp. 789–804, 2001. 9

[64] C. Huntzinger, P. Munro, S. Johnson, M. Miettinen, C. Zankowski, G. Ahlstrom, R. Glettig, R. Filliberti, W. Kaissl, M. Kamber, *et al.*, "Dynamic targeting image-guided radiotherapy," *Medical Dosimetry*, vol. 31, no. 2, pp. 113–125, 2006. 9

[65] D. A. Jaffray, K. Chawla, C. Yu, and J. W. Wong, "Dual-beam imaging for online verification of radiotherapy field placement," *International Journal of Radiation Oncology* Biology* Physics*, vol. 33, no. 5, pp. 1273–1280, 1995. 9

[66] D. A. Jaffray, J. H. Siewerdsen, J. W. Wong, and A. A. Martinez, "Flat-panel cone-beam computed tomography for image-guided radiation therapy," *International Journal of Radiation Oncology* Biology* Physics*, vol. 53, no. 5, pp. 1337–1349, 2002. 9

[67] I. S. Grills, G. Hugo, L. L. Kestin, A. P. Galerani, K. K. Chao, J. Wloch, and D. Yan, "Image-guided radiotherapy via daily online cone-beam CT substantially reduces margin requirements for stereotactic lung radiotherapy," *International Journal of Radiation Oncology* Biology* Physics*, vol. 70, no. 4, pp. 1045–1056, 2008. 9

[68] K. Ruchala, G. Olivera, E. Schloesser, and T. Mackie, "Megavoltage CT on a tomotherapy system," *Physics in Medicine & Biology*, vol. 44, no. 10, p. 2597, 1999. 9

[69] R. Mohan and D. Grosshans, "Proton therapy - present and future," *Advanced drug delivery reviews*, vol. 109, pp. 26–44, 2017. 9

[70] S. M. Bentzen, L. S. Constine, J. O. Deasy, A. Eisbruch, A. Jackson, L. B. Marks, R. K. Ten Haken, and E. D. Yorke, "Quantitative Analyses of Normal Tissue Effects in the Clinic (QUANTEC): an introduction to the scientific issues," *International Journal of Radiation Oncology* Biology* Physics*, vol. 76, no. 3, pp. S3–S9, 2010. 9, 10, 11

[71] B. Emami, "Tolerance of normal tissue to therapeutic radiation," *Reports of radiotherapy and Oncology*, vol. 1, no. 1, 2013. 9, 11, 22

[72] H. Curry, S. Parkes, J. Powell, and J. Mann, "Caring for survivors of childhood cancers: the size of the problem," *European Journal of Cancer*, vol. 42, no. 4, pp. 501–508, 2006. 9, 15, 41

[73] A. P. Panandiker, H. Ning, A. Likhacheva, K. Ullman, B. Arora, J. Ondos, S. Karimpour, R. Packer, R. Miller, and D. Citrin, "Craniospinal irradiation with spinal IMRT to improve target homogeneity," *International Journal of Radiation Oncology* Biology* Physics*, vol. 68, no. 5, pp. 1402–1409, 2007. 14

[74] *Health risks from exposure to low levels of ionizing radiation:* BEIR VII *phase 2*, vol. 7. National Academies Press, 2006. National Research Council and others, ISBN: 978-0-309-09156-5, https://doi.org/10.17226/11340.

[75] D. A. Mulrooney, M. W. Yeazel, T. Kawashima, A. C. Mertens, P. Mitby, M. Stovall, S. S. Donaldson, D. M. Green, C. A. Sklar, L. L. Robison, *et al.*, "Cardiac outcomes in a cohort of adult survivors of childhood and adolescent cancer: retrospective analysis of the Childhood Cancer Survivor Study cohort," *Bmj*, vol. 339, p. b4606, 2009. 10, 14, 36

[76] D. L. Friedman, J. Whitton, W. Leisenring, A. C. Mertens, S. Hammond, M. Stovall, S. S. Donaldson, A. T. Meadows, L. L. Robison, and J. P. Neglia, "Subsequent neoplasms in 5-year survivors of childhood cancer: the Childhood Cancer Survivor Study," *JNCI: Journal of the National Cancer Institute*, vol. 102, no. 14, pp. 1083–1095, 2010. 14, 36

[77] A. C. Mertens, Q. Liu, J. P. Neglia, K. Wasilewski, W. Leisenring, G. T. Armstrong, L. L. Robison, and Y. Yasui, "Cause-specific late mortality among 5-year survivors of childhood cancer: the Childhood Cancer Survivor Study," *Journal of the National Cancer Institute*, vol. 100, no. 19, pp. 1368–1379, 2008. 9

[78] E. J. Hall and A. J. Giaccia, *Radiobiology for the Radiologist*, vol. 6. Lippincott Williams & Wilkins, 2006. 9, 11

[79] R. A. Woo, M. T. Jack, Y. Xu, S. Burma, D. J. Chen, and P. W. Lee, "DNA damage-induced apoptosis requires the DNA-dependent protein kinase, and is mediated by the latent population of p53," *The EMBO journal*, vol. 21, no. 12, pp. 3000–3008, 2002. 9

[80] U. Schneider, S. Agosteo, E. Pedroni, and J. Besserer, "Secondary neutron dose during proton therapy using spot scanning," *International Journal of Radiation Oncology* Biology* Physics*, vol. 53, no. 1, pp. 244–251, 2002. 9

[81] J. Valentin *et al.*, *The 2007 recommendations of the international commission on radiological protection - Publication 103*, vol. 37. Elsevier Oxford, 2007. 9

[82] E. J. Hall, "Intensity-modulated radiation therapy, protons, and the risk of second cancers," *International Journal of Radiation Oncology* Biology* Physics*, vol. 65, no. 1, pp. 1–7, 2006. 9

[83] D. J. Brenner and E. J. Hall, "Secondary neutrons in clinical proton radiotherapy: a charged issue," *Radiotherapy and Oncology*, vol. 86, no. 2, pp. 165–170, 2008. 9

[84] B. Emami, J. Lyman, A. Brown, L. Cola, M. Goitein, J. Munzenrider, B. Shank, L. Solin, and M. Wesson, "Tolerance of normal tissue to therapeutic irradiation," *International Journal of Radiation Oncology* Biology* Physics*, vol. 21, no. 1, pp. 109–122, 1991. 10, 11

[85] C. Burman, G. Kutcher, B. Emami, and M. Goitein, "Fitting of normal tissue tolerance data to an analytic function," *International Journal of Radiation Oncology* Biology* Physics*, vol. 21, no. 1, pp. 123–135, 1991. 10, 11

[86] H. Holthusen, "Erfahrungen über die Verträglichkeitsgrenze für Röntgenstrahlen und deren Nutzanwendung zur Verhütung von Schäden," *Strahlentherapie*, vol. 57, pp. 254–269, 1936.

[87] L. Cohen, "The tissue volume factor in radiation oncology," *International Journal of Radiation Oncology* Biology* Physics*, vol. 8, no. 10, pp. 1771–1774, 1982. 10

[88] T. E. Schultheiss, C. G. Orton, and R. Peck, "Models in radiotherapy: volume effects," *Medical physics*, vol. 10, no. 4, pp. 410–415, 1983.

[89] H. R. Withers, J. M. Taylor, and B. Maciejewski, "Treatment volume and tissue tolerance," *International Journal of Radiation Oncology* Biology* Physics*, vol. 14, no. 4, pp. 751–759, 1988. 10

[90] P. Källman, A. Ågren, and A. Brahme, "Tumour and normal tissue responses to fractionated non-uniform dose delivery," *International journal of radiation biology*, vol. 62, no. 2, pp. 249–262, 1992. 10

[91] M. C. Joiner, A. Van der Kogel, M. Baumann, A. C. Begg, S. M. Bentzen, W. Dörr, V. Grégoire, K. Haustermans, M. R. Horsman, M. Koritzinsky, J. Lee, J. Overgaard, G. G. Steel, F. A. Stewart, K. R. Trott, B. G. Wouters, and D. Zips, *Basic clinical radiobiology fourth edition*. CRC press, 2009. 10, 11

[92] H. Thames, S. Bentzen, I. Turesson, M. Overgaard, and W. Van den Bogaert, "Fractionation parameters for human tissues and tumors," *International journal of radiation biology*, vol. 56, no. 5, pp. 701–710, 1989. 10

[93] S. M. Bentzen and S. L. Tucker, "Quantifying the position and steepness of radiation dose-response curves," *International journal of radiation biology*, vol. 71, no. 5, pp. 531–542, 1997. 10

[94] K. Markov, C. Schinkel, N. Stavreva, P. Stavrev, M. Weldon, and B. G. Fallone, "Reverse mapping of normal tissue complication probabilities onto dose volume histogram space: The problem of randomness of the dose volume histogram sampling," *Medical physics*, vol. 33, no. 9, pp. 3435–3443, 2006. 11

[95] J. A. Peñagarícano, N. Papanikolaou, C. Wu, and Y. Yan, "An assessment of biologically-based optimization (BORT) in the IMRT era," *Medical Dosimetry*, vol. 30, no. 1, pp. 12–19, 2005.

[96] X. S. Qi, V. A. Semenenko, and X. A. Li, "Improved critical structure sparing with biologically based IMRT optimization," *Medical physics*, vol. 36, no. 5, pp. 1790–1799, 2009.

[97] A. E. Nahum and J. Uzan, "(radio) biological optimization of external-beam radiotherapy," *Computational and mathematical methods in medicine*, vol. 2012, 2012.

[98] M. Alber and F. Nüsslin, "An objective function for radiation treatment optimization based on local biological measures," *Physics in Medicine & Biology*, vol. 44, no. 2, p. 479, 1999. 11

[99] H. Paganetti, A. Niemierko, M. Ancukiewicz, L. E. Gerweck, M. Goitein, J. S. Loeffler, and H. D. Suit, "Relative biological effectiveness (RBE) values for proton beam therapy," *International Journal of Radiation Oncology* Biology* Physics*, vol. 53, no. 2, pp. 407–421, 2002. 11

[100] H. Paganetti, "Relative biological effectiveness (RBE) values for proton beam therapy. variations as a function of biological endpoint, dose, and linear energy transfer," *Physics in Medicine & Biology*, vol. 59, no. 22, p. R419, 2014. 11

[101] L. E. Gerweck and S. V. Kozin, "Relative biological effectiveness of proton beams in clinical therapy," *Radiotherapy and oncology*, vol. 50, no. 2, pp. 135–142, 1999. 11

[102] G. Giovannini, T. Böhlen, G. Cabal, J. Bauer, T. Tessonnier, K. Frey, J. Debus, A. Mairani, and K. Parodi, "Variable RBE in proton therapy: comparison of different model predictions and their influence on clinical-like scenarios," *Radiation Oncology*, vol. 11, no. 1, p. 68, 2016. 11

[103] T. I. Marshall, P. Chaudhary, A. Michaelidesová, J. Vachelová, M. Davídková, V. Vondráček, G. Schettino, and K. M. Prise, "Investigating the implications of a variable RBE on proton dose fractionation across a clinical pencil beam scanned spread-out bragg peak," *International Journal of Radiation Oncology* Biology* Physics*, vol. 95, no. 1, pp. 70–77, 2016.

[104] A. Dasu and I. Toma-Dasu, "Impact of variable RBE on proton fractionation," *Medical physics*, vol. 40, no. 1, p. 011705, 2013.

[105] M. C. Frese, J. J. Wilkens, P. E. Huber, A. D. Jensen, U. Oelfke, and Z. Taheri-Kadkhoda, "Application of constant vs. variable relative biological effectiveness in treatment planning of intensity-modulated proton therapy," *International Journal of Radiation Oncology* Biology* Physics*, vol. 79, no. 1, pp. 80–88, 2011.

[106] A. Carabe, M. Moteabbed, N. Depauw, J. Schuemann, and H. Paganetti, "Range uncertainty in proton therapy due to variable biological effectiveness," *Physics in Medicine & Biology*, vol. 57, no. 5, p. 1159, 2012. 22, 36

[107] C. R. Peeler, D. Mirkovic, U. Titt, P. Blanchard, J. R. Gunther, A. Mahajan, R. Mohan, and D. R. Grosshans, "Clinical evidence of variable proton biological effectiveness in pediatric patients treated for ependymoma," *Radiotherapy and Oncology*, vol. 121, no. 3, pp. 395–401, 2016. 32, 36, 41

[108] T. Underwood and H. Paganetti, "Variable proton relative biological effectiveness: How do we move forward?," *International Journal of Radiation Oncology* Biology* Physics*, vol. 95, no. 1, pp. 56–58, 2016. 11

[109] L. B. Marks, E. D. Yorke, A. Jackson, R. K. Ten Haken, L. S. Constine, A. Eisbruch, S. M. Bentzen, J. Nam, and J. O. Deasy, "Use of normal tissue complication probability models in the clinic," *International Journal of Radiation Oncology* Biology* Physics*, vol. 76, no. 3, pp. S10–S19, 2010. 11

[110] M. Williams, J. Denekamp, and J. Fowler, "A review of $\alpha\beta$ ratios for experimental tumors: implications for clinical studies of altered fractionation," *International Journal of Radiation Oncology* Biology* Physics*, vol. 11, no. 1, pp. 87–96, 1985. 11, 22

[111] B. Lannering, P.-E. Sandström, S. Holm, J. Lundgren, S. Pfeifer, U. Samuelsson, B. Strömberg, G. Gustafsson, and Swedish Childhood CNS Tumor Working Group (VCTB), "Classification, incidence and survival analyses of children with CNS tumours diagnosed in sweden 1984–2005," *Acta paediatrica*, vol. 98, no. 10, pp. 1620–1627, 2009. 12

[112] V. Cokkinides, J. Albano, A. Samuels, M. Ward, and J. Thum, "American cancer society: Cancer facts and figures," *Atlanta: American Cancer Society*, 2005. 12

[113] J. Yu, W. Shi, and H. Li, "Factors affecting the prognosis of children with medulloblastoma: A single institution retrospective analysis of 40 cases," *Translational Neuroscience and Clinics*, vol. 3, no. 1, pp. 16–27, 2017. 12

[114] M. Zapotocky, D. Mata-Mbemba, D. Sumerauer, P. Liby, A. Lassaletta, J. Zamecnik, L. Krskova, M. Kyncl, J. Stary, S. Laughlin, *et al.*, "Differential patterns of metastatic dissemination across medulloblastoma subgroups," *Journal of Neurosurgery: Pediatrics*, vol. 21, no. 2, pp. 145–152, 2017. 12

[115] B. F. Danoff, F. S. Cowchock, C. Marquette, L. Mulgrew, and S. Kramer, "Assessment of the long-term effects of primary radiation. therapy for brain tumors in children," *Cancer*, vol. 49, no. 8, pp. 1580–1586, 1982. 12, 15

[116] R. K. Mulhern, S. L. Palmer, T. E. Merchant, D. Wallace, M. Kocak, P. Brouwers, K. Krull, M. Chintagumpala, R. Stargatt, D. M. Ashley, *et al.*, "Neurocognitive consequences of risk-adapted therapy for childhood medulloblastoma," *Journal of Clinical Oncology*, vol. 23, no. 24, pp. 5511–5519, 2005. 12, 15

[117] B. Danckert, J. Ferlay, G. Engholm, H. L. Hansen, T. B. Johannesen, S. Khan, J. E. Køtlum, E. Ólafsdóttir, L. K. H. Schmidt, A. Virtanen, and H. H. Storm, "NORDCAN: Cancer Incidence, Mortality, Prevalence and Survival in the Nordic Countries, version 8.2 (26.03.2019)." Association of the Nordic Cancer Registries. Danish Cancer Society. Available online from http://www.ancr.nu, last accessed 2020-05-06. 12

[118] H. M. Duvernoy, *The human hippocampus: functional anatomy, vascularization and serial sections with MRI*. Springer Science & Business Media, 2005. 12

[119] P. S. Eriksson, E. Perfilieva, T. Björk-Eriksson, A.-M. Alborn, C. Nordborg, D. A. Peterson, and F. H. Gage, "Neurogenesis in the adult human hippocampus," *Nature medicine*, vol. 4, no. 11, pp. 1313–1317, 1998. 13

[120] T. Toda, S. L. Parylak, S. B. Linker, and F. H. Gage, "The role of adult hippocampal neurogenesis in brain health and disease," *Molecular psychiatry*, vol. 24, no. 1, pp. 67–87, 2019. 13

[121] P. Peigneux, S. Laureys, S. Fuchs, F. Collette, F. Perrin, J. Reggers, C. Phillips, C. Degueldre, G. Del Fiore, J. Aerts, *et al.*, "Are spatial memories strengthened in the human hippocampus during slow wave sleep?," *Neuron*, vol. 44, no. 3, pp. 535–545, 2004. 13

[122] P.-F. Tsai, C.-C. Yang, C.-C. Chuang, T.-Y. Huang, Y.-M. Wu, P.-C. Pai, C.-K. Tseng, T.-H. Wu, Y.-L. Shen, and S.-Y. Lin, "Hippocampal dosimetry correlates with the change in neurocognitive function after hippocampal sparing during whole brain radiotherapy: a prospective study," *Radiation Oncology*, vol. 10, no. 1, p. 253, 2015. 13, 14, 15

[123] M. Connor, R. Karunamuni, C. McDonald, T. Seibert, N. White, V. Moiseenko, H. Bartsch, N. Farid, J. Kuperman, A. Krishnan, *et al.*, "Regional susceptibility to dose-dependent white matter damage after brain radiotherapy," *Radiotherapy and Oncology*, vol. 123, no. 2, pp. 209–217, 2017.

[124] A. M. Peiffer, C. M. Leyrer, D. M. Greene-Schloesser, E. Shing, W. T. Kearns, W. H. Hinson, S. B. Tatter, E. H. Ip, S. R. Rapp, M. E. Robbins, *et al.*, "Neuroanatomical target theory as a predictive model for radiation-induced cognitive decline," *Neurology*, vol. 80, no. 8, pp. 747–753, 2013. 13

[125] M. L. Monje, S. Mizumatsu, J. R. Fike, and T. D. Palmer, "Irradiation induces neural precursor-cell dysfunction," *Nature medicine*, vol. 8, no. 9, pp. 955–962, 2002. 13

[126] V. Gondi, W. A. Tomé, and M. P. Mehta, "Why avoid the hippocampus? A comprehensive review," *Radiotherapy and Oncology*, vol. 97, no. 3, pp. 370–376, 2010. 13, 14, 15, 36

[127] V. Gondi, S. L. Pugh, W. A. Tome, C. Caine, B. Corn, A. Kanner, H. Rowley, V. Kundapur, A. DeNittis, J. N. Greenspoon, *et al.*, "Preservation of memory with conformal avoidance of the hippocampal neural stem-cell compartment during whole-brain radiotherapy for brain metastases (RTOG 0933): a phase II multi-institutional trial," *Journal of Clinical Oncology*, vol. 32, no. 34, p. 3810, 2014. 13, 14, 15, 36

[128] J. S. Goda, D. Dutta, U. Krishna, S. Goswami, T. Gupta, V. Kothavade, S. Kannan, M. Maitre, N. Bano, and R. Jalali, "Hippocampal radiotherapy dose-constraints for predicting long-term neurocognitive outcomes: Mature data from a prospective trial in young patients with brain tumors," *Neuro-Oncology*, 2020. 13

[129] M. L. Smith and B. Milner, "The role of the right hippocampus in the recall of spatial location," *Neuropsychologia*, vol. 19, no. 6, pp. 781–793, 1981.

[130] V. D. Bohbot, M. Kalina, K. Stepankova, N. Spackova, M. Petrides, and L. Nadel, "Spatial memory deficits in patients with lesions to the right hippocampus and to the right parahippocampal cortex," *Neuropsychologia*, vol. 36, no. 11, pp. 1217–1238, 1998.

[131] A. H. Zureick, C. L. Evans, A. Niemierko, J. A. Grieco, A. J. Nichols, B. C. Fullerton, C. B. Hess, C. P. Goebel, S. L. Gallotto, E. A. Weyman, *et al.*, "Left hippocampal dosimetry correlates with visual and verbal memory outcomes in survivors of pediatric brain tumors," *Cancer*, vol. 124, no. 10, pp. 2238–2245, 2018. 13

[132] R. J. Packer, J. Goldwein, H. S. Nicholson, L. G. Vezina, J. C. Allen, M. D. Ris, K. Muraszko, L. B. Rorke, W. M. Wara, B. H. Cohen, *et al.*, "Treatment of children with medulloblastomas with reduced-dose craniospinal radiation therapy and adjuvant chemotherapy: A Children's Cancer Group Study," *Journal of clinical oncology*, vol. 17, no. 7, pp. 2127–2127, 1999. 14

[133] H. S. Greenberg, M. C. Chamberlain, M. J. Glantz, and S. Wang, "Adult medulloblastoma: multiagent chemotherapy," *Neuro-oncology*, vol. 3, no. 1, pp. 29–34, 2001. 14

[134] T. E. Merchant, L. E. Kun, M. J. Krasin, D. Wallace, M. M. Chintagumpala, S. Y. Woo, D. M. Ashley, M. Sexton, S. J. Kellie, V. Ahern, *et al.*, "Multi-institution prospective trial of reduced-dose craniospinal irradiation (23.4 Gy) followed by conformal posterior fossa (36 Gy) and primary site irradiation (55.8 Gy) and dose-intensive chemotherapy for average-risk medulloblastoma," *International Journal of Radiation Oncology* Biology* Physics*, vol. 70, no. 3, pp. 782–787, 2008. 14

[135] A. P. Brown, C. L. Barney, D. R. Grosshans, M. F. McAleer, J. F. De Groot, V. K. Puduvalli, S. L. Tucker, C. N. Crawford, M. Khan, S. Khatua, *et al.*, "Proton beam craniospinal irradiation reduces acute toxicity for adults with medulloblastoma," *International Journal of Radiation Oncology* Biology* Physics*, vol. 86, no. 2, pp. 277–284, 2013. 14

[136] D. M. Cochran, T. I. Yock, J. A. Adams, and N. J. Tarbell, "Radiation dose to the lens during craniospinal irradiation - an improvement in proton radiotherapy technique," *International Journal of Radiation Oncology* Biology* Physics*, vol. 70, no. 5, pp. 1336–1342, 2008. 14

[137] C. T. Lee, S. D. Bilton, R. M. Famiglietti, B. A. Riley, A. Mahajan, E. L. Chang, M. H. Maor, S. Y. Woo, J. D. Cox, and A. R. Smith, "Treatment planning with protons for pediatric retinoblastoma, medulloblastoma, and pelvic sarcoma: how do protons compare with other conformal techniques?," *International Journal of Radiation Oncology* Biology* Physics*, vol. 63, no. 2, pp. 362–372, 2005.

[138] B. Timmermann, A. J. Lomax, L. Nobile, M. A. Grotzer, M. Weiss, R.-D. Kortmann, A. Bolsi, and G. Goitein, "Novel technique of craniospinal axis proton therapy with the spot-scanning system," *Strahlentherapie und Onkologie*, vol. 183, no. 12, pp. 685–688, 2007. 14

[139] M. Blomstrand, N. P. Brodin, P. Munck af Rosenschöld, I. R. Vogelius, G. Sánchez Merino, A. Kiil-Berthlesen, K. Blomgren, B. Lannering, S. M. Bentzen, and T. Björk-Eriksson, "Estimated clinical benefit of protecting neurogenesis in the developing brain during radiation therapy for pediatric medulloblastoma," *Neuro-oncology*, vol. 14, no. 7, pp. 882–889, 2012. 14, 15, 20

[140] N. P. Brodin, P. Munck af Rosenschöld, M. Blomstrand, A. Kiil-Berthlesen, C. Hollensen, I. R. Vogelius, B. Lannering, S. M. Bentzen, and T. Björk-Eriksson, "Hippocampal sparing radiotherapy for pediatric medulloblastoma: impact of treatment margins and treatment technique," *Neuro-oncology*, vol. 16, no. 4, pp. 594–602, 2014.

[141] J. Stoker, S. Vora, A. Patel, D. Grosshans, P. D. Brown, T. Vern-Gross, M. Bues, T. Daniels, B. Allred, A. Uejo, *et al.*, "Advantages of intensity modulated proton therapy during hippocampal avoidance whole brain radiation therapy," *Physics and imaging in radiation oncology*, vol. 8, pp. 28–32, 2018.

[142] X. Ding, J. Zhou, X. Li, K. Blas, G. Liu, Y. Wang, A. Qin, P. Chinnaiyan, D. Yan, C. Stevens, *et al.*, "Improving dosimetric outcome for hippocampus and cochlea sparing whole brain radiotherapy using spot-scanning proton arc therapy," *Acta Oncologica*, vol. 58, no. 4, pp. 483–490, 2019. 14

[143] A. N. Gutiérrez, D. C. Westerly, W. A. Tomé, H. A. Jaradat, T. R. Mackie, S. M. Bentzen, D. Khuntia, and M. P. Mehta, "Whole brain radiotherapy with hippocampal avoidance and simultaneously integrated brain metastases boost: a planning study," *International Journal of Radiation Oncology* Biology* Physics*, vol. 69, no. 2, pp. 589–597, 2007. 14

[144] P. D. Brown, V. Gondi, S. Pugh, W. A. Tome, J. S. Wefel, T. S. Armstrong, J. A. Bovi, C. Robinson, A. Konski, D. Khuntia, *et al.*, "Hippocampal avoidance during whole-brain radiotherapy plus memantine for patients with brain metastases: Phase III trial NRG Oncology CC001," *Journal of Clinical Oncology*, pp. JCO–19, 2020. 14, 42

[145] V. Gondi, R. Tolakanahalli, M. P. Mehta, D. Tewatia, H. Rowley, J. S. Kuo, D. Khuntia, and W. A. Tomé, "Hippocampal-sparing whole-brain radiotherapy: a "How-to" technique using helical tomotherapy and

linear accelerator-based intensity-modulated radiotherapy," *International Journal of Radiation Oncology* Biology* Physics*, vol. 78, no. 4, pp. 1244–1252, 2010. 14, 15

[146] G. T. Armstrong, N. Jain, W. Liu, T. E. Merchant, M. Stovall, D. K. Srivastava, J. G. Gurney, R. J. Packer, L. L. Robison, and K. R. Krull, "Region-specific radiotherapy and neuropsychological outcomes in adult survivors of childhood CNS malignancies," *Neuro-oncology*, vol. 12, no. 11, pp. 1173–1186, 2010. 14, 15, 20, 35, 36

[147] B. Lannering, S. Rosberg, I. Marky, C. Moell, and K. Albertsson-Wikiand, "Reduced growth hormone secretion with maintained periodicity following cranial irradiation in children with acute lymphoblastic leukaemia," *Clinical endocrinology*, vol. 42, no. 2, pp. 153–159, 1995.

[148] J. P. Neglia, L. L. Robison, M. Stovall, Y. Liu, R. J. Packer, S. Hammond, Y. Yasui, C. E. Kasper, A. C. Mertens, S. S. Donaldson, *et al.*, "New primary neoplasms of the central nervous system in survivors of childhood cancer: a report from the Childhood Cancer Survivor Study," *Journal of the National Cancer Institute*, vol. 98, no. 21, pp. 1528–1537, 2006. 15

[149] R. J. Packer, J. G. Gurney, J. A. Punyko, S. S. Donaldson, P. D. Inskip, M. Stovall, Y. Yasui, A. C. Mertens, C. A. Sklar, H. S. Nicholson, *et al.*, "Long-term neurologic and neurosensory sequelae in adult survivors of a childhood brain tumor: Childhood Cancer Survivor Study," *Journal of Clinical Oncology*, vol. 21, no. 17, pp. 3255–3261, 2003. 14, 36

[150] N. P. Brodin, P. M. A. Rosenschöld, M. C. Aznar, A. Kiil-Berthelsen, I. R. Vogelius, P. Nilsson, B. Lannering, and T. Björk-Eriksson, "Radiobiological risk estimates of adverse events and secondary cancer for proton and photon radiation therapy of pediatric medulloblastoma," *Acta oncologica*, vol. 50, no. 6, pp. 806–816, 2011. 14

[151] J. Bates, R. Howell, Q. Liu, Y. Yasui, D. Mulrooney, S. Dhakal, W. Leisenring, D. Indelicato, T. Gibson, G. Armstromg, *et al.*, "Volumetric dose-effect analysis of late cardiotoxicity: a report from the Childhood Cancer Survivor Study (CCSS)," *International Journal of Radiation Oncology* Biology* Physics*, vol. 99, no. 2, p. S3, 2017. 15, 36

[152] T. R. Möller, S. Garwicz, L. Barlow, J. F. Winther, E. Glattre, G. Olafsdottir, J. H. Olsen, R. Perfekt, A. Ritvanen, R. Sankila, *et al.*, "Decreasing late mortality among five-year survivors of cancer in childhood and adolescence: a population-based study in the Nordic countries," *Journal of Clinical Oncology*, vol. 19, no. 13, pp. 3173–3181, 2001. 15, 41

[153] A. C. Mertens, Y. Yasui, J. P. Neglia, J. D. Potter, M. E. Nesbit Jr, K. Ruccione, W. A. Smithson, and L. L. Robison, "Late mortality experience in five-year survivors of childhood and adolescent cancer: the Childhood Cancer Survivor Study," *Journal of Clinical Oncology*, vol. 19, no. 13, pp. 3163–3172, 2001.

[154] G. T. Armstrong, Z. Pan, K. K. Ness, D. Srivastava, and L. L. Robison, "Temporal trends in cause-specific late mortality among 5-year survivors of childhood cancer," *Journal of clinical oncology*, vol. 28, no. 7, p. 1224, 2010.

[155] S. Garwicz, H. Anderson, J.H. Olsen, J. Falck Winther, R. Sankila, F. Langmark, L. Tryggvadóttir, T.R. Möller and Association of the Nordic Cancer Registries (ANCR) and the Nordic Society for Pediatric Hematology Oncology (NOPHO), "Late and very late mortality in 5-year survivors of childhood cancer: Changing pattern over four decades - Experience from the Nordic countries," *International journal of cancer*, vol. 131, no. 7, pp. 1659–1666, 2012.

[156] S. E. Lipshultz and M. J. Adams, "Cardiotoxicity after childhood cancer: Beginning with the end in mind," 2010.

[157] M. Tukenova, C. Guibout, O. Oberlin, F. Doyon, A. Mousannif, N. Haddy, S. Guérin, H. Pacquement, A. Aouba, M. Hawkins, *et al.*, "Role of cancer treatment in long-term overall and cardiovascular mortality after childhood cancer," *J Clin Oncol*, vol. 28, no. 8, pp. 1308–15, 2010. 15

[158] B. R. O'Driscoll, P. S. Hasleton, P. M. Taylor, L. W. Poulter, H. R. Gattamaneni, and A. A. Woodcock, "Active lung fibrosis up to 17 years after chemotherapy with carmustine (BCNU) in childhood," *New England Journal of Medicine*, vol. 323, no. 6, pp. 378–382, 1990. 15, 36

[159] G. W. Morgan, A. P. Freeman, R. G. McLean, B. H. Jarvie, and R. W. Giles, "Late cardiac, thyroid, and pulmonary sequelae of mantle radiotherapy for hodgkin's disease," *International Journal of Radiation Oncology* Biology* Physics*, vol. 11, no. 11, pp. 1925–1931, 1985.

[160] R. I. Jakacki, C. M. Schramm, B. R. Donahue, F. Haas, and J. C. Allen, "Restrictive lung disease following treatment for malignant brain tumors: a potential late effect of craniospinal irradiation.," *Journal of clinical oncology*, vol. 13, no. 6, pp. 1478–1485, 1995. 15, 36

[161] M. C. Cox, J. M. Kusters, C. E. Gidding, J. H. Schieving, E. J. van Lindert, J. H. Kaanders, and G. O. Janssens, "Acute toxicity profile of craniospinal irradiation with intensity-modulated radiation therapy in children with medulloblastoma: A prospective analysis," *Radiation Oncology*, vol. 10, no. 1, p. 241, 2015. 15

[162] F. N. Norsker, C. Rechnitzer, E. W. Andersen, K. M. Linnet, L. Kenborg, A. S. Holmqvist, L. Tryggvadottir, L.-M. Madanat-Harjuoja, I. Øra, H. K. Thorarinsdottir, *et al.*, "Neurologic disorders in long-term survivors of neuroblastoma - a population-based cohort study within the Adult Life after Childhood Cancer in Scandinavia (ALiCCS) research program," *Acta Oncologica*, vol. 59, no. 2, pp. 134–140, 2020. 15, 31

[163] D. L. Friedman, "The Childhood Cancer Survivor Study: an important research initiative for childhood cancer survivors," *Journal of Pediatric Oncology Nursing*, vol. 16, no. 3, pp. 172–175, 1999.

[164] M. Hawkins, E. Lancashire, D. Winter, C. Frobisher, R. Reulen, A. Taylor, M. Stevens, and M. Jenney, "The British Childhood Cancer Survivor Study: Objectives, methods, population structure, response rates and initial descriptive information," *Pediatric blood & cancer*, vol. 50, no. 5, pp. 1018–1025, 2008.

[165] T. Bolling, A. Schuck, H. Pape, C. Rube, B. Pollinger, B. Timmermann, R. D. Kortmann, K. Dieckmann, and N. Willich, "Study protocol of the German" Registry for the detection of late sequelae after radiotherapy in childhood and adolescence"(RiSK)," *Radiation Oncology*, vol. 3, no. 1, p. 10, 2008.

[166] L. Constine, C. Ronckers, C.-H. Hua, A. Olch, L. Kremer, A. Jackson, and S. Bentzen, "Pediatric normal tissue effects in the clinic (PENTEC): an international collaboration to analyse normal tissue radiation Dose-Volume response relationships for paediatric cancer patients," *Clinical Oncology*, vol. 31, no. 3, pp. 199–207, 2019.

[167] C. J. Bright, R. C. Reulen, D. L. Winter, D. P. Stark, M. G. McCabe, A. B. Edgar, C. Frobisher, and M. M. Hawkins, "Risk of subsequent primary neoplasms in survivors of adolescent and young adult cancer (Teenage and Young Adult Cancer Survivor Study): a population-based, cohort study," *The Lancet Oncology*, vol. 20, no. 4, pp. 531–545, 2019.

[168] J. Byrne, D. Alessi, R. S. Allodji, F. Bagnasco, E. Bárdi, A. Bautz, C. J. Bright, M. Brown, I. Diallo, E. A. L. Feijen, *et al.*, "The PanCareSurFup consortium: research and guidelines to improve lives for survivors of childhood cancer," *European journal of cancer*, vol. 103, pp. 238–248, 2018. 15, 31

[169] D. Gasic, P. M. af Rosenschöld, I. R. Vogelius, M. V. Maraldo, M. C. Aznar, K. Nysom, T. Björk-Eriksson, S. M. Bentzen, and N. P. Brodin, "Retrospective estimation of heart and lung doses in pediatric patients treated with spinal irradiation," *Radiotherapy and Oncology*, vol. 128, no. 2, pp. 209–213, 2018. 15, 41

[170] J. Cuzick, H. Stewart, L. Rutqvist, J. Houghton, R. Edwards, C. Redmond, R. Peto, M. Baum, B. Fisher, and H. Host, "Cause-specific mortality in long-term survivors of breast cancer who participated in trials of radiotherapy.," *Journal of Clinical Oncology*, vol. 12, no. 3, pp. 447–453, 1994. 15, 41

[171] R. K. Mulhern, T. E. Merchant, A. Gajjar, W. E. Reddick, and L. E. Kun, "Late neurocognitive sequelae in survivors of brain tumours in childhood," *The lancet oncology*, vol. 5, no. 7, pp. 399–408, 2004. 15

[172] P. D. Brown, J. C. Buckner, J. R. O'Fallon, N. L. Iturria, C. A. Brown, B. P. O'Neill, B. W. Scheithauer, R. P. Dinapoli, R. M. Arusell, W. J. Curran, *et al.*, "Effects of radiotherapy on cognitive function in patients with low-grade glioma measured by the folstein mini-mental state examination," *Journal of clinical oncology*, vol. 21, no. 13, pp. 2519–2524, 2003. 15, 36

[173] J. Grill, V. K. Renaux, C. Bulteau, D. Viguier, C. Levy-Piebois, C. Sainte-Rose, G. Dellatolas, M.-A. Raquin, I. Jambaqué, and C. Kalifa, "Long-term intellectual outcome in children with posterior fossa tumors according to radiation doses and volumes," *International Journal of Radiation Oncology* Biology* Physics*, vol. 45, no. 1, pp. 137–145, 1999.

[174] R. Jalali, I. Mallick, D. Dutta, S. Goswami, T. Gupta, A. Munshi, D. Deshpande, and R. Sarin, "Factors influencing neurocognitive outcomes in young patients with benign and low-grade brain tumors treated with stereotactic conformal radiotherapy," *International Journal of Radiation Oncology* Biology* Physics*, vol. 77, no. 4, pp. 974–979, 2010.

[175] R. K. Mulhern, J. L. Kepner, P. R. Thomas, F. D. Armstrong, H. S. Friedman, and L. E. Kun, "Neuropsychologic functioning of survivors of childhood medulloblastoma randomized to receive conventional or reduced-dose craniospinal irradiation: a Pediatric Oncology Group study.," *Journal of Clinical Oncology*, vol. 16, no. 5, pp. 1723–1728, 1998. 15, 36

[176] K. J. Redmond, E. M. Mahone, S. Terezakis, O. Ishaq, E. Ford, T. McNutt, L. Kleinberg, K. J. Cohen, M. Wharam, and A. Horska, "Association between radiation dose to neuronal progenitor cell niches and temporal lobes and performance on neuropsychological testing in children: a prospective study," *Neuro-oncology*, vol. 15, no. 3, pp. 360–369, 2013. 15

[177] K. D. Westover, J. T. Mendel, T. Dan, K. Kumar, A. Gao, S. Pulipparacharuv, P. Iyengar, L. Nedzi, R. Hannan, J. Anderson, *et al.*, "Phase II Trial of Hippocampal-Sparing Whole Brain Irradiation with Simultaneous Integrated Boost (HSIB-WBRT) for Metastatic Cancer," *Neuro-Oncology*, 2020. 15

[178] B. J. Spiegler, E. Bouffet, M. L. Greenberg, J. T. Rutka, and D. J. Mabbott, "Change in neurocognitive functioning after treatment with cranial radiation in childhood," *Journal of Clinical Oncology*, vol. 22, no. 4, pp. 706–713, 2004. 15

[179] M. Van Herk, P. Remeijer, C. Rasch, and J. V. Lebesque, "The probability of correct target dosage: dose-population histograms for deriving treatment margins in radiotherapy," *International Journal of Radiation Oncology* Biology* Physics*, vol. 47, no. 4, pp. 1121–1135, 2000. 17, 18, 19, 24, 25

[180] J. C. Stroom, H. C. de Boer, H. Huizenga, and A. G. Visser, "Inclusion of geometrical uncertainties in radiotherapy treatment planning by means of coverage probability," *International Journal of Radiation Oncology* Biology* Physics*, vol. 43, no. 4, pp. 905–919, 1999.

[181] A. L. McKenzie, M. van Herk, and B. Mijnheer, "The width of margins in radiotherapy treatment plans," *Physics in Medicine & Biology*, vol. 45, no. 11, p. 3331, 2000.

[182] B. C. Parker, A. S. Shiu, M. H. Maor, F. F. Lang, H. H. Liu, R. A. White, and J. A. Antolak, "PTV margin determination in conformal SRT of intracranial lesions," *Journal of applied clinical medical physics*, vol. 3, no. 3, pp. 176–189, 2002.

[183] A. McKenzie, M. van Herk, and B. Mijnheer, "Margins for geometric uncertainty around organs at risk in radiotherapy," *Radiotherapy and Oncology*, vol. 62, no. 3, pp. 299–307, 2002. 17

[184] E. Poskitt, "Defining childhood obesity: the relative body mass index (BMI)," *Acta Paediatrica*, vol. 84, no. 8, pp. 961–963, 1995. 18

[185] T. J. Cole and P. J. Green, "Smoothing reference centile curves: the LMS method and penalized likelihood," *Statistics in medicine*, vol. 11, no. 10, pp. 1305–1319, 1992. 18

[186] K. Nysom, C. Mølgaard, B. Hutchings, and K. F. Michaelsen, "Body mass index of 0 to 45-y-old danes: reference values and comparison with published european reference values," *International journal of obesity*, vol. 25, no. 2, pp. 177–184, 2001. 18

[187] G. J. Kutcher, G. S. Mageras, and S. A. Leibel, "Control, correction, and modeling of setup errors and organ motion," in *Seminars in radiation oncology*, vol. 5, pp. 134–145, Elsevier, 1995. 18, 19

[188] C. Njeh, "Tumor delineation: The weakest link in the search for accuracy in radiotherapy," *Journal of medical physics/Association of Medical Physicists of India*, vol. 33, no. 4, p. 136, 2008. 19, 25

[189] C. Rasch, R. Steenbakkers, and M. van Herk, "Target definition in prostate, head, and neck," in *Seminars in radiation oncology*, vol. 15, pp. 136–145, Elsevier, 2005. 19, 25

[190] N. P. Brodin, I. R. Vogelius, T. Björk-Eriksson, P. M. af Rosenschöld, and S. M. Bentzen, "Modeling freedom from progression for standard-risk medulloblastoma: A mathematical tumor control model with multiple modes of failure," *International Journal of Radiation Oncology* Biology* Physics*, vol. 87, no. 2, pp. 422–429, 2013. 20

[191] J. Michalski, A. Janss, G. Vezina, A. Gajjar, I. Pollack, T. Merchant, T. FitzGerald, T. Booth, N. Tarbell, Y. Li, *et al.*, "Results of COG ACNS0331: a phase III trial of involved-field radiotherapy (IFRT) and low dose craniospinal irradiation (LD-CSI) with chemotherapy in average-risk medulloblastoma: a report from the Children's Oncology Group," *International Journal of Radiation Oncology• Biology• Physics*, vol. 96, no. 5, pp. 937–938, 2016. 20, 35

[192] J. O. Deasy, A. I. Blanco, and V. H. Clark, "CERR: a computational environment for radiotherapy research," *Medical physics*, vol. 30, no. 5, pp. 979–985, 2003. 21

[193] B. Hidalgo and M. Goodman, "Multivariate or multivariable regression?," *American journal of public health*, vol. 103, no. 1, pp. 39–40, 2013. 21

[194] M. H. Katz, "Multivariable analysis: a primer for readers of medical research," *Annals of internal medicine*, vol. 138, no. 8, pp. 644–650, 2003.

[195] G. Van Belle, L. D. Fisher, P. J. Heagerty, and T. Lumley, *Biostatistics: a methodology for the health sciences*, vol. 519. John Wiley & Sons, 2004. 21

[196] R. Kohavi *et al.*, "A study of cross-validation and bootstrap for accuracy estimation and model selection," in *Ijcai*, vol. 14, pp. 1137–1145, Montreal, Canada, 1995. 22

[197] J.-H. Kim, "Estimating classification error rate: Repeated cross-validation, repeated hold-out and bootstrap," *Computational statistics & data analysis*, vol. 53, no. 11, pp. 3735–3745, 2009.

[198] C. Beleites, R. Baumgartner, C. Bowman, R. Somorjai, G. Steiner, R. Salzer, and M. G. Sowa, "Variance reduction in estimating classification error using sparse datasets," *Chemometrics and intelligent laboratory systems*, vol. 79, no. 1-2, pp. 91–100, 2005.

[199] S. Borra and A. Di Ciaccio, "Measuring the prediction error. A comparison of cross-validation, bootstrap and covariance penalty methods," *Computational statistics & data analysis*, vol. 54, no. 12, pp. 2976–2989, 2010. 22

[200] A. Bertolet, M. A. Cortés-Giraldo, K. Souris, M. Cohilis, and A. Carabe-Fernandez, "Calculation of clinical dose distributions in proton therapy from microdosimetry," *Medical physics*, vol. 46, no. 12, pp. 5816–5823, 2019. 22, 36

[201] A. Bertolet, A. Baratto-Roldán, S. Barbieri, G. Baiocco, A. Carabe, and M. Cortés-Giraldo, "Dose-averaged LET calculation for proton track segments using microdosimetric Monte Carlo simulations," *Medical physics*, vol. 46, no. 9, pp. 4184–4192, 2019.

[202] A. Bertolet, A. Baratto-Roldán, M. Cortés-Giraldo, and A. Carabe-Fernandez, "Segment-averaged LET concept and analytical calculation from microdosimetric quantities in proton radiation therapy," *Medical physics*, vol. 46, no. 9, pp. 4204–4214, 2019.

[203] A. Bertolet, M. Cortés-Giraldo, K. Souris, and A. Carabe, "A kernel-based algorithm for the spectral fluence of clinical proton beams to calculate dose-averaged LET and other dosimetric quantities of interest," *Medical Physics*, 2020. 22, 36

[204] N. Tilly, J. Johansson, U. Isacsson, J. Medin, E. Blomquist, E. Grusell, and B. Glimelius, "The influence of RBE variations in a clinical proton treatment plan for a hypopharynx cancer," *Physics in Medicine & Biology*, vol. 50, no. 12, p. 2765, 2005. 22

[205] J. Wilkens and U. Oelfke, "A phenomenological model for the relative biological effectiveness in therapeutic proton beams," *Physics in Medicine & Biology*, vol. 49, no. 13, p. 2811, 2004.

[206] Y. Chen and S. Ahmad, "Empirical model estimation of relative biological effectiveness for proton beam therapy," *Radiation protection dosimetry*, vol. 149, no. 2, pp. 116–123, 2012.

[207] M. Wedenberg, B. K. Lind, and B. Hårdemark, "A model for the relative biological effectiveness of protons: the tissue specific parameter α/β of photons is a predictor for the sensitivity to LET changes," *Acta oncologica*, vol. 52, no. 3, pp. 580–588, 2013.

[208] B. Jones, "Towards achieving the full clinical potential of proton therapy by inclusion of LET and RBE models," *Cancers*, vol. 7, no. 1, pp. 460–480, 2015.

[209] A. L. McNamara, J. Schuemann, and H. Paganetti, "A phenomenological relative biological effectiveness (RBE) model for proton therapy based on all published in vitro cell survival data," *Physics in Medicine & Biology*, vol. 60, no. 21, p. 8399, 2015.

[210] A. Mairani, I. Dokic, G. Magro, T. Tessonnier, J. Bauer, T. Böhlen, M. Ciocca, A. Ferrari, P. Sala, O. Jäkel, *et al.*, "A phenomenological relative biological effectiveness approach for proton therapy based on an improved description of the mixed radiation field," *Physics in Medicine & Biology*, vol. 62, no. 4, p. 1378, 2017.

[211] E. Rørvik, S. Thörnqvist, C. H. Stokkevåg, T. J. Dahle, L. F. Fjæra, and K. S. Ytre-Hauge, "A phenomenological biological dose model for proton therapy based on linear energy transfer spectra," *Medical physics*, vol. 44, no. 6, pp. 2586–2594, 2017. 22, 36

[212] S. Agostinelli, J. Allison, K. a. Amako, J. Apostolakis, H. Araujo, P. Arce, M. Asai, D. Axen, S. Banerjee, G. . Barrand, *et al.*, "GEANT4 - a simulation toolkit," *Nuclear instruments and methods in physics research section A: Accelerators, Spectrometers, Detectors and Associated Equipment*, vol. 506, no. 3, pp. 250–303, 2003. 22

[213] D. Sarrut, M. Bardiès, N. Boussion, N. Freud, S. Jan, J.-M. Létang, G. Loudos, L. Maigne, S. Marcatili, T. Mauxion, *et al.*, "A review of the use and potential of the GATE Monte Carlo simulation code for radiation therapy and dosimetry applications," *Medical physics*, vol. 41, no. 6, Part1, 2014. 22

[214] H. Paganetti, "Range uncertainties in proton therapy and the role of Monte Carlo simulations," *Physics in Medicine & Biology*, vol. 57, no. 11, p. R99, 2012. 28

[215] J. Seco, H. R. Panahandeh, K. Westover, J. Adams, and H. Willers, "Treatment of non-small cell lung cancer patients with proton beam-based stereotactic body radiotherapy: dosimetric comparison with photon plans highlights importance of range uncertainty," *International Journal of Radiation Oncology* Biology* Physics*, vol. 83, no. 1, pp. 354–361, 2012. 28

[216] G. T. Armstrong, "Long-term survivors of childhood central nervous system malignancies: the experience of the Childhood Cancer Survivor Study," *european journal of paediatric neurology*, vol. 14, no. 4, pp. 298–303, 2010. 28, 36

[217] D. Giantsoudi, R. V. Sethi, B. Y. Yeap, B. R. Eaton, D. H. Ebb, P. A. Caruso, O. Rapalino, Y.-L. E. Chen, J. A. Adams, T. I. Yock, *et al.*, "Incidence of CNS injury for a cohort of 111 patients treated with proton therapy for medulloblastoma: LET and RBE associations for areas of injury," *International Journal of Radiation Oncology* Biology* Physics*, vol. 95, no. 1, pp. 287–296, 2016. 32, 36

[218] H. Hinata, H. Inakoshi, K. Sakai, Y. Ogawa, M. Kobayashi, H. Wakushima, T. Obara, and Y. Shibamoto, "Estimation of time parameter of LQ-model in fractionated radiotherapy of medulloblastoma.," *Radiation medicine*, vol. 19, no. 2, pp. 61–70, 2001. 36

[219] K. K. Boman, F. Lindblad, and A. Hjern, "Long-term outcomes of childhood cancer survivors in Sweden: a population-based study of education, employment, and income," *Cancer: Interdisciplinary International Journal of the American Cancer Society*, vol. 116, no. 5, pp. 1385–1391, 2010. 36

[220] S. Acharya, S. Wu, J. M. Ashford, C. L. Tinkle, J. T. Lucas, I. Qaddoumi, A. Gajjar, M. J. Krasin, H. M. Conklin, and T. E. Merchant, "Association between hippocampal dose and memory in survivors of childhood or adolescent low-grade glioma: a 10-year neurocognitive longitudinal study," *Neuro-oncology*, vol. 21, no. 9, pp. 1175–1183, 2019. 36

[221] J. Li, S. M. Bentzen, J. Li, M. Renschler, and M. P. Mehta, "Relationship between neurocognitive function and quality of life after whole-brain radiotherapy in patients with brain metastasis," *International Journal of Radiation Oncology* Biology* Physics*, vol. 71, no. 1, pp. 64–70, 2008. 36

[222] L. Padovani, F. Chapon, N. André, M. Boucekine, A. Geoffray, F. Bourdeau, J. Masliah-Planchon, L. Claude, A. Huchet, A. Laprie, *et al.*, "Hippocampal sparing during craniospinal irradiation: what did we learn about the incidence of perihippocampus metastases?," *International Journal of Radiation Oncology* Biology* Physics*, vol. 100, no. 4, pp. 980–986, 2018. 36

[223] W. Rider, "Radiation damage to the brain - a new syndrome," *J. Can. Assoc. Radiologists*, vol. 14, 1963. 36

[224] N. G. Gottardo and A. Gajjar, "Current therapy for medulloblastoma," *Current treatment options in neurology*, vol. 8, no. 4, pp. 319–334, 2006. 41

[225] P. Fossati, U. Ricardi, and R. Orecchia, "Pediatric medulloblastoma: toxicity of current treatment and potential role of protontherapy," *Cancer treatment reviews*, vol. 35, no. 1, pp. 79–96, 2009. 41

[226] R. Mohan, C. R. Peeler, F. Guan, L. Bronk, W. Cao, and D. R. Grosshans, "Radiobiological issues in proton therapy," *Acta Oncologica*, vol. 56, no. 11, pp. 1367–1373, 2017. 41

[227] H. Willers, A. Allen, D. Grosshans, S. J. McMahon, C. von Neubeck, C. Wiese, and B. Vikram, "Toward a variable RBE for proton beam therapy," *Radiotherapy and Oncology*, vol. 128, no. 1, pp. 68–75, 2018. 41

[228] A. McNamara, H. Willers, and H. Paganetti, "Modelling variable proton relative biological effectiveness for treatment planning," *The British journal of radiology*, vol. 93, no. 1107, p. 20190334, 2020. 41

[229] H. Nystrom, M. F. Jensen, and P. W. Nystrom, "Treatment planning for proton therapy: what is needed in the next 10 years?," *The British Journal of Radiology*, vol. 93, no. 1107, p. 20190304, 2020. 41

[230] P. Munck af Rosenschold, S. A. Engelholm, P. N. Brodin, M. Jørgensen, D. R. Grosshans, R. X. Zhu, M. Palmer, C. N. Crawford, and A. Mahajan, "A retrospective evaluation of the benefit of referring pediatric cancer patients to an external proton therapy center," *Pediatric blood & cancer*, vol. 63, no. 2, pp. 262–269, 2016. 41

[231] N. P. Brodin, I. R. Vogelius, M. V. Maraldo, P. Munck af Rosenschöld, M. C. Aznar, A. Kiil-Berthelsen, P. Nilsson, T. Björk-Eriksson, L. Specht, and S. M. Bentzen, "Life years lost - comparing potentially fatal late complications after radiotherapy for pediatric medulloblastoma on a common scale," *Cancer*, vol. 118, no. 21, pp. 5432–5440, 2012. 41

[232] R. Leroy, N. Benahmed, F. Hulstaert, N. Van Damme, and D. De Ruysscher, "Proton therapy in children: a systematic review of clinical effectiveness in 15 pediatric cancers," *International Journal of Radiation Oncology* Biology* Physics*, vol. 95, no. 1, pp. 267–278, 2016. 41

[233] A. N. Schreuder and J. Shamblin, "Proton therapy delivery: what is needed in the next ten years?," *The British Journal of Radiology*, vol. 93, no. 1107, p. 20190359, 2020. 41

A

Appendix

This section provides additional and more detailed results from some of the studies included in the thesis.

A.1 Supplementary material
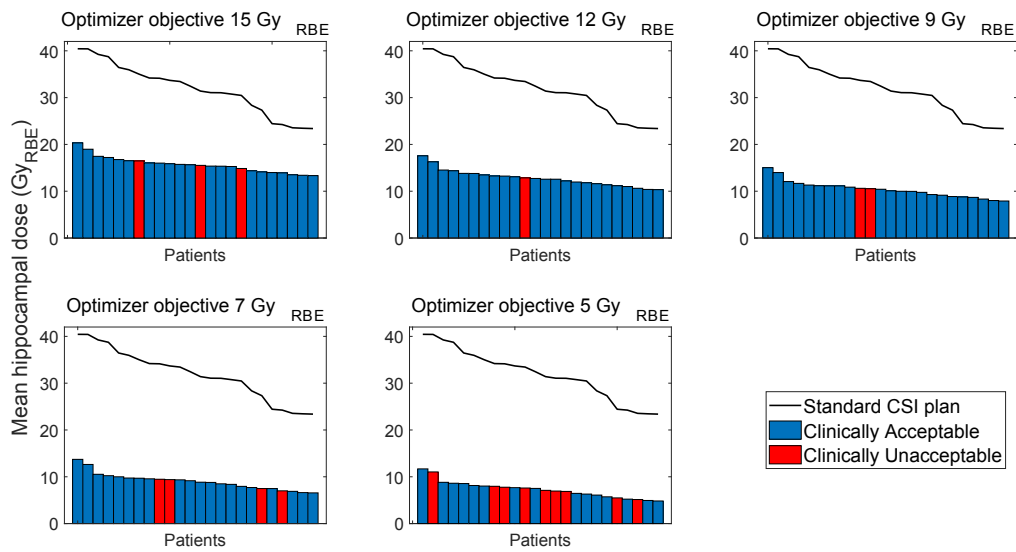
Figure A.1: Mean hippocampus dose (Gy$_{RBE}$) for all patients optimized with 1% / 1 mm. The blue bars indicate a clinically acceptable plan and the red bars indicate a plan that has been deemed unacceptable according to the parameters described in the chapter covering Methodological considerations for STUDY II. The black line is the mean hippocampus dose (Gy$_{RBE}$) for the standard CSI plans and corresponds to each of the patients.

Figure A.2: Mean hippocampus dose (Gy$_{RBE}$) for all patients optimized with 3.5% / 3 mm. The blue bars indicate a clinically acceptable plan and the red bars indicate a plan that has been deemed unacceptable according to the parameters described in the chapter covering Methodological considerations for STUDY II. The black line is the mean hippocampus dose (Gy$_{RBE}$) for the standard CSI plans and corresponds to each of the patients.
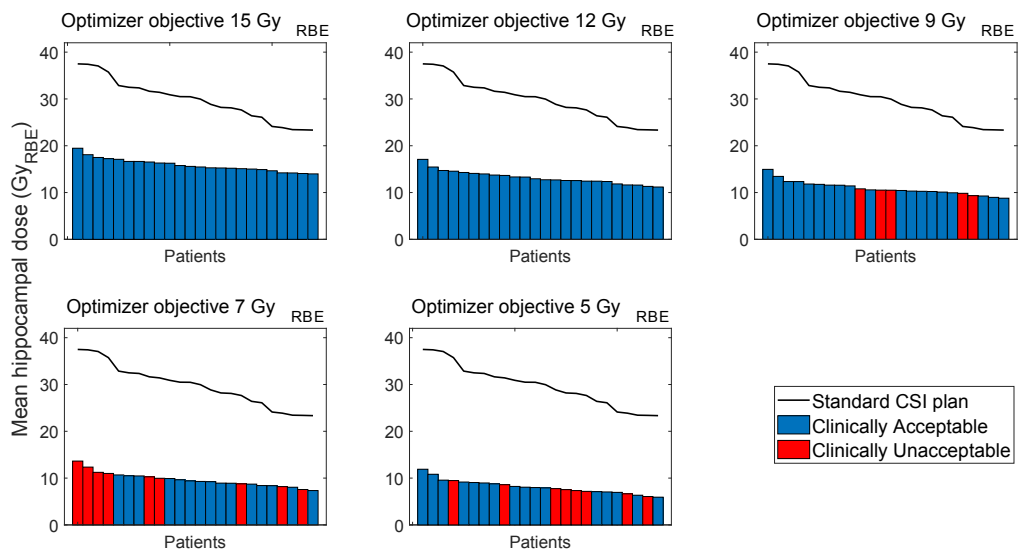
Table A.1: Mean translational (superior-inferior (SI), anterior-posterior (AP) and medial-lateral (ML)) and rotational positioning errors and uncertainties with corresponding range and standard deviations assuming setup based on skin-markers for both 3 and 6 degrees of freedom (DoF) and all isocenters (Units: cm and °/degrees).

	SI / Roll				AP / Yaw				ML / Pitch			
3DoF	SE	SU	RU	Range	SE	SU	RU	Range	SE	SU	RU	Range
Translational (cm)												
- Head	-0.01	0.23	0.21	-1.3 – 2.2	0.04	0.26	0.18	-1.1 – 1.0	0.07	0.17	0.16	-0.6 – 1.3
- Thoracic	0.01	0.21	0.22	-1.2 – 2.4	0.06	0.21	0.14	-0.9 – 0.8	0.08	0.15	0.16	-1.3 – 0.9
- Lumbal	0.04	0.26	0.31	-1.5 – 2.3	0.01	0.32	0.33	-1.0 – 2.1	0.06	0.22	0.30	-1.1 – 1.3
6DoF												
Translational (cm)												
- Head	-0.01	0.23	0.20	-1.3 – 2.2	0.03	0.27	0.23	-1.3 – 1.0	0.08	0.22	0.22	-1.0 – 1.3
- Thoracic	0.01	0.21	0.21	-1.3 – 2.4	0.03	0.22	0.18	-1.5 – 0.8	0.08	0.17	0.17	-1.3 – 1.0
- Lumbal	0.03	0.25	0.31	-1.5 – 2.3	0.00	0.36	0.33	-1.3 – 2.0	0.09	0.22	0.30	-1.1 – 1.4
Rotational (°)												
- Head	0.02	0.47	0.63	-3.5 – 3.5	0.05	0.48	0.60	-2.9 – 3.6	-0.11	0.64	0.70	-5.4 – 3.8
- Thoracic	-0.07	0.76	0.43	-3.6 – 2.0	0.02	0.37	0.40	-3.1 – 3.1	0.24	0.62	0.44	-3.6 – 3.7
- Lumbal	0.04	0.84	1.34	-4.9 – 4.6	0.00	0.51	0.72	-3.1 – 3.3	0.13	0.28	0.80	-3.9 – 4.2

Abbreviations: DoF = Degrees of freedom, SI = superior-inferior, AP = anteroposterior, ML = medial-lateral, SE = Systematic error (defined as the mean of all mean errors), SU = Systematic uncertainty (defined as the standard deviation of all mean errors), RU = Random uncertainty (defined as the root-mean-square deviation for all patients).

Table A.2: Mean translational (superior-inferior (SI), anterior-posterior (AP) and medial-lateral (ML)) and rotational positioning errors and uncertainties with corresponding range and standard deviations assuming setup based on NAL for both 3 and 6 degrees of freedom (DoF) and all isocenters (Units: cm and °/degrees).

	SI / Roll				AP / Yaw				ML / Pitch			
	SE	SU	RU	Range	SE	SU	RU	Range	SE	SU	RU	Range
3DoF												
Translational (cm)												
- Head	0.04	0.19	0.27	-1.3 − 2.2	0.03	0.12	0.23	-1.1 − 1.1	0.02	0.11	0.18	-0.7 − 0.9
- Thoracic	-0.02	0.17	0.27	-1.4 − 2.4	0.01	0.12	0.18	-0.7 − 0.9	0.05	0.11	0.19	-1.1 − 1.0
- Lumbal	-0.04	0.27	0.38	-1.5 − 2.3	-0.01	0.18	0.38	-1.2 − 1.6	-0.02	0.13	0.38	-0.9 − 1.5
6DoF												
Translational (cm)												
- Head	-0.03	0.19	0.25	-1.2 − 2.2	0.01	0.15	0.29	-1.1 − 1.1	0.04	0.13	0.25	-1.0 − 1.6
- Thoracic	-0.02	0.17	0.27	-1.3 − 2.4	-0.04	0.19	0.22	-2.1 − 0.9	0.05	0.15	0.21	-1.1 − 1.4
- Lumbal	0.03	0.13	0.35	-1.1 − 2.3	-0.01	0.19	0.39	-1.1 − 1.4	-0.02	0.13	0.39	-1.1 − 1.4
Rotational (°)												
- Head	-0.22	0.38	0.78	-3.4 − 3.5	0.00	0.42	0.66	-3.1 − 3-8	-0.12	0.64	0.78	-5.7 − 3.0
- Thoracic	-0.19	0.72	0.50	-3.6 − 2.0	-0.01	0.30	0.46	-4.0 − 3.1	0.13	0.46	0.51	-3.8 − 3.7
- Lumbal	-0.28	0.59	1.71	-6.1 − 4.3	-0.04	0.56	0.79	-3.5 − 3.3	0.15	0.41	0.88	-3.3 − 4.0

Abbreviations: DoF = Degrees of freedom, SI = superior-inferior, AP = anteroposterior, ML = medial-lateral, NAL = Non-action level, SE = Systematic error (defined as the mean of all mean errors), SU = Systematic uncertainty (defined as the standard deviation of all mean errors), RU = Random uncertainty (defined as the root-mean-square deviation for all patients).

Table A.3: Mean translational (superior-inferior (SI), anterior-posterior (AP) and medial-lateral (ML)) and rotational positioning errors and uncertainties with corresponding range and standard deviations assuming setup based on AL for both 3 and 6 degrees of freedom (DoF) and all isocenters (Units: cm and °/degrees).

	SI / Roll				AP / Yaw				ML / Pitch			
3DoF	SE	SU	RU	Range	SE	SU	RU	Range	SE	SU	RU	Range
Translational (cm)												
- Head	-0.03	0.22	0.19	-1.3 – 1.0	0.04	0.16	0.16	-0.8 – 1.1	0.01	0.09	0.15	-0.7 – 0.9
- Thoracic	-0.01	0.22	0.20	-1.4 – 1.4	0.02	0.09	0.14	-0.7 – 0.9	0.03	0.11	0.15	-1.1 – 1.0
- Lumbal	-0.04	0.27	0.38	-1.5 – 2.3	-0.02	0.20	0.30	-1.2 – 1.6	-0.04	0.19	0.26	-0.9 – 1.5
6DoF												
Translational (cm)												
- Head	-0.02	0.22	0.18	-1.2 – 1.0	0.01	0.19	0.22	-0.8 – 1.1	0.03	0.13	0.20	-1.0 – 1.6
- Thoracic	-0.01	0.21	0.19	-1.3 – 1.3	-0.03	0.17	0.18	-2.1 – 0.9	0.03	0.17	0.17	-1.1 – 1.4
- Lumbal	0.03	0.13	0.35	-1.1 – 2.3	-0.03	0.20	0.30	-1.1 – 1.4	-0.05	0.19	0.26	-1.1 – 1.3
Rotational (°)												
- Head	-0.28	0.47	0.59	-3.4 – 2.7	-0.02	0.47	0.55	-3.1 – 3-8	-0.11	0.70	0.67	-5.7 – 3.0
- Thoracic	-0.06	0.29	0.35	-2.0 – 1.6	-0.06	0.35	0.34	-4.0 – 3-1	0.00	0.36	0.35	-3.8 – 3.6
- Lumbal	-0.40	0.90	1.17	-6.1 – 4.0	-0.07	0.60	0.67	-3.5 – 3-3	0.17	0.44	0.78	-3.3 – 4.0

Abbreviations: DoF = Degrees of freedom, SI = superior-inferior, AP = anteroposterior, ML = medial-lateral, AL = Action level, SE = Systematic error (defined as the mean of all mean errors), SU = Systematic uncertainty (defined as the standard deviation of all mean errors), RU = Random uncertainty (defined as the root-mean-square deviation for all patients).

65

Table A.4: Mean translational (superior-inferior (SI), anterior-posterior (AP) and medial-lateral (ML)) and rotational positioning errors and uncertainties with corresponding range and standard deviations assuming setup based on IGRT$_{nj}$ for both 3 and 6 degrees of freedom (DoF) and all isocenters (Units: cm and °/degrees).

	SI / Roll				AP / Yaw				ML / Pitch			
	SE	SU	RU	Range	SE	SU	RU	Range	SE	SU	RU	Range
3DoF												
Translational (cm)												
- Head	-0.01	0.23	0.21	-1.3 – 2.2	0.01	0.03	0.04	-0.1 – 0.1	0.01	0.03	0.05	-0.1 – 0.1
- Thoracic	0.01	0.21	0.22	-1.2 – 2.4	0.02	0.03	0.04	-0.1 – 0.1	0.01	0.03	0.05	-0.1 – 0.1
- Lumbal	0.04	0.26	0.31	-1.5 – 2.3	0.00	0.01	0.04	-0.1 – 0.1	0.00	0.02	0.04	-0.1 – 0.1
6DoF												
Translational (cm)												
- Head	-0.01	0.23	0.20	-1.3 – 2.2	0.01	0.02	0.04	-0.1 – 0.1	0.01	0.02	0.05	-0.1 – 0.1
- Thoracic	0.01	0.21	0.21	-1.3 – 2.4	0.02	0.03	0.04	-0.1 – 0.1	0.01	0.03	0.05	-0.1 – 0.1
- Lumbal	0.03	0.25	0.31	-1.5 – 2.3	0.00	0.02	0.04	-0.1 – 0.1	0.00	0.02	0.04	-0.1 – 0.1
Rotational (°)												
- Head	0.00	0.02	0.04	-0.5 – 0.1	0.05	0.48	0.60	-2.9 – 3.6	-0.01	0.07	0.06	-2.4 – 0.8
- Thoracic	0.00	0.02	0.03	-0.1 – 0.1	0.02	0.37	0.40	-3.1 – 3.1	0.01	0.05	0.06	-0.6 – 0.7
- Lumbal	-0.02	0.06	0.11	-1.9 – 1.6	0.00	0.51	0.72	-3.1 – 3.3	0.03	0.06	0.11	-1.2 – 1.2

Abbreviations: DoF = Degrees of freedom, SI = superior-inferior, AP = anteroposterior, ML = medial-lateral, IGRT = Image-guided radiotherapy, nj = Narrow field junction, SE = Systematic error (defined as the mean of all mean errors), SU = Systematic uncertainty (defined as the standard deviation of all mean errors), RU = Random uncertainty (defined as the root-mean-square deviation for all patients).

Table A.5: Mean translational (superior-inferior (SI), anterior-posterior (AP) and medial-lateral (ML)) and rotational positioning errors and uncertainties with corresponding range and standard deviations assuming setup based on IGRT$_{wj}$ for both 3 and 6 degrees of freedom (DoF) and all isocenters (Units: cm and °/degrees).

	SI / Roll				AP / Yaw				ML / Pitch			
3DoF	SE	SU	RU	Range	SE	SU	RU	Range	SE	SU	RU	Range
Translational (cm)												
- Head	0.00	0.02	0.05	-0.1 – 0.1	0.01	0.03	0.04	-0.1 – 0.1	0.01	0.03	0.05	-0.1 – 0.1
- Thoracic	0.01	0.02	0.04	-0.1 – 0.1	0.02	0.03	0.04	-0.1 – 0.1	0.01	0.03	0.05	-0.1 – 0.1
- Lumbal	0.00	0.02	0.04	-0.1 – 0.1	0.00	0.01	0.04	-0.1 – 0.1	0.00	0.02	0.04	-0.1 – 0.1
6DoF												
Translational (cm)												
- Head	0.00	0.03	0.05	-0.1 – 0.1	0.01	0.02	0.04	-0.1 – 0.1	0.01	0.02	0.05	-0.1 – 0.1
- Thoracic	0.00	0.02	0.04	-0.1 – 0.1	0.02	0.03	0.04	-0.1 – 0.1	0.01	0.03	0.05	-0.1 – 0.1
- Lumbal	0.00	0.02	0.04	-0.1 – 0.1	0.00	0.02	0.04	-0.1 – 0.1	0.00	0.02	0.04	-0.1 – 0.1
Rotational (°)												
- Head	0.00	0.02	0.04	-0.5 – 0.1	0.00	0.02	0.04	-0.1 – 0.6	-0.01	0.07	0.06	-2.4 – 0.8
- Thoracic	0.00	0.02	0.03	-0.1 – 0.1	0.00	0.02	0.05	-0.1 – 0.1	0.01	0.05	0.06	-0.6 – 0.7
- Lumbal	-0.02	0.06	0.11	-1.9 – 1.6	0.00	0.02	0.05	-0.1 – 0.3	0.03	0.06	0.11	-1.2 – 1.2

Abbreviations: DoF = Degrees of freedom, SI = superior-inferior, AP = anteroposterior, ML = medial-lateral, IGRT = Image-guided radiotherapy, wj = Wide field junction, SE = Systematic error (defined as the mean of all mean errors), SU = Systematic uncertainty (defined as the standard deviation of all mean errors), RU = Random uncertainty (defined as the root-mean-square deviation for all patients).

B

Papers

71

B.1 STUDY I

Residual positioning errors and uncertainties for pediatric craniospinal irradiation and the impact of image guidance

Authors

Daniel Gram[1,2]*, M.Sc., André Haraldsson[3,4], M.Sc., N. Patrik Brodin[5], Ph.D., Karsten Nysom[6], M.D., Ph.D., Thomas Björk-Eriksson[7,8], M.D., Ph.D., Per Munck af Rosenschöld[3,4,2], Ph.D.

Affiliations

[1] Department of Oncology – Section of Radiotherapy, Rigshospitalet, Copenhagen, Denmark

[2] Niels Bohr Institute, University of Copenhagen, Copenhagen, Denmark

[3] Radiation Physics - Department of Hematology, Oncology and Radiation Physics, Skåne University Hospital, Lund, Sweden

[4] Medical Radiation Physics, Department of Clinical Sciences, Lund University, Lund, Sweden

[5] Institute for Onco-Physics, Albert Einstein College of Medicine and Montefiore Medical Center, Bronx, NY, USA

[6] Department of Paediatrics and Adolescent Medicine, The Juliane Marie Center, Rigshospitalet, Copenhagen, Denmark

[7] Department of Oncology, Institute of Clinical Sciences, Sahlgrenska Academy at the University of Gothenburg, Sweden

[8] Regional Cancer Centre West, Gothenburg, Sweden

Running Title: Residual positioning errors in pediatric CSI

Keywords

Positioning errors

Positioning uncertainties

Residual setup errors

Craniospinal irradiation

Image guidance

*Corresponding author: dgas0002@regionh.dk, +4535458922

Department of Oncology – Section of Radiotherapy 3993/3994, Rigshospitalet, Belgdamsvej 9, DK-2100 Copenhagen, Denmark

1

Abstract

Background

Optimal alignment is of utmost importance when treating pediatric patients with craniospinal irradiation (CSI), especially with regards to field junctions and multiple isocenters and techniques applying high dose gradients. Here, we investigated the setup errors and uncertainties for pediatric CSI using different setup verification protocols.

Methods

A total of 38 pediatric patients treated with CSI were identified for whom treatment records and setup images were available. The setup images were registered retrospectively to the reference image using an automated tool and matching on bony anatomy, subsequently, the impact of different correction protocols was simulated.

Results

For an action-level (AL)-protocol and a non-action level (NAL)-protocol, the translational residual setup error can be as large as 24 mm for an individual patient during a single fraction, and the rotational error as large as 6.1°. With daily IGRT, the maximum setup errors were reduced to 1 mm translational and 5.4° rotational versus 1 mm translational and 2.4° rotational for 3- and 6- degrees of freedom (DoF) couch shifts, respectively. With a daily 6-DoF IGRT protocol for a wide field junction irradiation technique, the residual positioning uncertainty was below 1 mm and 1° for translational and rotational directions, respectively. The largest rotational uncertainty was found for the patients' roll even though this was the least common type of rotational error, while the largest translational uncertainty was found in the patients' anterior-posterior-axis.

Conclusions

These results allow for informed margin calculation and robust optimization of treatments. Daily IGRT is the superior choice for setup of pediatric patients treated with CSI, although centers that do not have this option could use the results presented here to improve their margins and uncertainty estimates for a more accurate treatment alignment.

Background

Second only to leukemia, primary tumors in the central nervous system (CNS) are the most common malignancies in children [1]. The treatment usually consists of surgery, chemotherapy and irradiation, depending on age and tumor-related risk factors. When treating pediatric patients with CNS tumors it is of utmost importance that the patients are optimally aligned since this anatomical region contains many organs-at-risk (OARs) and since the developing brain is particularly vulnerable to the long-term toxicities of radiotherapy. Recently, studies investigating hippocampal-sparing cranial irradiation including craniospinal irradiation (CSI) for patients with medulloblastoma have emerged in order to minimize the common, treatment related, neurocognitive side effects [2,3]. When trying to avoid an important OAR such as the hippocampus, the importance of accurate alignment become even more apparent.

Setup corrections have typically been based on off-line setup images obtained from skin-mark based positioning protocols including different action level (AL)-protocols and non-action level (NAL)-protocols during the initial fractions of the treatment schedule [4,5]. Recently, setup correction decisions have changed from being based on AL/NAL-protocols to daily pre-treatment image-guided radiotherapy (IGRT) [6].

Setup uncertainties have been extensively studied in photon radiotherapy for various treatment sites [7-20]. Lately, proton radiotherapy has emerged as a prominent alternative to photon therapy for pediatric CSI and today, both treatment modalities are relevant when studying residual errors and uncertainties. For example, as setup errors will result in different dose distributions for photon treatments, they may cause even worse distortions of the dose distributions for proton therapy, due to the misalignment of the beams and the sensitivity to varying tissue densities [21,22].

In this multicenter study we investigated the setup errors for pediatric patients undergoing CSI by following image-guided correction protocols and explored how AL/NAL-protocols and daily IGRT impact the positioning uncertainty. These positioning uncertainty data may be used to estimate an uncertainty budget available for planning target volumes (PTV) and OAR margins as well as estimating criteria for robust optimization[23], which are essential components for the safe implementation of CSI for pediatric patients.

Methods

All patients ≤20 years at the time of treatment who received CSI (Childhood centers, oncology and radiotherapy departments from both Denmark and Sweden) between 2005 and 2018 were reviewed in accordance with approval from The Danish Patient Safety Authority and The Danish Data Protection Agency. A total of 38 eligible patients were identified, for whom treatment records and setup images (a minimum of the first four consecutive fractions were required for inclusion, up to all 20 fractions) were available, and included in the analysis (Table 1 provides the patients' characteristics).

3

Table 1: Characteristics of the 38 pediatric and adolescent patients included in the study. The number of fractions was 13 or 20 depending on tumor-related risk factors and are prescribed 1.8 Gy / fraction to either 23.4 Gy or 36 Gy to the craniospinal volume.

	Median	Range
Age (y)	8	4 - 19
Sex	n	%
Male	25	65.8
Female	13	34.2
Position		
Supine	35	92.1
Prone	3	7.9
Treatment fractions		
13	30	78.9
20	8	21.1
Anesthesia		
Yes	25	65.8
No	13	34.2
Isocenters		
1	20	52.6
2	6	15.8
3	12	31.6
Treatment unit		
Linac	18	47.4
3D-CRT	15	83.3
kV	13	86.7
MV	2	13.3
IMRT	3	16.7
kV	3	100
Tomo	20	52.6
Disease		
Medulloblastoma	21	55.3
Ependymoma	3	7.9
Germinoma	2	5.3
Astrocytoma gr. 2	2	5.3
Other	9	23.6
Unknown	1	2.6
	Mean	SD
Field length (cm)	65.2	10.7
BMI (Z-score)	0.07	2.0

Abbreviations: BMI = Body mass index, Tomo = Tomotherapy, Linac = Linear accelerator

The pediatric patients were setup according to the clinical procedure using image verification, in which only the three-dimensional couch corrections ("3- degrees of freedom, DoF") were used for positioning these patients during treatment, ignoring the rotational deviations. The most common patient immobilization

was a full body vacuum bag with a head mask together with a mouthpiece. Over the years, the immobilization was slightly adjusted since the patients were treated over the course of 13 years. The patients were aligned to wall mounted lasers followed by x-ray images taken at each isocenter and a shift was applied using a mean correction based on the images. New images were taken before the treatment at each isocenter. For the tomotherapy unit, a single full body scan was used for positioning of the patients.

For the current study, the setup images used for positioning were reanalyzed in order to estimate the set-up uncertainty of the patients, according to previously published methods; van Herk [24] and Kutcher et al. [7]. The positioning deviations quantified using the image data may be small and a correction may have been deemed unnecessary to perform clinically. We reexamined all the setup images and they were retrospectively registered to the reference image(s) using an automatic matching procedure based on bony anatomy. The match box volume of interest was set to cover the cranium, and the first two cervical vertebrae, ignoring as much as possible of the chin for the cranial isocenter while for the thoracic and lumbar isocenters, the spine was covered, omitting the top and bottom vertebrae. For the tomotherapy unit, the volume of interest was focused around the isocenter (thoracic region), however still trying to match the entire craniospinal volume. The different image modalities used were mega-voltage computed tomography (MVCT) for Tomotherapy and either kilo-voltage (kV) cone-beam computed tomography (CBCT) or planar kV/MV images using the on-board imaging device or electronic portal imaging device, respectively, for linear accelerators (Offline Review – multi-modality image review, ARIA™ Oncology Information System v. 13.7, Varian medical systems, Palo Alto, CA, USA and CTrue™, Accuray Inc., Madison, WI, USA). A 3- and 6-DoF match was performed, respectively, using both translational (superior-inferior (SI), anterior-posterior (AP) and medial-lateral (ML)) and rotational (yaw = rotation around the AP axis, pitch = rotation around the ML axis and roll = rotation around the SI axis) information. Using the image registration procedure, we calculated the mean correction, residual error and standard deviation (SD) for each patient. The mean correction is defined as the correction used in AL -protocols while the residual error is the mean discrepancy between the clinically applied and ideal registrations (found through retrospective matching) for all fractions for a single patient. Similar to van Herk [24] and Kutcher et al. [7], we used the data available to derive the systematic error (SE), systematic uncertainty (SU) and random uncertainty (RU) for all patients. The SE was calculated by taking the average mean residual error for all patients over their entire treatment and should thus be close to zero unless there is a systematic deviation affecting the procedure (e.g. misaligned lasers or similar). The SU and RU were calculated through the SD of the mean errors for all patients and the root mean square of the SD for all patients, again over the entire treatment, respectively.

Patient characteristics analyzed included the total length of the treatment field, body mass index (BMI, calculated at the start of treatment), age at treatment, sex, patient positioning (prone or supine), number of isocenters (these are associated with treatment modality, Tomotherapy patients had one isocenter while patients treated on linear accelerators had multiple isocenters) and whether the patient was treated under general anesthesia or not (Table 1). The majority of the younger aged (<10y) children were treated with a single isocenter. Since BMI of children and adolescents varies considerably with sex and age, the BMI was expressed as Z-scores [25], calculated according to previously published methods [26,27].

Using the positioning uncertainty data, we simulated four image guidance correction protocols; (1) an AL (based on the first three fractions with online corrections, followed by an isocenter shift according to the

5

average deviation), (2) a NAL (based on the first three fractions without online corrections, followed by an isocenter shift according to the average deviation), (3) daily IGRT protocol for narrow field junctions (nj) and (4) daily IGRT for wide field junctions (wj). Each protocol was simulated for image guidance with a 3-DoF and 6-DoF couch. We refer to "nj" as a treatment protocol with narrow field junctions and sharp dose gradients, i.e. where the field positions cannot be altered in the cranio-caudal direction without the risk of introducing considerable hot- or cold-spots in the dose distribution. For this protocol, no change in longitudinal position was allowed between isocenters. The "wj" protocol refers to the situation where wide field junctions and flat dose gradients are optimized to be overlapping, thus, dosimetric consequences of uncertainties in the cranio-caudal directions will be very small. For example, a narrow field junction can have a sharp dose gradient corresponding to 5% of the prescribed dose / mm deviation in the SI direction which corresponds to 1.8 Gy for a prescribed dose of 36 Gy with only a single millimeter misalignment. The flat dose gradient emanating from the wide field junction may have the equivalent of around 0.6% / mm deviation. The wide field junctions and flat dose gradients are usually obtainable using more modern techniques such as volumetric modulated arc therapy (VMAT) and intensity modulated proton therapy (IMPT), while the narrow junctions and sharp dose gradients are the result of three-dimensional conformal radiotherapy. Consequently, all available degrees of freedom were applied for this protocol. All simulations were performed based on the protocols previously described where all relevant shifts and corrections were applied to the images before the residual errors were assessed and the uncertainties were subsequently calculated.

Statistical analysis

The normality and linearity assumptions for the association between patient characteristics and residual errors were tested with Shapiro-Wilk tests and visual inspection of histograms and scatter plots. Data for positioning uncertainties for the different image-guided protocols were evaluated against pre-treatment image setup data and univariate linear regression models were fitted for the various positioning uncertainties and residual errors using all covariates. Bivariate associations between all patient characteristics (age, sex, position, anesthesia, number of isocenters, field length and BMI) and the positioning uncertainties and residual errors where quantified with Spearman's rank correlation coefficients or Wilcoxon's rank-sum tests for continuous and categorical variables, respectively.

Since the variance of each isocenter for all cardinal directions is assumed to be the same (based on a two-sample F-test that did not reject the null hypothesis that the samples comes from normal distributions and the same variance (p = 0.054 – 0.799)), this data is pooled to increase the statistical power of the comparison.

Results

Residual setup errors

The residual errors should only include rotational deviation since translational errors were corrected at treatment. However, rotational errors can affect the translational deviation as well. The SE was found to be well below 0.1 mm in all cardinal directions, for both 3-DoF and 6-DoF for the pooled data.

6

Translational positioning deviations greater than 1 cm occurred in 6% of all fractions and 33% of the patients had at least one such correction while rotational deviations greater than 1° occurred in 34% of all fractions and 80% of the patients had at least one such correction. The majority of the residual setup errors were found for the lumbar isocenter. Every patient in this study had at least one deviation larger than the PTV margin (SI=10mm, AP=12mm, ML=18mm) used for these patients and constituted therefore a geometric miss for all patients treated, not using a daily IGRT-protocol.

With an AL/NAL-protocol, the translational residual setup error was found to be as high as 2.4 cm for an individual patient during a single fraction, and the rotational error as high as 6.1°. If using daily IGRT the maximum setup error was reduced to 0.1 cm translational and 5.4° rotational and 0.1 cm translational and 2.4° rotational setup error for 3- and 6-DoF couch shifts, respectively (using maximum allowed pitch and roll correction of 3°).

There were no statistically significant correlations between the residual setup errors with gender and setup (prone/supine) position. We found moderate to strong positive correlations for total field length ($r = 0.5$ $p = 0.04$) and ($r = 0.6$ $p < 0.001$) for residual setup error and standard deviation, respectively, i.e. a longer total field length correlated with a larger residual setup error and standard deviation. For Linac-based multiple isocenter treatments, this presents an issue for standardizing margins where corrections in the SI direction cannot be applied after the first isocenter(s) position has been treated. The IGRT (nj) protocol eliminated correlations in all directions except SI while the IGRT (wj) protocol eliminated all significant correlations and relationships. Fewer isocenters were correlated with a lower mean residual setup error.

Setup uncertainties

When correcting the shifts according to any of the imaging protocols, large inter-fractional deviations occurred especially for rotational deviations (the uncertainties presented in table 2 and figures 1 and 2 illustrates the tendencies, with a larger uncertainty for larger deviations). The uncertainties for the pooled isocenters and all cardinal directions for all imaging protocols are presented in table 2 and figures 1 and 2. The largest rotational uncertainty was found for the patients' roll, even though this was the least common type of rotational error, while the largest translational uncertainty was found in the patients' AP-axis.

7

Table 2: Systematic uncertainty (SU), as calculated by the mean, and random uncertainty (RU), as calculated by the root mean square deviation, for all imaging protocols, both 3- and 6- degrees of freedom (DoF) and all isocenters pooled (Units: cm and °/degrees). Bold numbers indicate statistically significant difference compared to skin-mark based setup.

3DoF	SI		AP		ML	
	SU	RU	SU	RU	SU	RU
Translational						
- IGRT (nj)	0.18	0.26	**0.03**	**0.05**	**0.03**	**0.05**
- IGRT (wj)	**0.02**	**0.05**	**0.03**	**0.05**	**0.03**	**0.05**
- Skin	0.20	0.27	0.18	0.27	0.12	0.23
- AL	0.20	0.26	0.13	0.22	0.07	0.20
- NAL	0.18	0.32	0.09	0.28	0.07	0.24

6DoF	SI/Roll		AP/Yaw		ML/Pitch	
	SU	RU	SU	RU	SU	RU
Translational						
- IGRT (nj)	0.15	0.26	**0.02**	**0.05**	**0.02**	**0.05**
- IGRT (wj)	**0.02**	**0.05**	**0.02**	**0.05**	**0.02**	**0.05**
- Skin	0.20	0.26	0.19	0.31	0.14	0.27
- AL	0.15	0.26	0.14	0.26	0.09	0.24
- NAL	0.13	0.31	0.11	0.32	0.09	0.29
Rotational						
- IGRT (nj)	**0.02**	**0.12**	0.22	0.66	**0.04**	**0.14**
- IGRT (wj)	**0.02**	**0.12**	**0.02**	**0.05**	**0.04**	**0.14**
- Skin	0.39	0.91	0.27	0.67	0.42	0.86
- AL	0.37	0.87	0.25	0.66	0.39	0.79
- NAL	0.31	1.10	0.22	0.74	0.38	0.88

Abbreviations: DoF = Degrees of freedom, SI = Superior-inferior, AP = Anteroposterior, ML = Medial-lateral, SU = Systematic uncertainty, RU = Random uncertainty, IGRT = Image-guided radiotherapy, nj = Narrow field junction, wj = Wide field junction, AL = Action level, NAL = Non-action level

There were no statistically significant correlations between uncertainties with gender and setup position. We found that a higher BMI correlated with a larger SU in the SI direction ($r = 0.35 – 0.46$, $p = 0.008 – 0.04$) but not in the other cardinal directions. The number of isocenters, age and anesthesia showed weak to moderate correlations ($r = -0.63 – 0.45$, $p = 0.008 – 0.02$). Younger children are usually treated under general anesthesia and we found that being under general anesthesia could reduce the setup uncertainties in the SI direction since there were smaller deviations for these patients ($r = -0.39 – -0.19$, $p = 0.02 – 0.46$).

If a daily 6-DoF IGRT (wj) protocol was used, the residual systematic positioning uncertainty was 0.2 – 0.3 mm and 0.02 – 0.04° for translational and rotational directions, respectively. The residual random positioning uncertainty was 0.5 mm and 0.05 – 0.14° for translational and rotational directions, respectively. This is significantly smaller than for the corresponding 1.2 – 2.0 mm and 0.3 – 0.4° (p = 0.03, based on mean values) systematic uncertainties and 2.3 – 3.1 mm and 0.7 – 0.9° (p = 0.03) random uncertainties, when using only the skin-marks for setup. Both AL- and NAL-protocols with 6-DoF had lower uncertainties compared to only using skin-marks, but the results were not statistically significant ($p = 0.06$, $p = 0.41$, respectively) with similar results for 3-DoF.

Since the data stem from patients treated over the course of 13 years, both immobilization and imaging strategies have changed throughout. A vacuum bag with a mask and/or a mouthpiece was the most common immobilization type and the immobilization changes were conjecturally inconsiderable. However, the setup images revealed that patients treated in the earlier years were more accurately positioned to the skin-marks compared to the patients treated later in the cohort. No other time-trends were observed.

Rotational uncertainties are generally more considerable than translational (Table 2 and figure 1 – 4), and the effect of rotational uncertainty peaks farthest away from the isocenter and rapidly decreases closer to it. Typically, the largest uncertainties were found to be in the SI direction or around the SI direction (roll). The single largest deviation was found to be 9.6° for the roll rotation around the SI-axis for a NAL-protocol.

Documents for machine quality assurance for the last 5 years were assessed and all radiation isocenter vs imaging isocenter agreements were within 1 mm.

9

a) Mean residual setup error for skin-marks and each cardinal direction

b) Mean residual setup error for AL and each cardinal direction

c) Mean residual setup error for NAL and each cardinal direction
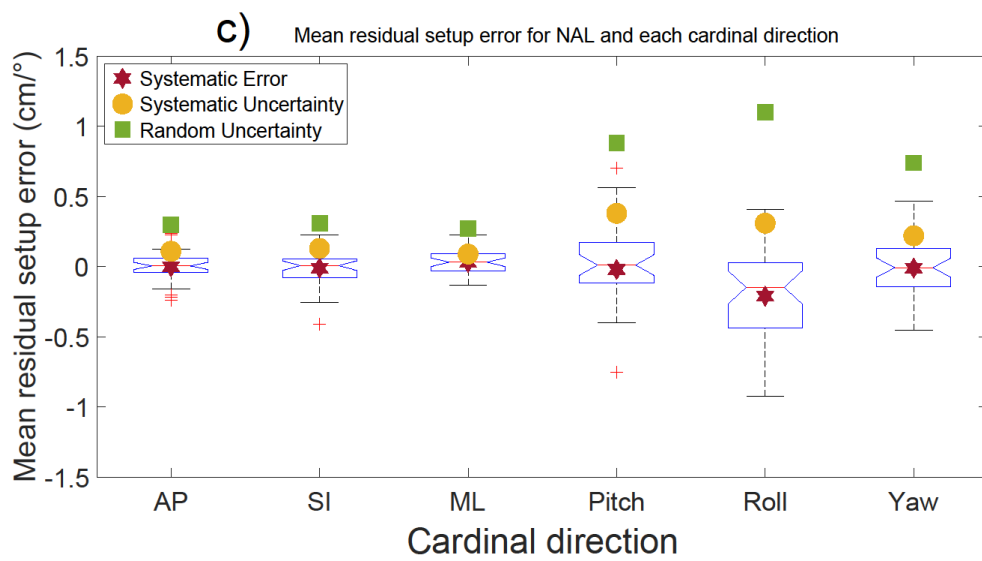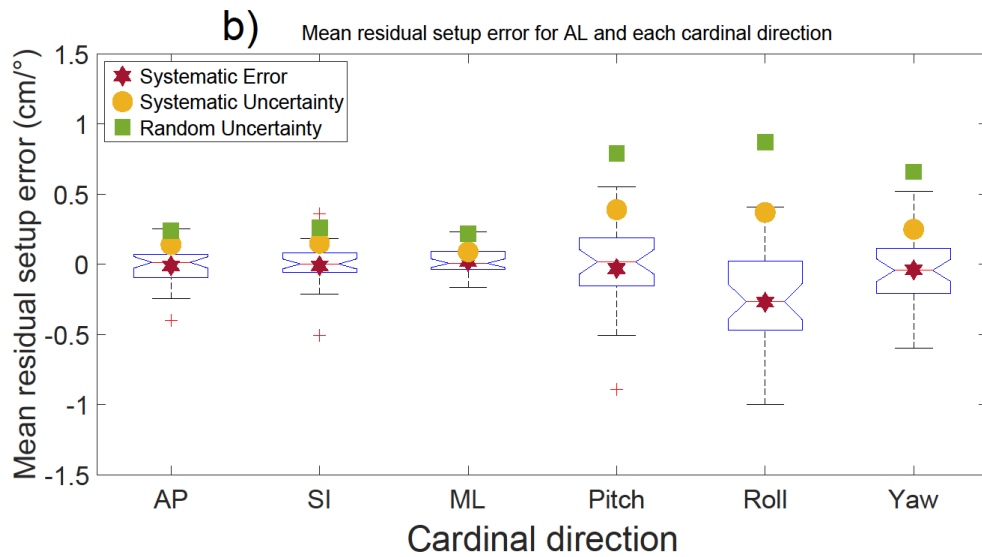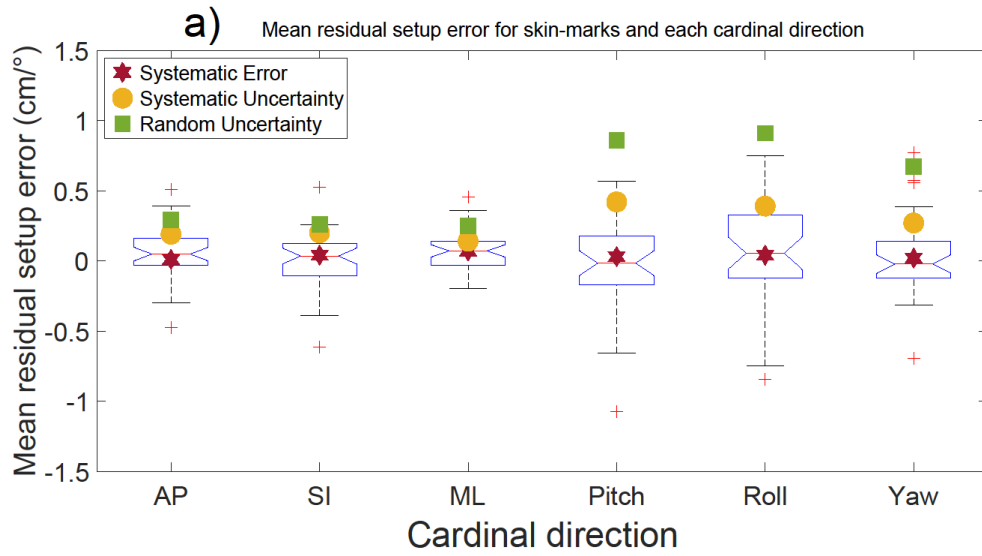
10

*Figure 1: Mean setup error(mm) presented with blue notched boxplots for **a)** skin-marks, **b)** AL-protocol and **c)** NAL-protocol and all six cardinal directions examined. The boxplots show the median (central red line), 25th and 75th percentile (blue notched box) and the whiskers (black dashed lines) which extend to the most extreme data points that are considered non-outliers. The individually plotted red plus signs indicate the outliers. Please note that the plots are showing two different dimensions (cm and °).*
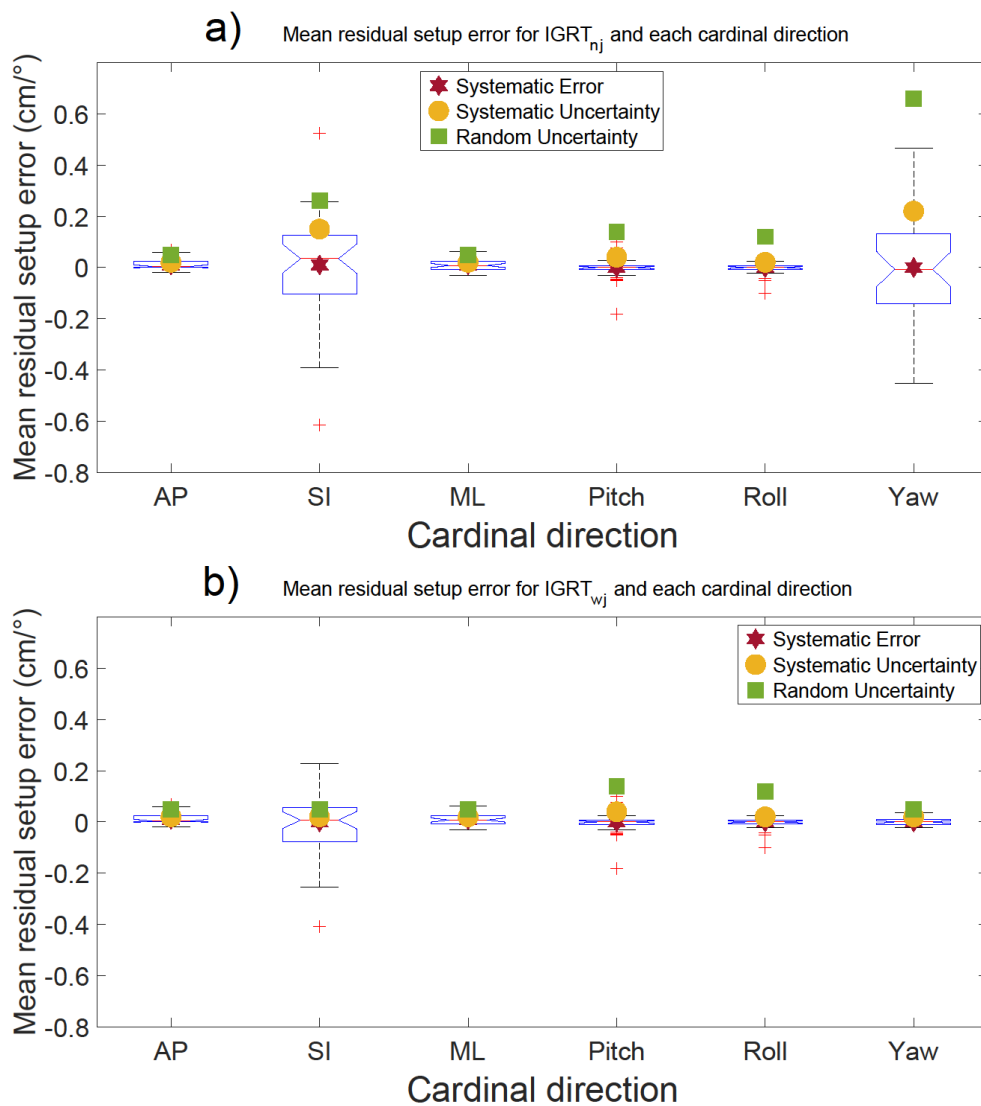

*Figure 2: Mean setup error(mm) presented with blue notched boxplots for **a)** IGRT (nj)-protocol and **b)** IGRT (wj)-protocol and all six cardinal directions examined. The boxplots show the median (central red line), 25th and 75th percentile (blue notched box) and the whiskers (black dashed lines) which extend to the most extreme data points that are considered non-outliers. The individually plotted red plus signs indicate the outliers. Please note that the plots are showing two different dimensions (cm and °).*

11

a) Standard deviation for skin-marks and each cardinal direction

b) Standard deviation for AL and each cardinal direction

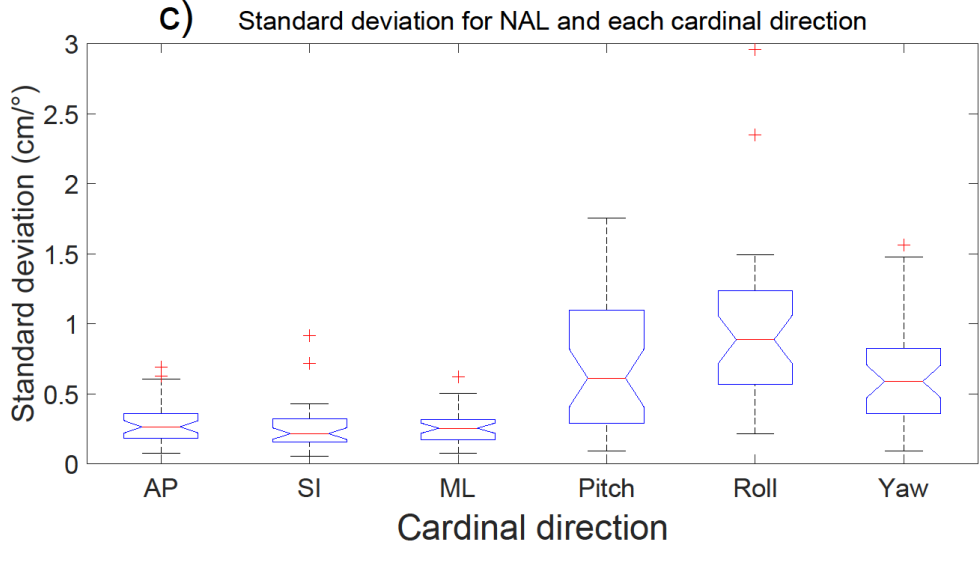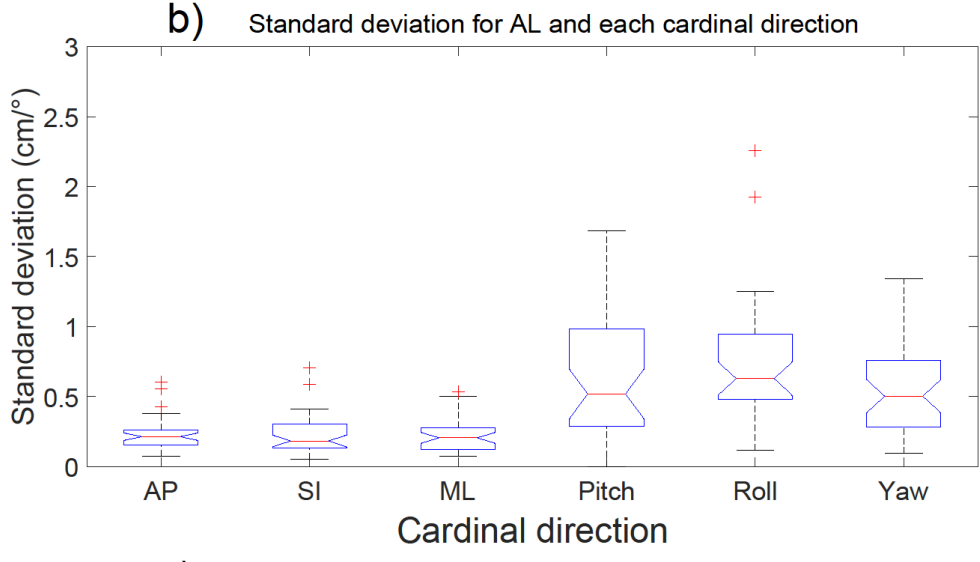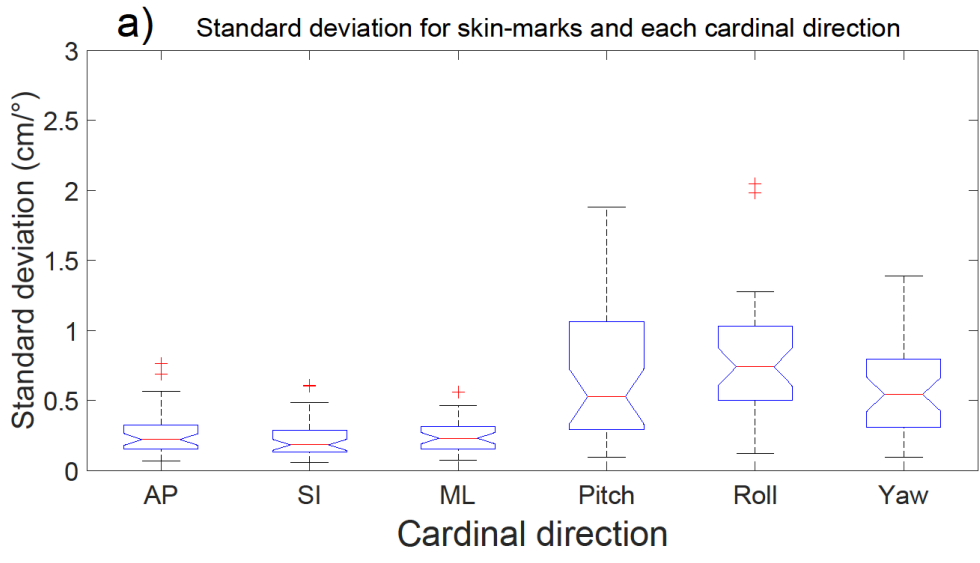c) Standard deviation for NAL and each cardinal direction

12

*Figure 3: Standard deviation (mm) presented with blue notched boxplots for **a)** skin-marks, **b)** AL-protocol and **c)** NAL-protocol and all six cardinal directions examined. The boxplots show the median (central red line), 25th and 75th percentile (blue notched box) and the whiskers (black dashed lines) which extend to the most extreme data points that are considered non-outliers. The individually plotted red plus signs indicate the outliers. Please note that the plots are showing two different dimensions (cm and °).*

*Figure 4: Standard deviation (mm) presented with blue notched boxplots for **a)** IGRT (nj)-protocol and **b)** IGRT (wj)-protocol and all six cardinal directions examined. The boxplots show the median (central red line), 25th and 75th percentile (blue notched box) and the whiskers (black dashed lines) which extend to the most extreme data points that are considered non-outliers. The individually plotted red plus signs indicate the outliers. Please note that the plots are showing two different dimensions (cm and °).*
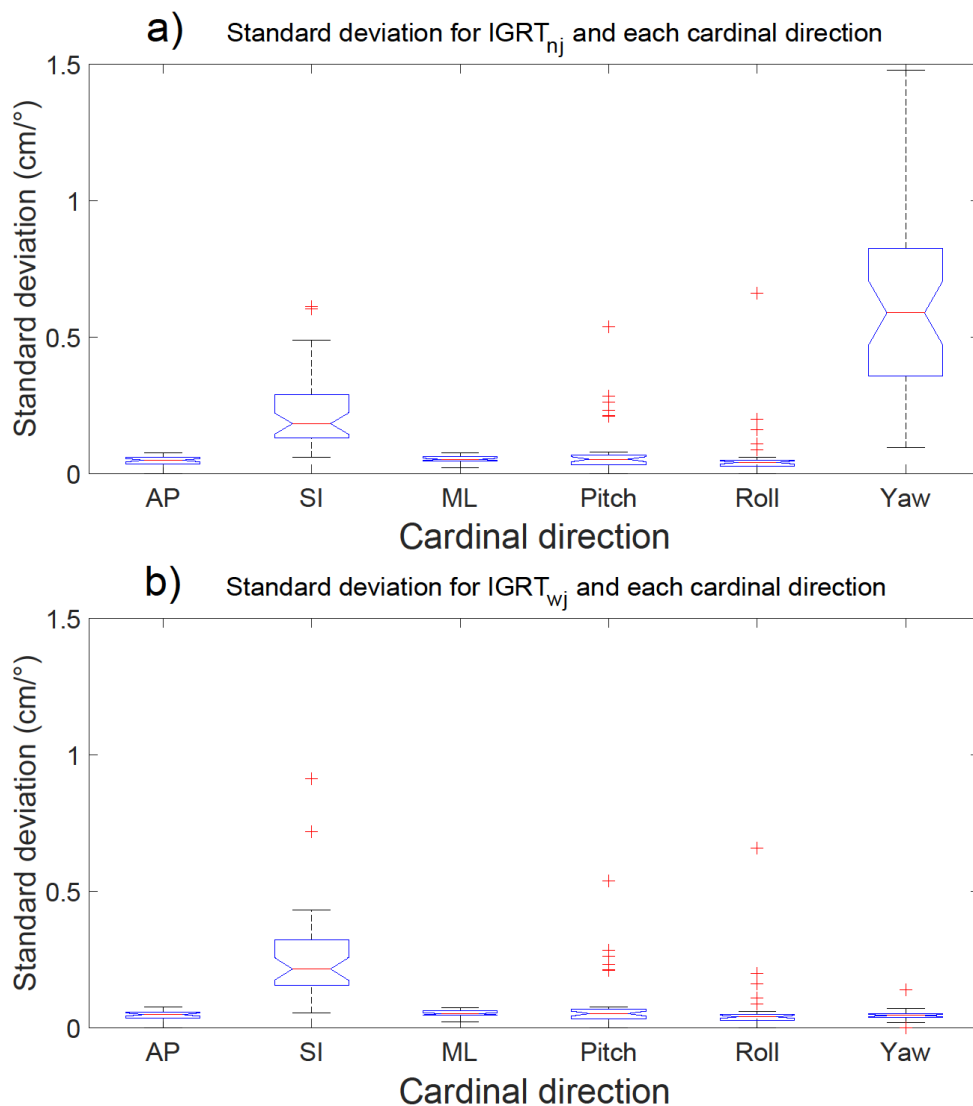
13

Discussion

In this study we mainly provide the uncertainties that stem from setup images as there are a wide variety of treatment and imaging units, many with different inherent uncertainties. With these results we hope that clinics providing pediatric CSI will have a possibility to personalize the treatment margins regardless of imaging protocol or number of isocenters in use. Important to note when calculating margins for CSI treatments is that different margin strategies in respect to inter-fractional effects of the organ or structure the margin is based on, e.g. spinal column length, need to be considered. These results could also act as a reference to older methods or when comparing setup verification technique. To the authors' knowledge, this is the first analysis dealing with positioning uncertainties based solely on pediatric CSI treatments.

According to our results, the random uncertainty increases by using a NAL-protocol to correct for the couch shifts. This could, however, be because the correction merely shifts the scatter of the corrected points (where each point is a patient's fraction) whilst still using the two starting points (that were not corrected for in a NAL-protocol) when calculating the RU. If the starting points were removed from the calculation, there was a minimal increase in RU by using a NAL-protocol for some directions and isocenters (both pooled and un-pooled data), it was, however, not statistically significant. There is also a small general decrease in RU when removing the starting points which could be an indication that some of the most extreme correction values tend to occur in the first couple of fractions.

It is important to keep in mind that there are two different types of uncertainties with different sources. The random component of the uncertainties is inter-fractional and stem from positioning on external markers on either the patient's skin or mask or due to internal motion relative to the external markers. The systematic component stems from events such as changes in patient anatomy over the course of treatment or mechanical mismatches between CT simulation and the treatment machine. There can still be quite large errors even if using a daily IGRT-protocol since there is a 3° physical restraint (maximum allowed couch movement in clinical treatment mode) on the couch. Shifts larger than this should trigger a re-positioning of the patient but since we do not have access to the specific circumstances for each treatment fraction, we were restricted to analyzing only the setup images in this study.

Previous studies have developed widely used algorithms for calculating margins [28,29] and there are multiple alternatives, reported by van Herk [24]. With these algorithms standardized or personalized margins can be calculated. We also wanted to supply information for both narrow- and wide field junctions irradiation techniques, since some centers that use conformal techniques do not allow for imaging-based corrections in the SI direction, and simply apply the planned SI isocenter shift, after treating the first isocenter due to narrow field junctions and steep dose gradients. Most IMPT centers have that option since the wide junctions and more flat dose gradients often result in a smaller dose difference compared to incorrect heterogeneity correction arising from positional errors [21,23]. This might also explain some of the effects seen in the SI direction. It is important to note that there could be variations in the relative distance between isocenters (Linac patients with multiple isocenters) which can lead to large differences between the expected and actual dose distribution if an IGRT protocol is used to correct the shift in all directions without considerations to the junction. One would also expect that the yaw would contribute largely to the uncertainties in the SI direction, but this is not supported by our results. Hadley et al. [30] studied the effect of a wide single gradient dose junction using intensity modulated radiotherapy for spinal

14

fields which is similar to the technique utilized by many proton centers. They found that this improved uncertainties for spinal fields compared to narrow multiple junction shifts. The patients with longer field lengths appear to be the most relevant for a closer examination of the margins (mainly for the lumbar isocenter) or alternatively, a more comprehensive imaging protocol can be applied for these patients, such as daily IGRT. Based on our results, IGRT generally, and IGRT (wj) specifically is the superior choice for these patients. Centers that do not have this option should investigate their margins according to these uncertainties, especially for longer field lengths and higher number of isocenters.

Like previous studies [31,32], we found that applying any type of imaging protocol reduces the uncertainties and residual setup errors compared to only using skin-marks for patient alignment. This difference was smaller for patients treated in the earlier years. Both imaging protocols and immobilizations have changed over the years, which affects this trend. In the era of daily image guidance, the difference might also originate from less time being spent on patient alignment when a verification image is pending.

When investigating the isocenters individually, the positioning errors and uncertainties found in this study are comparable to previously published research for other sites [8,13-15]. Al-Wassia et al. [33] studied the effect of a 3-DoF couch correction, and found uncertainties that were substantially lower than ours for the single isocenter treatment. Their maximum mean deviation, in any direction, was found to be 6 mm while ours was 24 mm. Our results were, however, comparable to other similar studies investigating errors, uncertainties and margins for craniospinal treatments [34-36]. Stoiber et al. [34] found a maximum deviation of 18 mm and 10 °, again compared to our 24 mm and 9.6 °. Gupta et al. [35] found a maximum deviation of 20 mm. Interestingly, Thondykandy et al. [36] found the SU to be larger than the RU for CSI while our results show the opposite. The SE was investigated as an additional control to check that there were no systematic setup errors occurring in our imaging that potentially could bias the results, and indeed we found a SE close to zero.

Conclusions

Our results show that daily IGRT substantially reduces setup uncertainties for pediatric CSI patients. Following a daily IGRT-protocol does, however, not guarantee satisfactory alignment when only a 3-DoF couch shift is applied. There are still quite large residual errors, some of which are the result of using multiple isocenters and narrow field junctions even if a 6-DoF couch shift would be applied. In conclusion, daily IGRT is the superior choice for setup of pediatric craniospinal patients, however, for centers that do not have this option, these results could be used to improve their margins and uncertainties for a more accurate treatment or used as a reference when comparing setup verification techniques.

Abbreviations

CSI	Craniospinal irradiation
IGRT	Image-guided radiotherapy
AL	Action-level
NAL	Non-action level
DoF	Degrees of freedom
CNS	Central nervous system
OARs	Organs-at-risk
PTV	Planning target volume
MVCT	Mega-voltage computed tomography
kV	Kilo-voltage
CBCT	Cone-beam computed tomography
SI	Superior-inferior
AP	Anterior-posterior
ML	Medial-lateral
SD	Standard deviation
SE	Systematic error
SU	Systematic uncertainty
RU	Random uncertainty
BMI	Body mass index
nj	Narrow field junctions
wj	Wide field junctions
VMAT	Volumetric modulated arc therapy
IMPT	Intensity modulated proton therapy

16

References

1. Lannering B, Sandström P-E, Holm S, et al. Classification, incidence and survival analyses of children with CNS tumours diagnosed in Sweden 1984-2005. Acta Paediatrica. 2009;98(10):1620-1627.
2. Blomstrand M, Brodin NP, Munck Af Rosenschold P, et al. Estimated clinical benefit of protecting neurogenesis in the developing brain during radiation therapy for pediatric medulloblastoma. Neuro Oncol. 2012 Jul;14(7):882-9.
3. Brodin NP, Munck af Rosenschold P, Blomstrand M, et al. Hippocampal sparing radiotherapy for pediatric medulloblastoma: impact of treatment margins and treatment technique. Neuro Oncol. 2014 Apr;16(4):594-602.
4. Craig T, Sharpe M, Haycocks T, et al. Comparison Of Correction Protocols for Image-Guided Radiation Therapy. International Conference on Medical Image Computing and Computer-Assisted Intervention. 2003;November:264-270.
5. Bortfeld T, van Herk M, Jiang SB. When should systematic patient positioning errors in radiotherapy be corrected. Phys Med Biol. 2002;47(23):N297-N302.
6. Das S, Liu T, Jani AB, et al. Comparison of image-guided radiotherapy technologies for prostate cancer. Am J Clin Oncol. 2014 Dec;37(6):616-23.
7. Kutcher GJ, Mageras GS, Leibel SA. Control, Correction, and Modeling of Setup Errors and Organ Motion. Seminars in Radiation Oncology. 1995;5(2):134-145.
8. Munck af Rosenschold P, Desai NB, Oh JH, et al. Modeling positioning uncertainties of prostate cancer external beam radiation therapy using pre-treatment data. Radiother Oncol. 2014 Feb;110(2):251-5.
9. Aristophanous M, Chi PM, Kao J, et al. Deep-Inspiration Breath-Hold Intensity Modulated Radiation Therapy to the Mediastinum for Lymphoma Patients: Setup Uncertainties and Margins. Int J Radiat Oncol Biol Phys. 2018 Jan 1;100(1):254-262.
10. Han C, Schiffner DC, Schultheiss TE, et al. Residual setup errors and dose variations with less-than-daily image guided patient setup in external beam radiotherapy for esophageal cancer. Radiother Oncol. 2012 Feb;102(2):309-14.
11. Crook JM, Raymond Y, Salhani D, et al. Prostate motion during standard radiotherapy as assessed by fiducial markers. Radiother Oncol. 1995;37:35-42.
12. Yu Y, Michaud AL, Sreeraman R, et al. Comparison of daily versus nondaily image-guided radiotherapy protocols for patients treated with intensity-modulated radiotherapy for head and neck cancer. Head Neck. 2014 Jul;36(7):992-7.
13. Kershaw L, van Zadelhoff L, Heemsbergen W, et al. Image Guided Radiation Therapy Strategies for Pelvic Lymph Node Irradiation in High-Risk Prostate Cancer: Motion and Margins. Int J Radiat Oncol Biol Phys. 2018 Jan 1;100(1):68-77.
14. Hawkins MA, Aitken A, Hansen VN, et al. Set-up errors in radiotherapy for oesophageal cancers--is electronic portal imaging or conebeam more accurate? Radiother Oncol. 2011 Feb;98(2):249-54.
15. Zhou J, Uhl B, Dewit K, et al. Analysis of daily setup variation with tomotherapy megavoltage computed tomography. Med Dosim. 2010 Spring;35(1):31-7.
16. Yang M, Timmerman R. Stereotactic Ablative Radiotherapy Uncertainties: Delineation, Setup and Motion. Semin Radiat Oncol. 2018 Jun;28(3):207-217.
17. Huijskens SC, van Dijk I, Visser J, et al. Abdominal organ position variation in children during image-guided radiotherapy. Radiat Oncol. 2018 Sep 12;13(1):173.
18. Nazmy MS, Khafaga Y, Mousa A, et al. Cone beam CT for organs motion evaluation in pediatric abdominal neuroblastoma. Radiother Oncol. 2012 Mar;102(3):388-92.
19. Beltran C, Krasin MJ, Merchant TE. Inter- and intrafractional positional uncertainties in pediatric radiotherapy patients with brain and head and neck tumors. Int J Radiat Oncol Biol Phys. 2011 Mar 15;79(4):1266-74.

20.   van Dijk I, Huijskens SC, de Jong R, et al. Interfractional renal and diaphragmatic position variation during radiotherapy in children and adults: is there a difference? Acta Oncol. 2017 Aug;56(8):1065-1071.
21.   Lomax AJ. Intensity modulated proton therapy and its sensitivity to treatment uncertainties 2: the potential effects of inter-fraction and inter-field motions. Phys Med Biol. 2008 Feb 21;53(4):1043-56.
22.   Lomax AJ, Pedroni E, Rutz HP, et al. The Clinical Potential of Intensity Modulated Proton Therapy. Zeitschrift für Medizinische Physik. 2004;14(3):147-152.
23.   Tasson A, Laack NN, Beltran C. Clinical Implementation of Robust Optimization for Craniospinal Irradiation. Cancers. 2018;10(1):E7.
24.   van Herk M. Errors and margins in radiotherapy. Semin Radiat Oncol. 2004 Jan;14(1):52-64.
25.   Poskitt EME. Defining childhood obesity - the relative body mass index (BMI). Acta Paediatr. 1995;84:961-963.
26.   Cole TJ, Green PJ. Smoothing reference centile curves - the LMS method and penalized likelihood. Stat Med. 1992;11:1305-19.
27.   Nysom K, Mølgaard C, Hutchings B, et al. Body mass index of 0 to 45-y-old Danes - reference values and comparison with published European reference values. Int J Obes. 2001;25:177-84.
28.   Van Herk M, Remeijer P, Rasch C, et al. The Probability of Correct Target Dosage - Dose-Population Histograms for Deriving Treatment Margins in Radiotherapy. Int J Radiat Oncol Biol Phys. 2000;47(4):1121-35.
29.   Stroom JC, De Boer HC, Huizenga H, et al. Inclusion of Geometrical Uncertainties in Radiotherapy Treatment Planning by Means of Coverage Probability. Int J Radiat Oncol Biol Phys. 1999;43(4):905-19.
30.   Hadley A, Ding GX. A single-gradient junction technique to replace multiple-junction shifts for craniospinal irradiation treatment. Med Dosim. 2014 Winter;39(4):314-9.
31.   de Boer HC, van Os MJ, Jansen PP, et al. Application of the No Action Level (NAL) protocol to correct for prostate motion based on electronic portal imaging of implanted markers. Int J Radiat Oncol Biol Phys. 2005 Mar 15;61(4):969-83.
32.   Bel A, Van Herk M, Bartelink H, et al. A verification procedure to improve patient set-up accuracy using portal images. Radiother Oncol. 1993;29:253-260.
33.   Al-Wassia R, Bahig H, Poon E, et al. Daily setup uncertainty analysis for craniospinal irradiation using helical tomotherapy. Pract Radiat Oncol. 2013 Oct-Dec;3(4):349-55.
34.   Stoiber EM, Giske K, Schubert K, et al. Local setup reproducibility of the spinal column when using intensity-modulated radiation therapy for craniospinal irradiation with patient in supine position. Int J Radiat Oncol Biol Phys. 2011 Dec 1;81(5):1552-9.
35.   Gupta T, Upasani M, Master Z, et al. Assessment of three-dimensional set-up errors using megavoltage computed tomography (MVCT) during image-guided intensity-modulated radiation therapy (IMRT) for craniospinal irradiation (CSI) on helical tomotherapy (HT). Technol Cancer Res Treat. 2015 Feb;14(1):29-36.
36.   Thondykabdy B, Swamidas J, Agarwal J, et al. Setup error analysis in helical tomotherapy based image-guided radiation therapy treatments. J Med Phys. 2015;40(4):233-9.

18

Declarations

Ethics approval and consent to participate

The Danish Patient Safety Authority and The Danish Data Protection Agency approved this study.

Consent for publication

Not applicable

Availability of data and materials

The datasets generated and/or analyzed during the current study are not publicly available due to that individual privacy could be compromised. Some restrictions apply to the availability of this data and parts of the data could become available from the corresponding author on reasonable request and with permission of PMR and KN.

Competing interests

PMR and AH reports research agreement with Accuray Inc. to the department, all outside the submitted work.

Authors' contributions

DG, AH, PB, KN, TBE and PMR contributed to the conception and the design of the study. DG, AH and PB drafted the first version of the manuscript. DG, AH, KN and PMR contributed to the collection of data and data interpretation was performed by DG and PB. All authors contributed critical revision of the manuscript and have reviewed and approved the final version for publication.

19

STUDY II

B.2 STUDY II

The risk of radiation-induced neurocognitive impairment and the impact of sparing the hippocampus during pediatric proton cranial irradiation

Authors

Daniel Gram[1,2]*, M.Sc., N. Patrik Brodin[3], Ph.D., Thomas Björk-Eriksson[4,5], M.D., Ph.D., Karsten Nysom[6], M.D., Ph.D., Per Munck af Rosenschöld[7,8,2], Ph.D.

Affiliations

[1] Department of Oncology – Section of Radiotherapy, Rigshospitalet, Copenhagen, Denmark

[2] Niels Bohr Institute, University of Copenhagen, Copenhagen, Denmark

[3] Institute for Onco-Physics, Albert Einstein College of Medicine and Montefiore Medical Center, Bronx, NY, USA

[4] Department of Oncology, Institute of Clinical Sciences, Sahlgrenska Academy at the University of Gothenburg, Sweden

[5] Regional Cancer Centre West, Gothenburg, Sweden

[6] Department of Paediatrics and Adolescent Medicine, The Juliane Marie Center, Rigshospitalet, Copenhagen, Denmark

[7] Radiation Physics - Department of Hematology, Oncology and Radiation Physics, Skåne University Hospital, Lund, Sweden

[8] Medical Radiation Physics, Department of Clinical Sciences, Lund University, Lund, Sweden

*Corresponding author: dgas0002@regionh.dk, +4535458922

Department of Oncology – Section of Radiotherapy 3993/3994, Rigshospitalet, Belgdamsvej 9, DK-2100 Copenhagen, Denmark

Highlights

- Hippocampal sparing (HS) IMPT for medulloblastoma patients can be constructed using realistic positioning uncertainty estimates and robust treatment planning methods
- We provide estimates of potential benefit of clinically realistic and robust HS IMPT regarding neurocognitive impairment as compared to standard radiotherapy
- In this simulation study, HS IMPT considerably reduced predicted neurocognitive adverse effects with marginal effect to target coverage and estimated tumor control probability

Abstract

Background and purpose:

Hippocampus is a central component for neurocognitive function and memory. We investigated the predicted risk of neurocognitive impairment from the cranial part, including boost, of craniospinal irradiation (CSI) and the deliverability and effects of hippocampal sparing. Specifically, we leveraged the estimated benefit of reduced neurocognitive impairment with the risk of reduced tumor control.

Material and methods:

A total of 504 hippocampal sparing intensity modulated proton therapy (HS-IMPT) plans were generated for 24 pediatric patients whom had previously received CSI. Plans were evaluated with respect to target coverage and homogeneity index to target volumes, maximum and mean dose to OARs. Paired t-tests were used to compare hippocampal mean doses and normal tissue complication probability estimates.

Results:

The median mean dose to the hippocampus could be reduced from 31.3 Gy$_{RBE}$ to 7.3 Gy$_{RBE}$ (p<0.001), though 20% of these plans were not considered clinically acceptable. Reducing the median mean hippocampus dose to 10.6 Gy$_{RBE}$ was possible with all plans passing clinical acceptance criterion. By sparing the hippocampus to the lowest dose level, the risk estimation of neurocognitive impairment could be reduced from 89.6%, 62.1% and 51.1% to 41.0% (p<0.001), 20.1% (p<0.001) and 29.9% (p<0.001) for task efficiency, organization and memory, respectively. Estimated tumor control probability was not adversely affected by HS-IMPT, ranging from 78.5-80.5% for all plans.

Conclusions:

We present estimates of potential clinical benefit in terms of neurocognitive impairment and demonstrate the possibility of considerably reducing neurocognitive adverse effects, minimally compromising target coverage locally using HS-IMPT.

Introduction

Primary central nervous system (CNS) tumors are the second most common type of cancer in children [1]. The most frequent malignant CNS tumor in children is medulloblastoma. In children above 3-5 years of age, most medulloblastomas are treated with a combination of surgery, chemotherapy and craniospinal irradiation (CSI). The treatment depends on age and tumor-related risk factors, such as residual tumor volume, M-stage, histology, molecular subgroups including various genetic mutations[2]. Although treatment has become more stratified over the last decade, it has remained rather consistent. Most long-term survivors of malignant pediatric CNS tumors treated with CSI have significant neurocognitive late effects, and patients irradiated at a younger age tend to have worse outcomes [3,4]. Recently, in order to reduce the common, treatment related, neurocognitive side effects, several studies have investigated hippocampal-sparing (HS) irradiation modalities [5-10].

Long term childhood cancer survivors constitute a rapidly growing group of young adults [11]. Since the frequency and severity of late side effects generally increase with time, they are especially debilitating for pediatric cancer survivors as they mature into adulthood [12-14]. Certain parts of the brain (e.g. the hippocampus) are more sensitive to radiation [8,15,16] and neurogenesis occurs within the dentate gyrus of the hippocampus [17]. Radiation further damages hippocampal stem cell differentiation [18] and it is associated with reduced memory preservation. Consequently, avoiding high-dose irradiation of the hippocampus should be a priority [7,19].

No clinical trials of hippocampal sparing in children with CNS tumors have yet been published. The most compelling evidence to date comes from the randomized phase III trial NRG Oncology CC001 that showed significantly lower risk of cognitive failure in adults with brain metastases in the arm receiving hippocampal-sparing whole-brain irradiation [20].

We previously studied the feasibility of reducing the dose to the hippocampi and found IMPT to be remarkably promising [5]. However, the study was based on generic proton data and without consideration to clinically accepted proton therapy protocol for planning and delivery.

In the current work we studied the risk of neurocognitive impairment from the cranial part (whole-brain and boost) of intensity-modulated proton therapy (IMPT) craniospinal treatment. Specifically, we investigated the possibility of lowering the hippocampal dose significantly without compromising dose to the whole-brain target, regarding clinically acceptable objectives. The deliverability of the HS IMPT plans was evaluated based on different plan uncertainty and robustness criteria.

Materials and Methods

Patients and delineation

We identified 24 eligible patients treated at our institution between 2005 and 2015. The patients in this study had all undergone photon CSI treatment. All patients were re-planned and a total of 504 HS IMPT plans were generated for the 24 patients (table 1), with 432 plans evaluating different levels of HS and robustness for the elective whole-brain treatment and 72 plans evaluating the dose contribution from the

boost treatment. The elective target volume was defined as the whole-brain (clinical target volume, CTV) denoted as CTV$_{elective}$, disregarding the spinal part of the target in this study. The hippocampi and the postoperative resection volume, including residual tumor if any, (denoted GTV) were contoured on MRI co-registered with CT images (figure 1) by an experienced senior radiologist. The boost target volume (denoted CTV$_{boost}$) was defined as the GTV plus a 5 mm margin. Two patients treated in earlier years had no GTV contoured; their boost volumes consisted of the entire posterior fossa.

Table 1: *Characteristics of the 24 pediatric patients included in the study.*

	n	%
Sex		
Male	12	50
Female	12	50
	Median	Range
Age (y)	9	4-18
Distance* (cm)		
CTV - Hippocampus	1.4	1.0 – 4.3
Target and OAR volumes (cm^3)		
CTV$_{elective}$	1427.2	1137.7 – 1770.7
CTV$_{boost}$	44.7	11.5 – 228.3
Hippocampus	3.4	0.8 – 10.6

* Defined as the distance between the center of the hippocampus to the closest point of CTV$_{boost}$

Treatment planning

The total prescribed dose (PD) was 54 Gy$_{RBE}$ in 1.8 Gy$_{RBE}$ per fraction, 23.4 Gy$_{RBE}$ from the elective whole-brain plan and 30.6 Gy$_{RBE}$ from the boost plan. All plans were normalized so the mean target volume dose was 100% of the PD dose and robustly optimized using 1%/1mm, 2%/2mm and 3.5%/3mm uncertainty criteria in all directions. The treatment plans were generated using the Eclipse™ treatment planning system (TPS) v.13.7 (Varian medical systems, Palo Alto, CA, USA). Three incident fields (90°, 180° and 270° with the patient's positioned head first supine) with field specific targets, with no range shifter used and multi-field optimization. For each plan, the target, normal tissue and organs-at-risk (OARs, with the exception of the hippocampus for the different dose levels) objectives were kept constant to minimize planner bias.

The hippocampal dose objectives were defined in relation to five different levels of avoidance; 5, 7, 9 (figure 1), 12 and 15 Gy$_{RBE}$ with the intent of studying how the target coverage and plan quality was affected by the different levels of hippocampal sparing. Treatment plans with no priority or dose restriction to the hippocampus (denoted standard CSI plan), were generated for comparison.

Analysis and evaluation metrics

Treatment plans were exported to the Computational Environment for Radiotherapy Research (CERR) [21] and subsequently analyzed in MATLAB release 2019a (The MathWorks Inc., Natick, MA, USA). The plans were evaluated with respect to target coverage, homogeneity index (HI), maximum dose to target and mean and maximum doses to the OARs.

The target coverage was evaluated by calculating the percentage of the target volume receiving ≥95% ($V_{95\%}$) and ≤107% ($V_{107\%}$) of the PD. The HI was calculated according to a definition proposed by Spruijt et al. [22]. The dose to 0.03cm^3 of the target volume and brainstem was used to represent clinically relevant maximum dose received by these structures.

The plans were deemed clinically acceptable if the following conditions were met: $V_{95\%}$ ≥95% of PD, $D_{0.03cc}$ ≤110% of PD, $D_{0.03cc}$ ≤107% of the PD to the brainstem, dose to the chiasm ≤50 Gy$_{RBE}$ and a HI for CTV$_{elective}$ of ≥95 where 100 constitutes a completely homogenous dose to the region of interest.
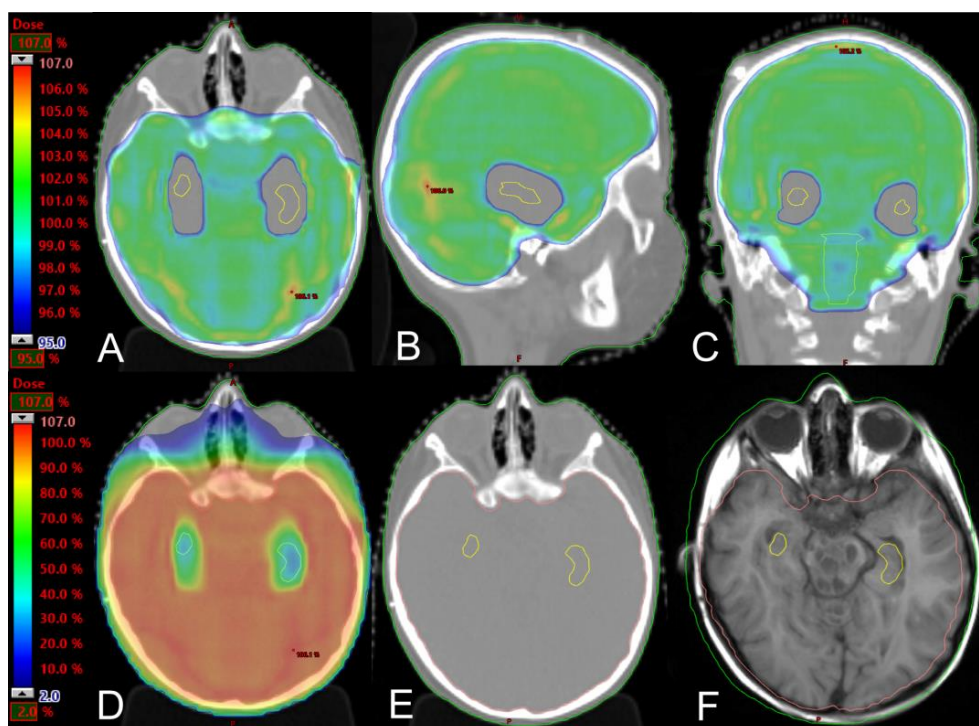

Figure 1: *Absorbed dose in color-wash 95 – 107% for a) transversal, b) sagittal and c) frontal view and absorbed dose in color-wash 2 – 107% for d) transversal. A transversal slice of the e) CT image and f) T1-weighted MRI. All images*

show the contoured hippocampus (yellow contour). The hippocampal dose constraint was set to 9 Gy$_{RBE}$ for the elective target.

The association between hippocampal dose and patient characteristics such as GTV size, hippocampal size and the distance between CTV$_{boost}$ and the hippocampus (defined as the center of the hippocampus to the closest point of CTV$_{boost}$) was evaluated using scatter plots and regression models.

Tumor control probability (TCP) and neurocognitive impairment normal tissue complication probability (NTCP) was estimated using previously published models [5,23,24]. The TCP dose-response model has been evaluated against recently published data [25] to test their applicability and updated for use in this study.

Statistical analysis

The Shapiro-Wilk test and visual histogram inspection were used to assess normality and equal variance. Paired t-tests were used to compare hippocampal mean doses and NTCP estimates, where p <0.05 was considered statistically significant. Stepwise comparison between each of the hippocampal dose objectives was performed; Standard CSI plan vs. 15 Gy$_{RBE}$ vs. 12 Gy$_{RBE}$ vs. 9 Gy$_{RBE}$ vs. 7 Gy$_{RBE}$ vs. 5 Gy$_{RBE}$, respectively.

Results

It was possible to reduce the dose to the hippocampus considerably without compromising whole-brain target coverage. However, the lowest dose constraint to the hippocampus was related to a higher risk of one or multiple target objectives failing clinically acceptable criteria (figure 2). The different robust optimization parameters used resulted in similar plan quality with some minor differences (Supplementary figures s1A, B and C). The 2%/2mm criteria resulted in the fewest failed plans, whereas 3.5%/3mm and 1%/1mm both resulted in a higher number of failed plans.
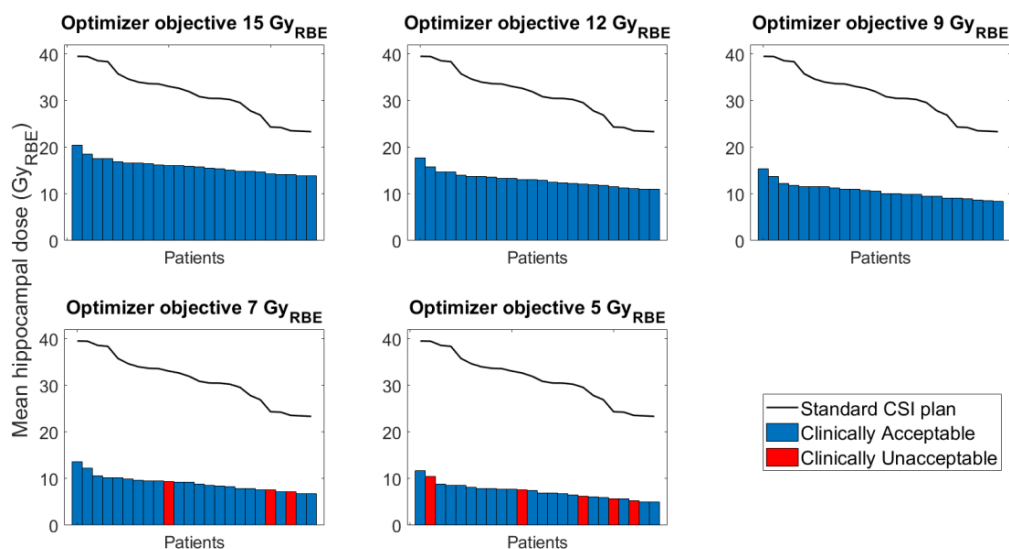
Figure 2: *Mean hippocampus dose (Gy$_{RBE}$) for all patients optimized with 2%/2mm where blue bars indicate a clinically acceptable plan and red bars a plan deemed unacceptable regarding target coverage (V$_{95\%}$ ≥95% of PD), homogeneity (≥95), maximum target dose (D$_{0.03cc}$ ≤110% of PD) and doses to the OARs (D$_{0.03cc}$ ≤107% of the PD to the brainstem, dose to the chiasm ≤50 Gy$_{RBE}$). The black line corresponds to each of the patients showing mean hippocampus dose (Gy$_{RBE}$) for the plans optimized without any priority or dose restriction (standard CSI plan).*

The median mean dose (range) to the hippocampus from whole-brain and boost plans was 7.1 Gy$_{RBE}$ (5.0 to 11.7 Gy$_{RBE}$, p<0.001), 9.0 Gy$_{RBE}$ (6.8 to 13.7 Gy$_{RBE}$, p<0.001), 10.4 Gy$_{RBE}$ (8.4 to 15.4 Gy$_{RBE}$, p<0.001), 13.0 Gy$_{RBE}$ (11.0 to 17.8 Gy$_{RBE}$, p<0.001), 15.9 Gy$_{RBE}$ (13.9 to 20.5 Gy$_{RBE}$, p<0.001) and 31.4 Gy$_{RBE}$ (23.3 to 39.5 Gy$_{RBE}$, p<0.001) for 5, 7, 9, 12, 15 Gy$_{RBE}$ and standard CSI plans, respectively (figure 2).

There was a clear correlation between hippocampus dose and distance between the hippocampus and CTV$_{boost}$ (figure 3a). Trends were seen for the correlation between GTV and hippocampal size with mean hippocampal dose (figure 3b and 3c). The strongest correlation was seen for standard CSI plans where HS was not applied. The hippocampus dose was reduced with approximately 4.7 Gy$_{RBE}$ and 1.3 Gy$_{RBE}$ per cm distance between the hippocampi and CTV$_{boost}$ for standard CSI plan and 9 Gy$_{RBE}$ for HS plans, respectively.
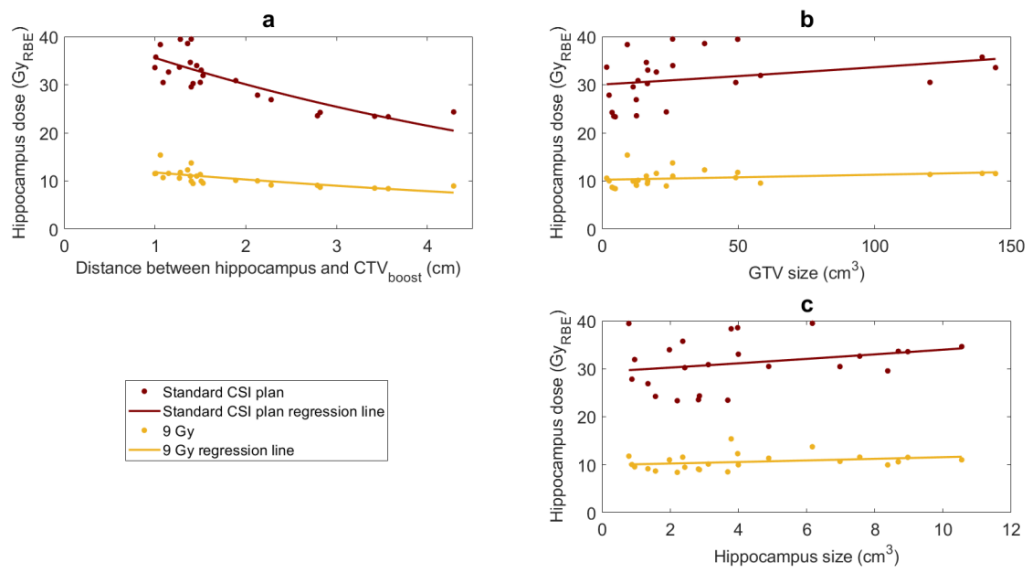
Figure 3: *Hippocampus dose (Gy$_{RBE}$) visualized in contrast to a) the distance between the center of hippocampus and closest point of CTV$_{elective}$, b) GTV size and c) hippocampus size including values for all patients and corresponding regression lines. Only the standard CSI plan and plans with 9 Gy$_{RBE}$ constraint are featured for visual purposes. Full image is available in Supplementary figure s2.*

The TCP remained relatively consistent with an estimated 78.5-80.5% event free survival (EFS) for all evaluated plans and patients. The NTCP was calculated for cognitive impairment (table 2) which was divided into three major domains; Task efficiency (figure 4a), Organization (figure 4b) and Memory (figure 4c).

Table 2: *Normal tissue complication probability calculations; median mean estimated risk of impairment and average mean reduced estimated risk of impairment for task efficiency, organization and memory, with corresponding 95% confidence intervals or standard deviations. All parameters presented here are statistically significant compared to their closest higher neighboring value (p<0.001).*

	Task efficiency	(Range)	Organization	(Range)	Memory	(Range)
Risk of impairment						
- 5 Gy$_{RBE}$	40.6%	(35.3 – 52.9%)	19.8%	(17.3 – 26.2%)	29.8%	(28.2 – 33.5%)
- 7 Gy$_{RBE}$	45.5%	(39.6 – 58.0%)	22.3%	(19.3 – 29.3%)	31.3%	(29.5 – 35.1%)
- 9 Gy$_{RBE}$	49.2%	(43.9 – 62.5%)	24.2%	(21.4 – 32.2%)	32.4%	(30.8 – 36.6%)
- 12 Gy$_{RBE}$	56.3%	(50.8 – 68.4%)	28.2%	(25.1 – 36.5%)	34.6%	(32.9 – 38.7%)
- 15 Gy$_{RBE}$	63.8%	(58.6 – 74.3%)	33.1%	(29.6 – 41.6%)	37.1%	(35.3 – 41.1%)
- Standard CSI plan	90.4%	(79.8 – 95.8)	62.8%	(47.2 – 76.3%)	51.2%	(43.7 – 58.6%)
	Task efficiency	SD	Organization	SD	Memory	SD
Reduced risk of impairment						
- 5 Gy$_{RBE}$	48.2%	3.1	42.1%	7.7	21.1%	3.7
- 7 Gy$_{RBE}$	43.7%	3.1	39.8%	7.6	19.7%	3.7
- 9 Gy$_{RBE}$	39.4%	3.1	37.5%	7.4	18.4%	3.6
- 12 Gy$_{RBE}$	32.9%	2.9	33.8%	7.3	16.4%	3.6
- 15 Gy$_{RBE}$	25.4%	2.8	29.0%	7.1	13.9%	3.6

Abbreviations: RBE = Radiobiological effect, CSI = Craniospinal irradiation, SD = Standard deviation.
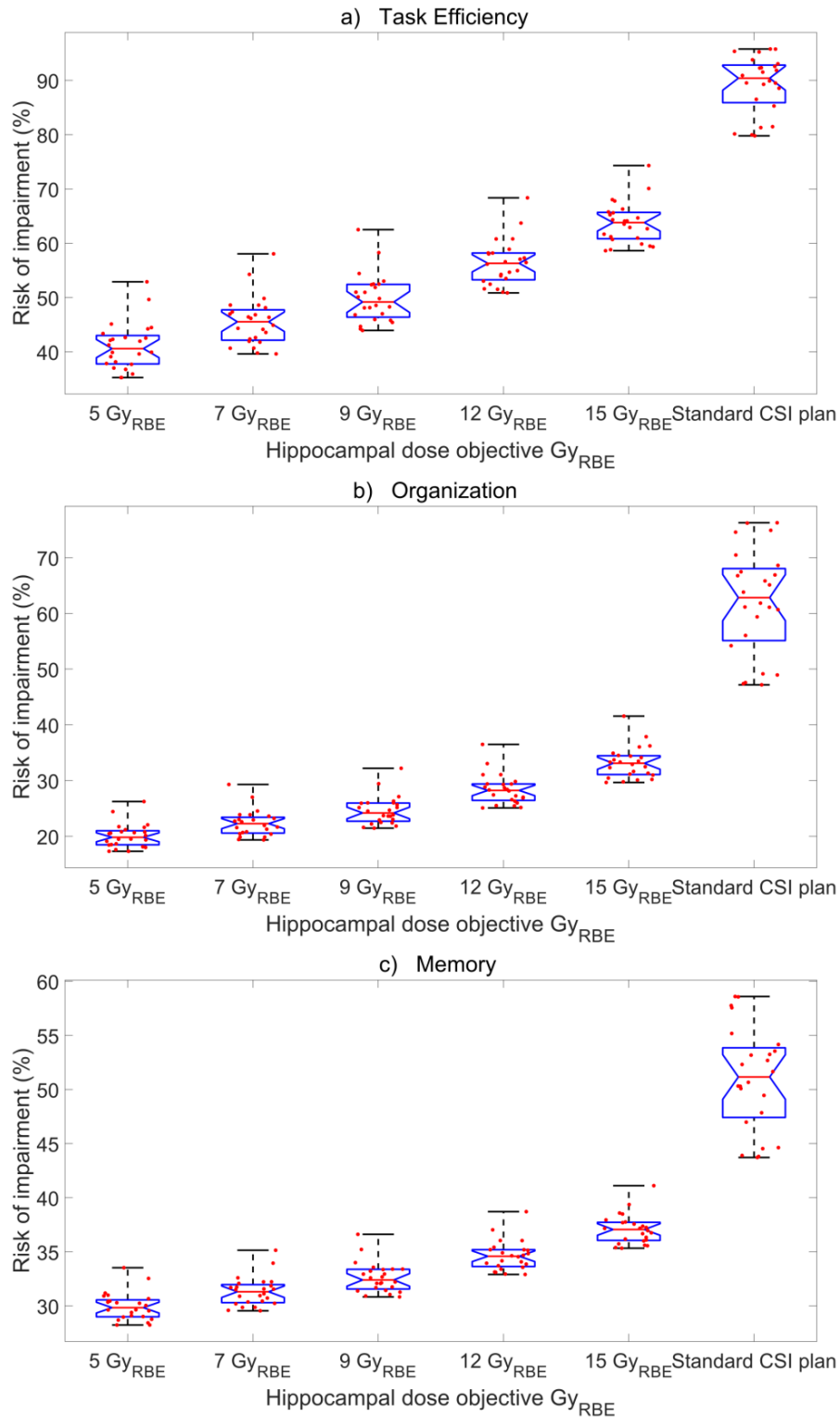
Figure 4: *The boxplots represent the distribution of risk of impairment (%) among the 24 patients (red scatter) given as median, 25th – 75th percentiles and range for each of the optimizer objectives for a) task efficiency, b) organization and c) memory. For clarification purpose, the y-axes are presented in different ranges, most suitable for each dataset.*

Discussion

This study shows that it is possible to reduce the dose to the hippocampus considerably with minimal impact on whole-brain target coverage with IMPT, in particular when inspecting dose-volume histograms. Even with acceptable target coverage, there might, however, be hot- and cold-spots throughout that would affect clinical acceptability, which is why this was explicitly evaluated. The high HI can be explained by the fact that the hippocampus only constitutes roughly 1% of the total irradiated volume. Gondi et al. [26] found that the HS volume with added planning-risk expansion accounted for about 2.1% of the whole-brain in adults. The lowest HS dose constraints tested in this study (5 Gy_{RBE}) might be difficult to achieve for some patients, especially depending on tumor location and GTV size. This is in agreement with results from a previous study [6] where plans were not based on a clinical protocol for treatment planning as well as on robust plan optimization. For the 9 Gy_{RBE} HS constraint, all plans were deemed clinically acceptable, demonstrating the possibility to lower the mean dose to the hippocampus by 20 Gy_{RBE} and still achieve acceptable plans.

Since tumor control remains the primary goal of HS-CSI, it might be inappropriate to spare the hippocampus for patients with high-risk medulloblastoma (MB), as their risk of recurrence may be higher [27]. Recently, it was also shown that lowering the dose to the entire craniospinal volume to 18 Gy for patients with standard-risk MB resulted in lower EFS and is currently not recommended [25]. Lately, laudable efforts have been made towards HS and the comprehensive phase III NRG Oncology CC001 trial demonstrated that for adults with CNS metastases, it is possible to significantly spare short-term cognitive function without deterioration of either progression-free survival and overall survival in a randomized setting [20].

Most modern radiotherapy techniques are able to spare the hippocampus to some extent [5,8-10,26] although the data suggests that IMPT would be the preferred alternative [5,10], especially for novel proton radiotherapy techniques [28]. In this study, we show that it is possible to considerably spare the hippocampus using IMPT. Doses to the hippocampus found in this study are comparable to previously published research [5,6,10]. Blomstrand et al. [5] determined that it was possible to spare the hippocampus to approximately 10 Gy_{RBE} using IMPT without compromising the $V_{95\%}$ $CTV_{elective}$ coverage. An important addition from this study is the use of robust optimization instead of using approaches mainly used for photon treatments, ensuring that IMPT plans will be deliverable.

We estimated the clinical benefit in terms of the reduced risk of neurocognitive impairment using published dose-response models. The data presented here suggests the possibility of reducing the risk from roughly 90%, 60% and 50% to 40%, 20% and 30% for task efficiency, organization and memory impairment, respectively. These dose-response models are of course subject to considerable uncertainty but a lower dose to the hippocampus clearly estimates a reduced risk of neurocognitive impairment. The available TCP model is not stratified based on different molecular subgroups or patient's performance status and is based on data from standard-risk MB patients. The current multimodality treatment results in a 5-year EFS of 75-80% for standard-risk patients [29] which compares well to our TCP estimates of a 5-year EFS of 78.5-80.5%. As the hippocampus constitutes only a small volume of the whole-brain, a very limited drop in estimated TCP was found for our HS treatment plans.

According to our risk estimates, there is a statistically significant reduction in the risk of cognitive impairment for all dose levels where the hippocampus was avoided. Gondi et al. [30] determined that there was a dosimetric threshold at 7.3 Gy to 40% of the bilateral hippocampi volume for a significant cognitive benefit in adults with brain metastases. Goda et al. [31] found that a hippocampal mean dose of less than 30 Gy did not affect intelligence quotient in children, adolescents and young adults. Although not fully comparable to our results, these studies further support treatment strategies avoiding irradiation of the hippocampi.

When sparing a critical OAR such as the hippocampus, it is crucial that the delineation is correct, which is not always trivial [32]. Another challenge is the central location and somewhat odd shape of the hippocampus where the use of IMPT might be of particular advantage. It is, however, important to consider the complexities of linear energy transfer of protons and the relative biological effect along the proton beam, where physical dose may no longer be the best indicator of biologic effect [33,34]. Encouragingly, a recent study found no increase in CNS injury from proton treatment for MB, and no correlation with RBE compared to photon treatments [35].

In conclusion, we demonstrate the potential clinical benefit of reduced neurocognitive impairment based on robustly optimized HS IMPT plans, without compromising target coverage and thereby estimated tumor control. Our results suggest that any dose reduction to the hippocampus could have valuable impact in terms of cognitive function for pediatric patients treated with CSI.

Conflict of Interest statement

No conflict of interest to report.

References

1.   Lannering B, Sandström P-E, Holm S, et al. Classification, incidence and survival analyses of children with CNS tumours diagnosed in Sweden 1984-2005. Acta Paediatrica. 2009;98(10):1620-1627.
2.   Yu J, Shi W, Li H. Factors affecting the prognosis of children with medulloblastoma: A single institution retrospective analysis of 40 cases. Translational Neuroscience and Clinics. 2017;3(1):16-27.
3.   Mulhern RK, Palmer SL, Merchant TE, et al. Neurocognitive consequences of risk-adapted therapy for childhood medulloblastoma. J Clin Oncol. 2005 Aug 20;23(24):5511-9.
4.   Danoff BF, Cowchock SF, Marquette C, et al. Assessment of the Long-Term Effects of Primary Radiation Therapy for Brain Tumors in Children. Cancer. 1982;49(8):1580-1586.

5. Blomstrand M, Brodin NP, Munck Af Rosenschold P, et al. Estimated clinical benefit of protecting neurogenesis in the developing brain during radiation therapy for pediatric medulloblastoma. Neuro Oncol. 2012 Jul;14(7):882-9.

6. Brodin NP, Munck af Rosenschold P, Blomstrand M, et al. Hippocampal sparing radiotherapy for pediatric medulloblastoma: impact of treatment margins and treatment technique. Neuro Oncol. 2014 Apr;16(4):594-602.

7. Gondi V, Pugh SL, Tome WA, et al. Preservation of memory with conformal avoidance of the hippocampal neural stem-cell compartment during whole-brain radiotherapy for brain metastases (RTOG 0933): a phase II multi-institutional trial. J Clin Oncol. 2014 Dec 1;32(34):3810-6.

8. Tsai PF, Yang CC, Chuang CC, et al. Hippocampal dosimetry correlates with the change in neurocognitive function after hippocampal sparing during whole brain radiotherapy: a prospective study. Radiat Oncol. 2015 Dec 10;10:253.

9. Gutierrez AN, Westerly DC, Tome WA, et al. Whole brain radiotherapy with hippocampal avoidance and simultaneously integrated brain metastases boost: a planning study. Int J Radiat Oncol Biol Phys. 2007 Oct 1;69(2):589-97.

10. Stoker J, Vora S, Patel A, et al. Advantages of intensity modulated proton therapy during hippocampal avoidance whole brain radiation therapy. Physics and Imaging in Radiation Oncology. 2018;8:28-32.

11. Curry HL, Parkes SE, Powell JE, et al. Caring for survivors of childhood cancers: the size of the problem. Eur J Cancer. 2006 Mar;42(4):501-8.

12. Spiegler BJ, Bouffet E, Greenberg ML, et al. Change in neurocognitive functioning after treatment with cranial radiation in childhood. J Clin Oncol. 2004 Feb 15;22(4):706-13.

13. Williams NL, Rotondo RL, Bradley JA, et al. Late Effects After Radiotherapy for Childhood Low-grade Glioma. Am J Clin Oncol. 2018 Mar;41(3):307-312.

14. Grill J, Renaux VK, Bulteau C, et al. Long-term intellectual outcome in childre with posterior fossa tumors according to radiation doses and volumes. Int J Radiat Oncol Biol Phys. 1999;45(1):137-145.

15. Connor M, Karunamuni R, McDonald C, et al. Regional susceptibility to dose-dependent white matter damage after brain radiotherapy. Radiotherapy and Oncology. 2017;123(2):209-217.

16. Peiffer AM, Leyrer MC, Greeneschloesser DM, et al. Neuroanatomical target theory as a predictive model for radiation-induced cognitive decline. Neurology. 2013;80:747-753.

17. Eriksson PS, Perfilieva E, Björk-Eriksson T, et al. Neurogenesis in the adult human hippocampus. Nat Med. 1998;4(11):1313-1317.

18. Monje ML, Mizumatsu S, Fike JR, et al. Irradiation induces neural precursor-cell dysfunction. Nat Med. 2002 Sep;8(9):955-62.

19. Gondi V, Tome WA, Mehta MP. Why avoid the hippocampus? A comprehensive review. Radiother Oncol. 2010 Dec;97(3):370-6.

20. Brown PD, Gondi V, Pugh S, et al. Hippocampal Avoidance During Whole-Brain Radiotherapy Plus Memantine for Patients With Brain Metastases: Phase III Trial NRG Oncology CC001. J Clin Oncol. 2020;38(10):1019-1029.

21. Deasy JO, Blanco AI, Clark VH. CERR: a computational environment for radiotherapy research. Med Phys. 2003 May;30(5):979-85.

22. Spruijt KH, Dahele M, Cuijpers JP, et al. Flattening filter free vs flattened beams for breast irradiation. Int J Radiat Oncol Biol Phys. 2013 Feb 1;85(2):506-13.

23. Armstrong GT, Jain N, Liu W, et al. Region-specific radiotherapy and neuropsychological outcomes in adult survivors of childhood CNS malignancies. Neuro Oncol. 2010 Nov;12(11):1173-86.

24. Brodin NP, Vogelius IR, Bjork-Eriksson T, et al. Modeling freedom from progression for standard-risk medulloblastoma: a mathematical tumor control model with multiple modes of failure. Int J Radiat Oncol Biol Phys. 2013 Oct 1;87(2):422-9.

25. Michalski JM, Janss A, Vezina G, et al. Results of COG ACNS0331: A Phase III Trial of Involved-Field Radiotherapy (IFRT) and Low Dose Craniospinal Irradiation (LD-CSI) with Chemotherapy in Average-
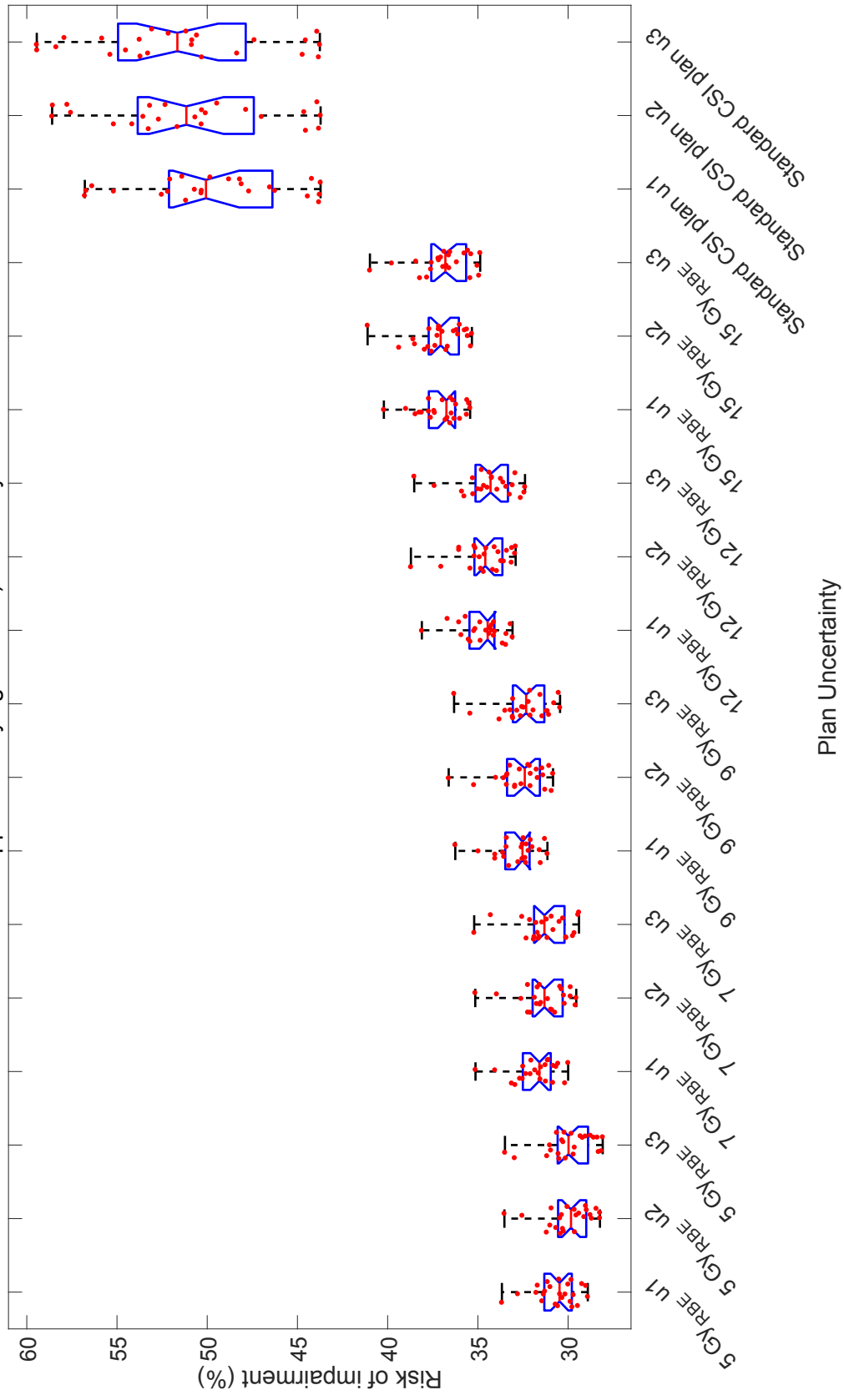
Risk Medulloblastoma: A Report from the Children's Oncology Group. Int J Radiat Oncol Biol Phys. 2016;96(5):937-938.

26. Gondi V, Tolakanahalli R, Mehta MP, et al. Hippocampal-sparing whole-brain radiotherapy: a "how-to" technique using helical tomotherapy and linear accelerator-based intensity-modulated radiotherapy. Int J Radiat Oncol Biol Phys. 2010 Nov 15;78(4):1244-52.

27. Padovani L, Chapon F, Andre N, et al. Hippocampal Sparing During Craniospinal Irradiation: What Did We Learn About the Incidence of Perihippocampus Metastases? Int J Radiat Oncol Biol Phys. 2018 Mar 15;100(4):980-986.

28. Ding X, Zhou J, Li X, et al. Improving dosimetric outcome for hippocampus and cochlea sparing whole brain radiotherapy using spot-scanning proton arc therapy. Acta Oncol. 2019 Apr;58(4):483-490.

29. Gottardo NG, Gajjar A. Current Therapy for Medulloblastoma. Curr Treat Options Neurol. 2006;8(4):319-334.

30. Gondi V, Hermann BP, Mehta MP, et al. Hippocampal dosimetry predicts neurocognitive function impairment after fractionated stereotactic radiotherapy for benign or low-grade adult brain tumors. Int J Radiat Oncol Biol Phys. 2012 Jul 15;83(4):e487-93.

31. Goda JS, Dutta D, Krishna U, et al. Hippocampal radiotherapy dose-constraints for predicting long-term neurocognitive outcomes: Mature data from a prospective trial in young patients with brain tumors [https://doi.org/10.1093/neuonc/noaa076]. Neuro Oncol. 2020 noaa076:[Epub ahead of print].

32. Gondi V, Cui Y, Mehta MP, et al. Real-time pretreatment review limits unacceptable deviations on a cooperative group radiation therapy technique trial: quality assurance results of RTOG 0933. Int J Radiat Oncol Biol Phys. 2015 Mar 1;91(3):564-70.

33. Jones B. Towards Achieving the Full Clinical Potential of Proton Therapy by Inclusion of LET and RBE Models. Cancers (Basel). 2015 Mar 17;7(1):460-80.

34. Giovannini G, Bohlen T, Cabal G, et al. Variable RBE in proton therapy: comparison of different model predictions and their influence on clinical-like scenarios. Radiat Oncol. 2016 May 17;11:68.

35. Giantsoudi D, Sethi RV, Yeap BY, et al. Incidence of CNS Injury for a Cohort of 111 Patients Treated With Proton Therapy for Medulloblastoma: LET and RBE Associations for Areas of Injury. Int J Radiat Oncol Biol Phys. 2016 May 1;95(1):287-296.
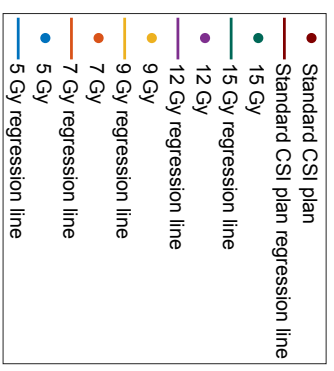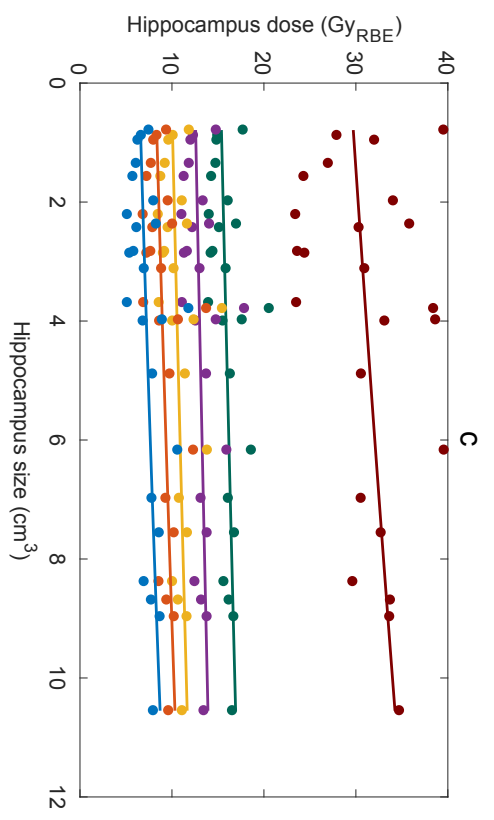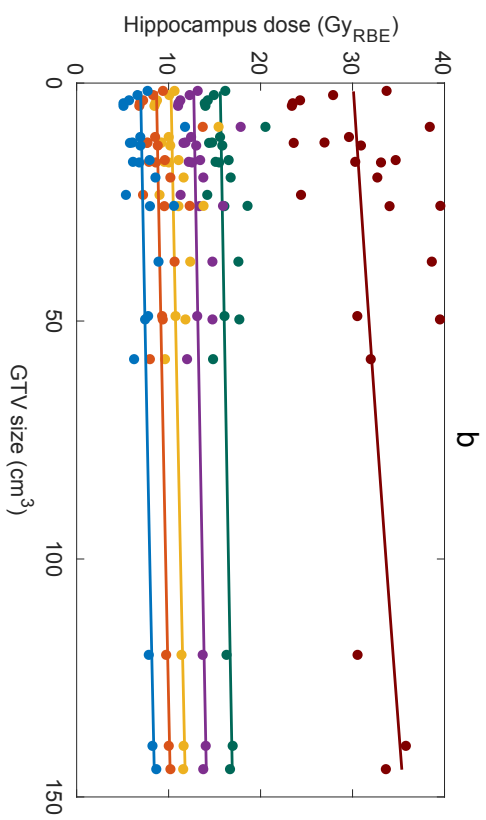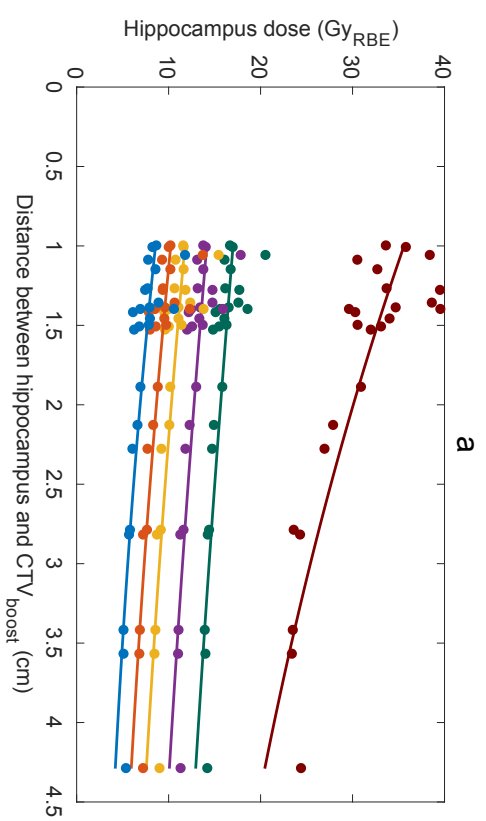
Supplementary figure S1 A) - Task Efficiency

Hippocampal dose objective and plan uncertainty

Supplementary figure S1 B) - Organization
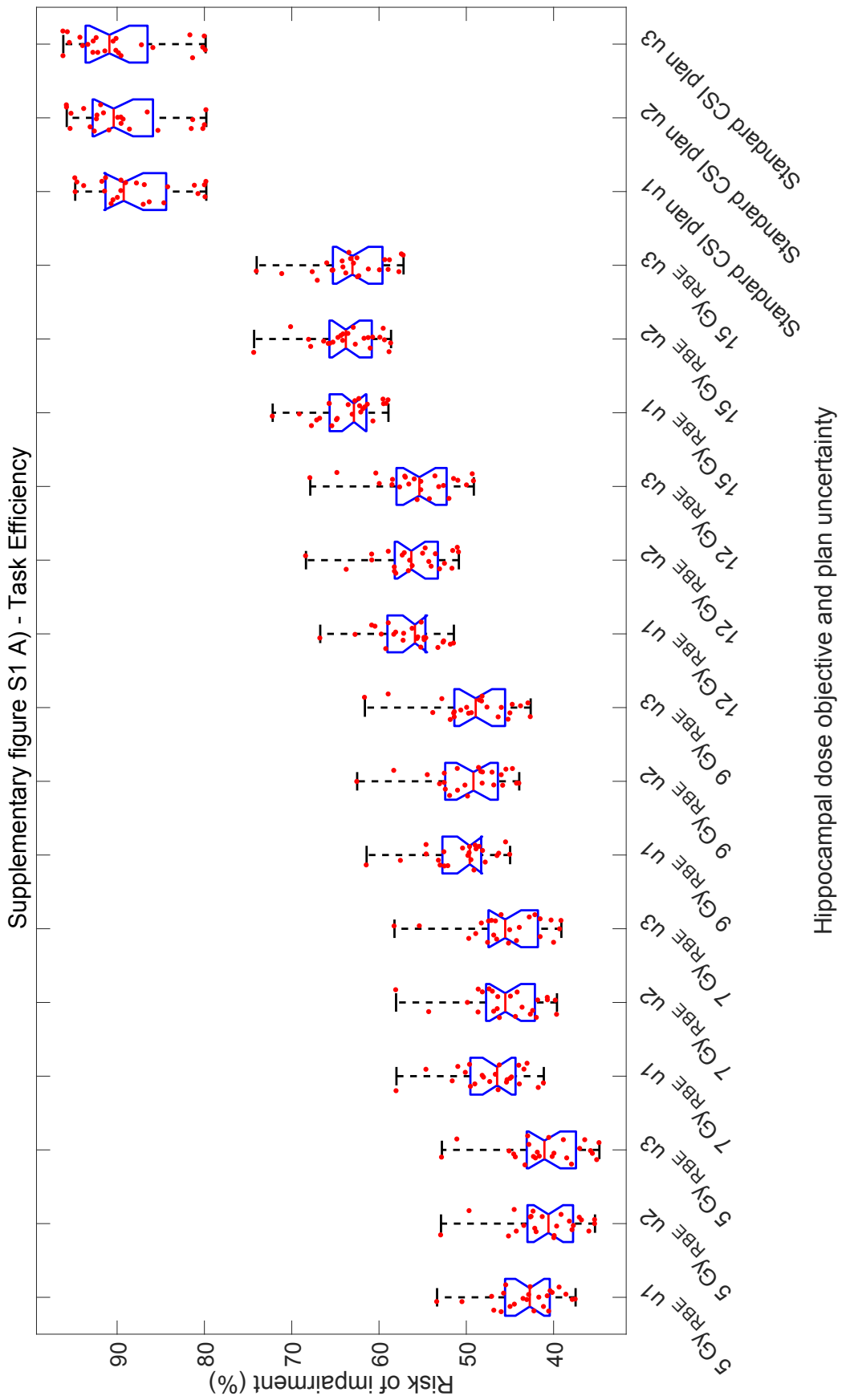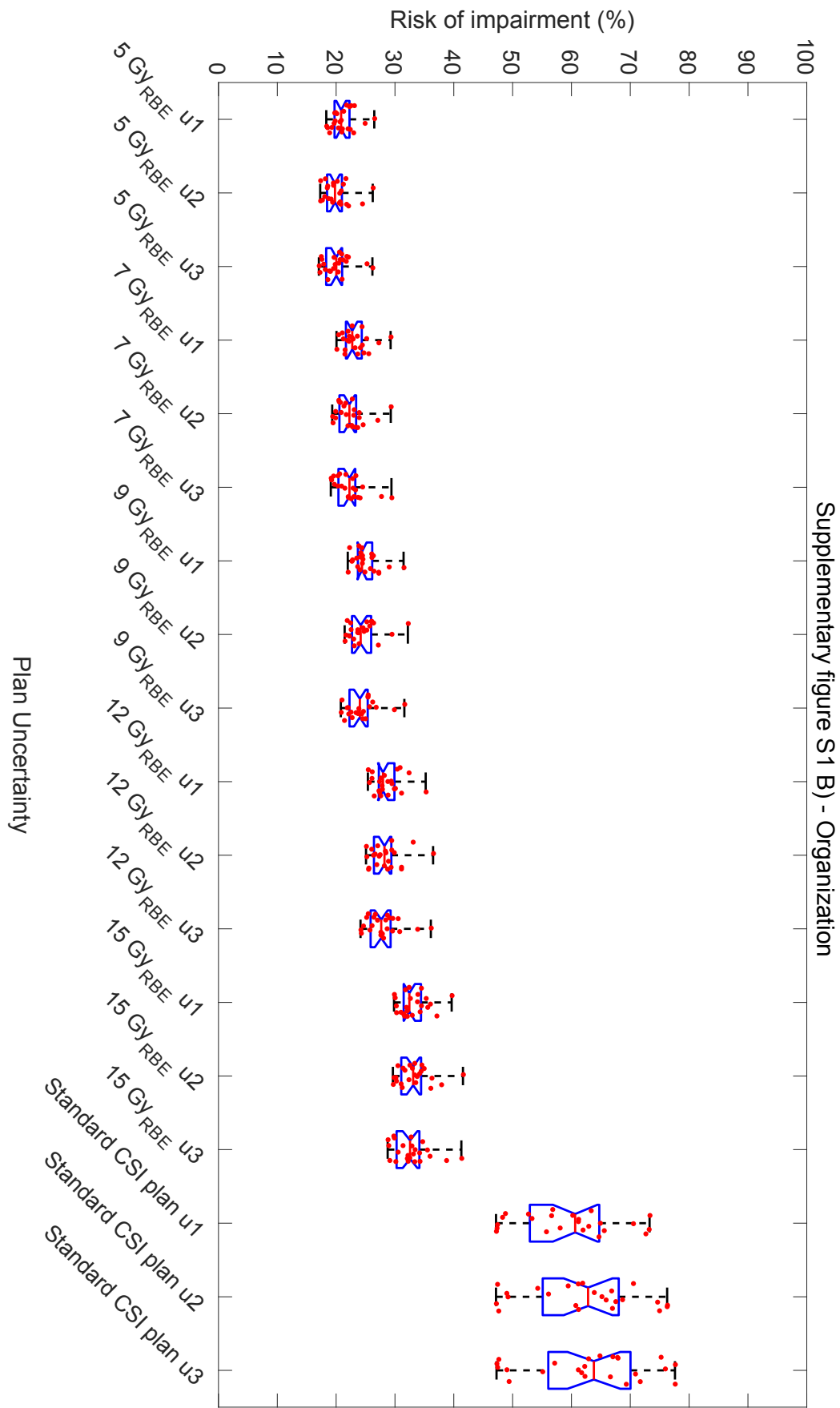
Supplementary figure S1 C) - Memory

STUDY III

Contents lists available at ScienceDirect

Radiotherapy and Oncology

journal homepage: www.thegreenjournal.com

STUDY III

Pediatric radiotherapy

Retrospective estimation of heart and lung doses in pediatric patients treated with spinal irradiation

Daniel Gasic [a,b,*], Per Munck af Rosenschöld [c,b], Ivan R. Vogelius [a,d], Maja V. Maraldo [a], Marianne C. Aznar [e], Karsten Nysom [f], Thomas Björk-Eriksson [g,h], Søren M. Bentzen [i], Nils Patrik Brodin [j]

[a] Department of Oncology, Section of Radiotherapy, Rigshospitalet; [b] Niels Bohr Institute, University of Copenhagen, Copenhagen, Denmark; [c] Department of Radiation Physics, Skåne University Hospital, Lund, Sweden; [d] Faculty of Health and Medical Sciences, University of Copenhagen, Copenhagen, Denmark; [e] Manchester Cancer Research Centre, University of Manchester, Manchester Academic Health Sciences Centre, Manchester, UK; [f] Department of Pediatrics and Adolescent Medicine, The Juliane Marie Center, Rigshospitalet, Copenhagen, Denmark; [g] Department of Oncology, Institute of Clinical Sciences, Sahlgrenska Academy at the University of Gothenburg; [h] Regional Cancer Centre West, Gothenburg, Sweden; [i] Department of Epidemiology and Public Health, University of Maryland School of Medicine, Baltimore; and [j] Institute for Onco-Physics, Albert Einstein College of Medicine, Bronx, USA

ARTICLE INFO

ABSTRACT

Background and purpose: The purpose of this study was to investigate whether treatment information from medical records can be used to estimate radiation doses to heart and lungs retrospectively in pediatric patients receiving spinal irradiation with conventional posterior fields.

Material and methods: An algorithm for retrospective dosimetry in children treated with spinal irradiation was developed in a cohort of 21 pediatric patients with available CT-scans and treatment plans. We developed a multivariable linear regression model with explanatory variables identifiable in case note review for retrospective estimation of minimum, maximum, mean and $V_{10\%}$–$V_{80\%}$ doses to the heart and lungs. Doses were estimated for both linear accelerator (Linac) and ^{60}Co radiation therapy modalities.

Results: Age and spinal field width were identified as statistically significant predictors of heart and lung doses in multivariable analyses (p < 0.01 in all models). Models showed excellent predictive performance with R^2 = 0.70 for mean heart dose and 0.79 for mean lung dose, for Linac plans. In leave-one-out cross-validation analysis the average difference between predicted and actual mean heart dose was 6.7% and 7.6% of the prescription dose for Linac and ^{60}Co plans, respectively, and 5.2% and 4.9% for mean lung dose. Due to the small sample size and large inter-patient variation in heart and lung dose, prospective studies validating these findings are highly warranted.

Conclusions: The models presented here provide retrospective estimates of heart and lung doses for historical cohorts of pediatric patients, thus facilitating studies of long-term adverse effects of radiation.

Pediatric cancer survivors comprise a rapidly growing group of young adults [1]. However, a longer survival is associated with long-term morbidity and mortality [2]. The most common cause of death among pediatric cancer survivors is cardiovascular disease [3]. Congestive heart failure in the form of coronary artery disease is also a serious late effect due to mediastinal radiation [4], other late effects, that also might cause death are pulmonary fibrosis, acute pulmonary toxicity and restrictive lung disease [5–7].

Recent technological advances in radiation therapy optimization and delivery, often provide several competing treatment options and the resulting dose distributions throughout the patient's body can vary considerably [8]. These in turn may yield substantially different risks of late complications such as severely debilitating cardiac and pulmonary toxicity. Considerable clinical research efforts have aimed at developing empirical models for clinical decision support in pediatric patients [9], as well as young adults with Hodgkin lymphoma [10] and breast cancer patients [11–13], relating the dose and dose distribution delivered to an organ-at-risk (OAR) to the risk of long-term toxicity. This is a challenging research field in both pediatric and adult patient populations, and due to the considerable differences between children and adults, it is not straightforward to translate results from an adult population directly to pediatric cohorts. However, important long-term outcome data emerging from large cohort studies of childhood cancer survivors has the potential to greatly improve our ability to predict the risk of late toxicity in patients treated today [14–17]. Furthermore, a comprehensive systematic review of available dose–volume data related to toxicity after pediatric radiation therapy is currently undertaken by the Pediatric Normal Tissue Effects in the Clinic (PENTEC) collaboration [18].

Because of the long latent period of many late effects, for some endpoints 10–20 years or more, many dose–response modeling studies of late-effects analyze outcome data from cohorts treated decades ago. This poses the further challenge of reconstructing the dose distribution for cases treated in an era without 3D computed tomography (CT) based planning and detailed dosimetry, and with radiation modalities that are less commonly used now. In some clinical indications at least a crude relationship exists between organ doses and patient characteristics that are available from case note review. If unadjusted for, these associations may confound the results of retrospective analyses if organ doses are solely based on the prescribed dose. For example, it is possible that the dose delivered to the heart and lungs of a pediatric patient correlates with patient age due to the relative change in body composition and organ size as the child grows. This may cause a bias in a retrospective analysis as an observed correlation between age at exposure and risk of toxicity could be wrongfully attributed to age, when in fact the heart or lung dose is driving the association. This issue and the need for accurate retrospective dosimetry have been well recognized in the adult setting for example in Hodgkin lymphoma [19–23].

In this study we test whether age, as well as several other characteristics that can be retrieved from treatment records, can be used to estimate doses to the heart and lungs in a group of pediatric patients treated with spinal irradiation. Furthermore, we investigate if different radiation beam qualities (i.e. ^{60}Cobalt (^{60}Co) machines vs. linear accelerators (Linacs)) would yield a systematic difference in organ dose that may further confound retrospective studies.

Materials and methods

Data collection

All patients, ≤20 years of age at the time of treatment and who received spinal irradiation between 2005 and 2012 at our institution were retrospectively reviewed. We identified a cohort of 21 eligible patients that were included in the analysis (see Table 1 for patient characteristics), all treated for medulloblastoma with Linac-based cranio-spinal radiation therapy using a 6 MV beam. Treatment plan information and CT scans were available for all patients in the treatment planning system (TPS, Eclipse™ v. 13.7 (Varian Medical Systems, Palo Alto, CA, USA). The heart and lungs were segmented (ARIA® contouring suite v. 13.6, Varian Medical Systems, Palo Alto, CA, USA) on the treatment planning CT scans. The heart was manually segmented and the lungs were automatically segmented with manual adjustment when needed.

Treatment plans were exported to CERR [24] and subsequently analyzed in MATLAB release 2014b (The MathWorks, Inc., Natick, MA, USA) and the minimum, maximum, mean and $V_{10\%}$–$V_{80\%}$ doses

Table 1
Characteristics of the 21 pediatric patients included in the study.

	Median	Range
Age (y)	9	2–20
	n	%
Sex		
Male	11	52
Female	10	48
Position		
Supine	15	71
Prone	6	29
	Mean	SD
Field length (cm)	31.1	3.7
Field width (cm)	6.2	1.2

to the heart and lungs were extracted from the spinal irradiation plan for each patient. Further patient characteristics that were extracted were the length and width of the spinal field (at the patient's skin level from the incident beam direction), age at exposure, sex, and patient positioning (prone or supine).

Comparison to ^{60}Co

To test the possible difference in minimum, maximum, mean and $V_{10\%}$–$V_{80\%}$ heart and lung doses from ^{60}Co and 6 MV Linac beams, we implemented a ^{60}Co machine in our TPS with beam data from a Siemens Gammatron-3. ^{60}Co treatment plans required the dose to be calculated using a pencil beam algorithm (i.e. a type A algorithm, PBC version 10.0.28), while the Linac plans were calculated using a Monte Carlo-like algorithm (i.e. a type C algorithm, Acuros XB®, version 13.7). The field set-up was identical in the Linac and the ^{60}Co plans. All Linac and ^{60}Co plans were normalized to a reference point at the dorsal edge of the Th8-Th11 (depending on patient size) vertebral body receiving 90% of the prescribed dose. To assess the effect of differences between the Acuros XB® algorithm and PBC algorithm used for ^{60}Co calculations, all Linac plans were also calculated with the PBC algorithm.

Statistical analysis

The Shapiro–Wilk tests and visual histogram inspection were used to test for a normal distribution of a variable. Bivariate associations between all patient characteristics (age, sex, position, field length and width) and heart or lung doses were quantified by Pearson's or Spearman's rank correlation coefficients for continuous variables and *t*-tests or Wilcoxon's rank-sum tests for categorical variables, depending on the assessment of normality and linearity. Similarly, differences between heart and lung doses between Linac and ^{60}Co plans were assessed using paired *t*-tests or Wilcoxon's sign-rank tests depending on the normality test.

Multivariable linear regression models were fitted for the various heart and lung dose metrics using all covariates with $p < 0.2$ from the tests of bivariate association as candidate predictor variables. Stepwise elimination was performed manually using a $p < 0.05$ cutoff for inclusion in the final models. The resulting multivariable linear regression models provide the following relationship for dose estimation:

$$D_{\text{Est}} = X_1\beta_1 + X_2\beta_2 + \cdots + X_n\beta_n + k \tag{1}$$

where D_{Est} is the estimated dose metric, x_i is the value of the *i*:th predictor, β_i the corresponding regression coefficient and k a constant. Despite the large number of statistical tests performed, correction for multiple comparisons was not applied since it is expected that highly correlated dose metrics would depend on the same predictor variables, so it is unlikely that spurious associations would be found for a certain dose metric and not the others. However, a leave-one-out (LOO) cross-validation was performed to assess the predictive performance of the final models. This was done by fitting the regression coefficients of the final models to subsets of the data, subsequently leaving out each of the 21 patients. The heart and lung dose metrics for each excluded patient were then estimated using the models and compared to that patient's dose data from the TPS. The root-mean-square deviation (RMSD) of this difference was then calculated as an average estimate of how well the predicted doses compared to the actual values in the LOO setting. To determine if the Linac-based models would be able to estimate doses from ^{60}Co and vice versa, the predicted doses from one radiation modality were compared to the TPS doses from the other.

Results

Age and the size of the spinal irradiation field (length and width) showed strong association with mean heart and lung doses (Table 2), with similar trends for the other analyzed dose metrics (see supplementary material). The association with age supports the general assumption that age is a good surrogate for heart and lung volume, which is confirmed in our data where age showed a strong correlation with both heart volume (Spearman's $r_s = 0.85$ with 95% CI: 0.64–0.95, $p < 0.001$) and lung volume $r_s = 0.79$ with 95% CI: 0.51–0.94, $p < 0.001$).

In multivariable analysis only age and spinal field width were found to be significant predictors of heart and lung dose as shown in Table 3 for mean doses ($p < 0.01$) and Supplementary material (Tables S1 and S2) for other dose metrics. Since the length of the heart and lungs in the superior–inferior direction was fully encompassed by the spinal fields for all patients we found that field length was not a significant predictor of heart and lung doses. The models based on age and spinal field width showed excellent predictive performance with 69.7% of the variance in mean heart dose, and 78.9% of the mean lung dose, explained by the model for the Linac plans. Patient position, sex and field length were not significant predictors of heart and lung dose in multivariable analysis.

Fig. 1 shows the association between age and mean heart and lung dose for the Linac plans and Fig. 2 shows the corresponding association for spinal field width, along with box-and-whiskers plots of the population mean heart and lung doses. We further explored the association between organ volume and mean heart and lung dose to demonstrate whether age indeed acts as a surrogate marker for this association. In fact, heart volume seems to be a good predictor for mean heart dose ($R^2 = 50.5\%$ in univariable linear regression), as compared to $R^2 = 31.5\%$ using age as the only predictor variable. Conversely, lung volume does not appear to be a particularly good univariable predictor for mean lung dose ($R^2 = 5.6\%$) and rather it appears that the combination of age and spinal field width ($R^2 = 78.9\%$) provides a surrogate measure for the proportion of the lungs receiving incident irradiation (arbitrarily defined as the proportion receiving > 10% of prescription dose, $R^2 = 98.8\%$).

The leave-one-out analysis shows that the models based on age and spinal field width provide fairly accurate estimates of the heart and lung doses when compared with the actual dose for the excluded patients. The average relative accuracy (given by the $RMSD_{LOO}$) of the estimates of the mean heart dose was 6.7% and 7.6% of the prescribed dose for Linac and ^{60}Co plans respectively. The respective $RMSD_{LOO}$ for the mean lung dose was 5.2% and 4.9%. Table 4 shows the relative accuracy for Linac and ^{60}Co models for the heart and lung dose metrics through calculating the RMSD.

Table 3
Final multivariable regression models for mean heart and lung dose for Linac and ^{60}Co plans, respectively. Model performance is given by R^2 and $RMSD_{LOO}$.

Predictor variable Linac	Regression coefficient (β)	95% CI	*p*-Value
Mean heart dose ($R^2 = 0.70$, $RMSD_{LOO} = 6.7\%$)			
Age (y)	−1.37	(−1.95, −0.78)	<0.001
Field width (cm)	5.68	(3.17, 8.18)	<0.001
Constant	31.4		
Mean lungs dose ($R^2 = 0.79$, $RMSD_{LOO} = 5.2\%$)			
Age (y)	−1.05	(−1.51, −0.59)	<0.001
Field width (cm)	6.69	(4.73, 8.64)	<0.001
Constant	−7.90		
Predictor variable ^{60}Co	**Regression coefficient (β)**	**95% CI**	**_p_-Value**
Mean heart dose ($R^2 = 0.58$, $RMSD_{LOO} = 7.6\%$)			
Age (y)	−1.17	(−1.82, −0.51)	0.001
Field width (cm)	5.85	(2.54, 9.17)	0.002
Constant	34.4		
Mean lungs dose ($R^2 = 0.78$, $RMSD_{LOO} = 4.9\%$)			
Age (y)	−0.88	(−1.31, −0.45)	<0.001
Field width (cm)	7.64	(5.45, 9.84)	<0.001
Constant	−6.37		

Abbreviations: $RMSD_{LOO}$ = The root-mean-square deviation for the leave-one-out cross validation.

Fig. 1. Mean heart dose (circles) and, mean lung dose (triangles) vs. patient's age with the multivariable linear regression models. The boxplots represent the distribution of mean heart and lung doses among the 21 patients given as mean, 25th–75th percentile and range. Please note that the range of the boxplots overlap.

Table 2
Results of the analysis of bivariate associations between mean heart and lung dose and the various patient characteristics for Linac and ^{60}Co plans. As sex and position are categorical variables, correlation coefficients can't be given.

Variable	Mean heart dose		Mean lungs dose	
	Corr. Coef.	*p*-Value	Corr. Coef.	*p*-Value
Age	−0.56 (r_p)	0.008	−0.43 (r_p)	0.05
Sex		0.13		0.17
Position		0.11		0.36
Field length	0.38 (r_s)	0.09	0.47 (r_s)	0.03
Field width	0.55 (r_p)	0.01	0.72 (r_p)	<0.001
Age	−0.50 (r_p)	0.02	−0.36 (r_p)	0.11
Sex		0.10		0.14
Position		0.11		0.43
Field length	0.34 (r_s)	0.13	0.47 (r_s)	0.03
Field width	0.49 (r_p)	0.02	0.75 (r_p)	<0.001

Abbreviations: r_p = Pearson's product-moment correlation coefficients; r_s = Spearman's rank correlation coefficients.
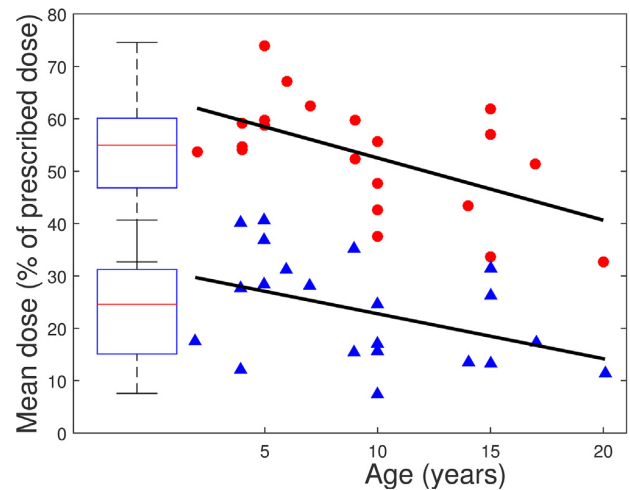
Fig. 2. Mean heart dose (circles) and, mean lung dose (triangles) vs. spinal field width with the multivariable linear regression models. The boxplots represent the distribution of mean heart and lung doses among the 21 patients given as mean, 25th–75th percentile and range. Please note that the range of the boxplots overlap.
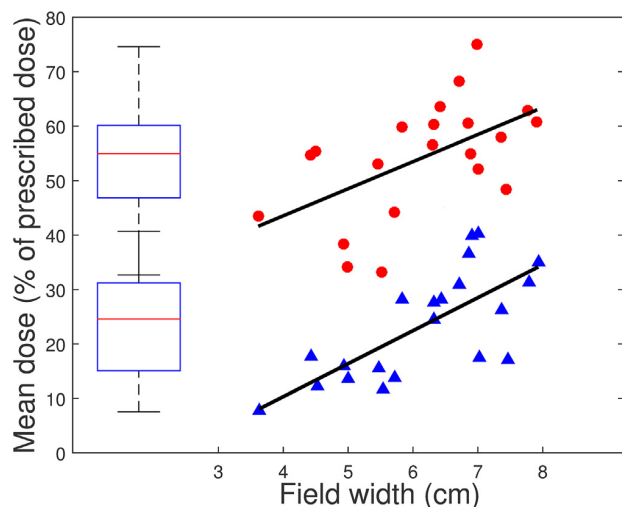
Table 4
The RMSD$_{LOO}$ comparisons show the performance of using Linac derived models to estimate Linac doses and ^{60}Co derived models to estimate ^{60}Co doses for all dose metrics. The ^{60}Co$_{Linac}$ comparisons show the performance of using the Linac dose models to estimate ^{60}Co doses, and vice versa.

Variable	RMSD$_{LOO}$ (%)		RMSD (%)	
	Linac	^{60}Co	^{60}Co$_{Linac}$	Linac$_{60Co}$
Mean heart dose	6.7	7.6	7.5	7.3
Min. heart dose	1.3	4.0	4.0	2.4
Max. heart dose	6.2	10.5	9.7	7.6
V$_{10\%}$ heart dose	8.3	8.3	12.8	13.3
V$_{20\%}$ heart dose	8.7	8.9	11.2	11.8
V$_{30\%}$ heart dose	9.1	9.4	9.9	10.3
V$_{40\%}$ heart dose	9.2	10.0	9.7	9.8
V$_{50\%}$ heart dose	9.5	12.1	12.1	11.1
V$_{60\%}$ heart dose	10.9	13.5	17.6	16.7
V$_{70\%}$ heart dose	11.6	11.2	16.1	16.7
V$_{80\%}$ heart dose	8.3	7.0	8.0	9.1
Mean lungs dose	5.2	4.9	5.8	5.2
Min. lungs dose	0.3	0.4	0.7	0.7
Max. lungs dose	7.6	12.6	11.6	8.5
V$_{10\%}$ lungs dose	7.0	6.5	9.8	8.6
V$_{20\%}$ lungs dose	6.6	6.4	9.6	8.5
V$_{30\%}$ lungs dose	6.3	6.4	8.2	7.1
V$_{40\%}$ lungs dose	6.6	7.7	7.3	6.3
V$_{50\%}$ lungs dose	6.1	6.5	7.2	6.2
V$_{60\%}$ lungs dose	6.1	6.6	7.8	7.1
V$_{70\%}$ lungs dose	6.3	5.6	7.5	7.6
V$_{80\%}$ lungs dose	5.5	4.1	6.3	6.8

Abbreviations: RMSD = The root-mean-square deviation for the final model; RMSD$_{LOO}$ = The root-mean-square deviation for the leave-one-out cross validation.

Furthermore, Table 4 shows that using the Linac-based models to estimate ^{60}Co doses and vice versa provides less accurate estimates compared to the LOO analysis within the same modality, suggesting that separate dose estimation models are needed for patients treated with Linac and ^{60}Co irradiation. To ensure that this was not simply attributable to the use of different calculation algorithms, we compared the results when using the PBC algorithm to calculate Linac doses and concluded that this had minimal effect on the various dose metrics (see Supplementary Figure S1).

Discussion

The models including age and spinal field width derived in this study provide an effective means of retrospectively estimating heart and lung doses in pediatric patients treated with spinal irradiation, when 3D dose data from a TPS are not available. Based on Figs. 1 and 2 it is clear that there is considerable variation in the heart and lung doses between patients and estimating organ doses based on prescription dose alone could lead to biased results.

There are various databases with long-term follow-up of large cohorts of pediatric cancer patients treated up to several decades ago [14–17]. Along with these laudable efforts of collecting data on long-term toxicity, we believe that the models derived in this study can considerably aid the process of linking doses to the heart and lungs with the documented long-term effects. Furthermore, it should be possible to expand this analysis to encompass other OAR in a similar manner and to further refine OAR dose estimation for example by following the suggestions in the AAPM TG-158 report on out of field dosimetry [25]. Similarly, due to the relatively large inter-patient variation in heart and lung dose, prospective studies validating these results are warranted.

Accurate models linking organ dose to late toxicity can aid in the clinical decision making when competing radiation techniques are considered and could help identify patients in need of closer post-treatment surveillance for late adverse events.

Previous studies of adult malignancies have investigated the possibility of applying individual retrospective estimates based on a type of standard phantom or standard patient [12,20–22]. One such example is retrospectively estimating cardiac doses from breast cancer radiation therapy based on a standardized female patient [12]. Other studies used virtual simulation and CT scans to reconstruct treatment fields [19,23]. There have also been studies that instead chose to utilize dose measured to a water phantom, along with tumor location details from clinical records, to estimate the doses at the site of secondary tumor development [21]. Hybrid computational phantoms created from CT scans have been shown to be feasible for retrospective heart dosimetry following breast irradiation [26]. By also adding the use of Monte Carlo based dose calculations to pediatric hybrid phantoms, organ doses could be reconstructed to add further accuracy in future secondary cancer risk studies [27].

Given the relatively homogenous setup of spinal irradiation between different patients, the simple models based on age and field width developed here may be sufficient to explain most of the dosimetric variation, and this information can be extracted from previous treatment records. Although the leave-one-out analysis provides an internal validation of the models' accuracy, potential institutional variation in treatment setup and prescription depth was not considered. Since all data came from a single institution the generalizability to patient cohorts and treatment techniques employed in other institutions may be limited. It should also be mentioned that these models are derived from a relatively small patient sample and are only applicable to treatments with conventional posterior spinal fields.

In conclusion, this study provides a simple recipe for retrospectively estimating heart and lung doses from pediatric spinal irradiation, giving researchers a useful tool to aid them in analyzing heart and lung dose effect relationships in retrospective studies of late effects in long-term pediatric cancer survivors.

Conflict of interest statement

Dr. Vogelius has a master research agreement with Varian Medical Systems and Dr. Aznar reports grants to the department from both Varian Medical Systems and Siemens, all outside the submitted work.

Acknowledgements

Appendix A. Supplementary data

Supplementary data associated with this article can be found, in the online version, at https://doi.org/10.1016/j.radonc.2018.05.013.

References

[1] Curry HL, Parkes SE, Powell JE, Mann JR. Caring for survivors of childhood cancers: the size of the problem. Eur J Cancer 2006;42:501–8.
[2] Möller TR, Garwicz S, Barlow L, et al. Decreasing late mortality among five-year survivors of cancer in childhood and adolescence: a population-based study in the Nordic Countries. J Clin Oncol 2001;19:3173–81.
[3] Bates JE, Howell RM, Liu Q, et al. Volumetric dose-effect analysis of late cardiotoxicity: a report from the Childhood Cancer Survivor Study (CCSS). Int J Radiat Oncol Biol Phys 2017;99. Supplement:S3 (Abstract).
[4] Hancock SL, Donaldson SS, Hoppe RT. Cardiac disease following treatment of Hodgkin's disease in children and adolescents. J Clin Oncol 1993;11:1208–15.
[5] O'Driscoll BR, Hasleton PS, Taylor PM, et al. Active lung fibrosis up to 17 years after chemotherapy with carmustine (BCNU) in childhood. N Engl J Med 1990;323:378–82.
[6] Morgan GW, Freeman AP, McLean RG, Jarvie BH, Giles RW. Late cardiac, thyroid and pulmonary sequelae of mantle radiotherapy for Hodgkin's disease. Int J Radiat Oncol Biol Phys 1985;11:1925–31.
[7] Jakacki RI, Schramm CM, Donahue BR, Haas F, Allen JC. Restrictive lung disease following treatment for malignant brain tumors: a potential late effect of craniospinal irradiation. J Clin Oncol 1995;13:1478–85 (Abstract).
[8] Saran F. New technology for radiotherapy in paediatric oncology. Eur J Cancer 2004;40:2091–105.
[9] Brodin NP, Vogelius IR, Maraldo MV, et al. Life years lost-comparing potentially fatal late complications after radiotherapy for paediatric medulloblastoma on a common scale. Cancer 2012;118:5432–40.
[10] Schneider U, Sumila M, Robotka J. Site-specific dose-response relationships for cancer induction from the combined Japanese A-bomb and Hodgkin cohorts for doses relevant to radiotherapy. Theor Biol Med Model 2011;8:27.
[11] Taylor CW, Nisbet A, McGale P, et al. Cardiac doses from Swedish breast cancer radiotherapy since the 1950s. Radiother Oncol 2009;90:127–35.
[12] Taylor CW, Bronnum D, Darby SC, et al. Cardiac dose estimates from Danish and Swedish breast cancer radiotherapy during 1977–2001. Radiother Oncol 2011;100:176–83.
[13] Darby SC, Ewertz M, McGale P, et al. Risk of ischemic heart disease in women after radiotherapy for breast cancer. N Engl J Med 2013;368:987–98.
[14] Adult Life after Childhood Cancer in Scandinavia (ALiCCS). Available from: www.aliccs.org Accessed: August 7, 2017.
[15] Friedman DL. The childhood cancer survivor study: an important research initiative for childhood cancer survivors. J Pediatr Oncol Nurs 1999;16:172–5.
[16] Hawkins MM, Lancashire ER, Winter DL, et al. The British childhood cancer survivor study: objectives, methods, population structure, response rates and initial descriptive information. Pediatr Blood Cancer 2008;50:1018–25.
[17] Bolling T, Schuck A, Pape H, et al. Study protocol of the German "Registry for the detection of late sequelae after radiotherapy in childhood and adolescence" (RiSK). Radiat Oncol 2008;3:10.
[18] Pediatric Normal Tissue Effects in the Clinic (PENTEC). Available from: www.pentecradiation.org Accessed: September 6, 2017.
[19] Maraldo MV, Lundemann M, Vogelius IR, Specht L. A new method to estimate doses to the normal tissues after past extended and involved field radiotherapy for Hodgkin lymphoma. Radiother Oncol 2015;114:206–11.
[20] Ng A, Brock KK, Sharpe MB, Moseley JL, Craig T, Hodgson DC. Individualized 3D reconstruction of normal tissue dose for patients with long-term follow-up: a step toward understanding dose risk for late toxicity. Int J Radiat Oncol Biol Phys 2012;84:e557–63.
[21] van Leeuwen FE, Klokman WJ, Stovall M, et al. Roles of radiation dose, chemotherapy, and hormonal factors in breast cancer following Hodgkin's disease. J Natl Cancer Inst 2003;95:971–80.
[22] Travis LB, Hill DA, Dores GM, et al. Breast cancer following radiotherapy and chemotherapy among young women with Hodgkin disease. JAMA 2003;290:465–75.
[23] van Nimwegen FA, Cutter DJ, Schaapveld M, et al. Simple method to estimate mean heart dose from Hodgkin lymphoma radiation therapy according to simulation X-rays. Int J Radiat Oncol Biol Phys 2015;92:153–60.
[24] Deasy JO, Blanco AI, Clark VH. CERR: a computational environment for radiotherapy research. Med Phys 2003;30:979–85.
[25] Kry SF, Bednarz B, Howell RM, et al. AAPM TG 158: measurement and calculation of doses outside the treated volume from external beam radiation therapy. Med Phys 2017;44(10):e391–429.
[26] Moignier A, Derreumaux S, Broggio D, et al. Potential of hybrid computational phantoms for retrospective heart dosimetry after breast radiation therapy: a feasibility study. Int J Radiat Oncol Biol Phys 2013;85:492–9.
[27] Lee C, Jung JW, Pelletier C, et al. Reconstruction of organ dose for external radiotherapy patients in retrospective epidemiologic studies. Phys Med Biol 2015;60:2309–24.

STUDY III

B.5 STUDY III - SUPPLEMENTARY MATERIAL

Figure S1: The dose difference between TPS values for different dose calculation algorithms. Results are presented as % of prescribed dose for minimum, maximum and mean dose, and % volume receiving a given dose for $V_{10\%} - V_{80\%}$. The Boxplots represent the distribution of all heart and lung dose metrics among the 21 patients given as mean, $25^{th} - 75^{th}$ percentile and range.

STUDY III

Supplementary material – Dose calculation algorithm comparisons

Supplementary material – All models for Linac doses

Table S1: *Final multivariable regression models for all heart and lung doses for Linac plans. Model performance is given by R^2 and $RMSD_{LOO}$.*

Predictor variable	Regression coefficient (β)	95% CI	p-value
Mean heart dose (R^2 = 0.70, $RMSD_{LOO}$ = 6.7%)			
Age (y)	-1.37	(-1.95 , -0.78)	< 0.001
Field width (cm)	5.68	(3.17 , 8.18)	< 0.001
Constant	31.4		
Min. heart dose (R^2 = 0.55, $RMSD_{LOO}$ = 1.3%)			
Age (y)	-0.14	(-0.26 , -0.03)	0.01
Field width (cm)	0.93	(0.45 , 1.41)	< 0.001
Constant	0.12		
Max. heart dose (R^2 = 0.10, $RMSD_{LOO}$ = 6.2%)			
Age (y)	-0.19	(-0.71 , 0.34)	0.47
Field width (cm)	1.40	(-0.83 , 3.62)	0.20
Constant	84.3		
$V_{10\%}$ heart (R^2 = 0.68, $RMSD_{LOO}$ = 8.3%)			
Age (y)	-0.07	(-0.10 , -0.03)	< 0.001
Field width (cm)	0.30	(0.17 , 0.43)	< 0.001
Constant	2.15		
$V_{20\%}$ heart (R^2 = 0.66, $RMSD_{LOO}$ = 8.7%)			
Age (y)	-0.07	(-0.10 , -0.04)	< 0.001
Field width (cm)	0.30	(0.16 , 0.44)	< 0.001
Constant	1.98		
$V_{30\%}$ heart (R^2 = 0.65, $RMSD_{LOO}$ = 9.1%)			
Age (y)	-0.07	(-0.10 , -0.03)	< 0.001
Field width (cm)	0.31	(1.16 , 0.45)	< 0.001
Constant	1.87		
$V_{40\%}$ heart (R^2 = 0.64, $RMSD_{LOO}$ = 9.2%)			
Age (y)	-0.07	(-0.10 , -0.03)	< 0.001
Field width (cm)	0.31	(1.16 , 0.46)	< 0.001
Constant	1.75		
$V_{50\%}$ heart (R^2 = 0.66, $RMSD_{LOO}$ = 9.5%)			
Age (y)	-0.07	(-0.11 , -0.04)	< 0.001
Field width (cm)	0.35	(0.19 , 0.50)	< 0.001
Constant	1.50		

$V_{60\%}$ heart (R^2 = 0.74, $RMSD_{LOO}$ = 10.9%)

1

Predictor variable	Regression coefficient (β)	95% CI	p-value
Age (y)	-0.11	(-0.15 , -0.07)	< 0.001
Field width (cm)	0.41	(0.24 , 0.59)	< 0.001
Constant	1.17		
$V7_{0\%}$ heart (R^2 = 0.65, $RMSD_{LOO}$ = 11.6%)			
Age (y)	-0.10	(-0.14 , -0.06)	< 0.001
Field width (cm)	0.32	(0.13 , 0.50)	0.002
Constant	0.66		
$V_{80\%}$ heart (R^2 = 0.36, $RMSD_{LOO}$ = 8.3%)			
Age (y)	-0.04	(-0.07 , -0.01)	0.01
Field width (cm)	0.12	(-0.01 , 0.25)	0.07
Constant	0.21		

Predictor variable	Regression coefficient (β)	95% CI	p-value
Mean lung dose (R^2 = 0.79, $RMSD_{LOO}$ = 5.2%)			
Age (y)	-1.05	(-1.51 , -0.59)	< 0.001
Field width (cm)	6.69	(4.73 , 8.64)	< 0.001
Constant	-7.9		
Min. lung dose (R^2 = 0.79, $RMSD_{LOO}$ = 0.3%)			
Age (y)	-0.07	(-0.10 , -0.05)	< 0.001
Field width (cm)	0.37	(0.25 , 0.49)	< 0.001
Constant	0.22		
Max. lung dose (R^2 = 0.06, $RMSD_{LOO}$ = 7.6%)			
Age (y)	0.06	(-0.60 , 0.72)	0.84
Field width (cm)	1.29	(-1.51 , 4.10)	0.35
Constant	96.5		
$V_{10\%}$ lungs (R^2 = 0.82, $RMSD_{LOO}$ = 7.0%)			
Age (y)	-0.07	(-0.09 , -0.04)	< 0.001
Field width (cm)	0.42	(0.30 , 0.53)	< 0.001
Constant	-0.38		
$V_{20\%}$ lungs (R^2 = 0.80, $RMSD_{LOO}$ = 6.6%)			
Age (y)	-0.06	(-0.09 , -0.04)	< 0.001
Field width (cm)	0.36	(0.25 , 0.46)	< 0.001
Constant	-0.42		
$V_{30\%}$ lungs (R^2 = 0.79, $RMSD_{LOO}$ = 6.3%)			
Age (y)	-0.06	(-0.08 , -0.04)	< 0.001
Field width (cm)	0.34	(0.24 , 0.44)	< 0.001
Constant	-0.42		
$V_{40\%}$ lungs (R^2 = 0.79, $RMSD_{LOO}$ = 6.6%)			
Age (y)	-0.06	(-0.08 , -0.03)	< 0.001
Field width (cm)	0.32	(0.23 , 0.42)	< 0.001
Constant	-0.50		

2

$V_{50\%}$ lungs (R^2 = 0.78, $RMSD_{LOO}$ = 6.1%)			
Age (y)	-0.05	(-0.08 , -0.03)	< 0.001
Field width (cm)	0.31	(0.22 , 0.41)	< 0.001
Constant	-0.53		
$V_{60\%}$ lungs (R^2 = 0.76, $RMSD_{LOO}$ = 6.1%)			
Age (y)	-0.05	(-0.07 , -0.03)	< 0.001
Field width (cm)	0.30	(0.20 , 0.40)	< 0.001
Constant	-0.56		
$V_{70\%}$ lungs (R^2 = 0.68, $RMSD_{LOO}$ = 6.3%)			
Age (y)	-0.04	(-0.06 , -0.02)	0.002
Field width (cm)	0.27	(0.16 , 0.37)	< 0.001
Constant	-0.58		
$V_{80\%}$ lungs (R^2 = 0.65, $RMSD_{LOO}$ = 5.5%)			
Age (y)	-0.03	(-0.05 , -0.009)	0.007
Field width (cm)	0.22	(0.13 , 0.31)	< 0.001
Constant	-0.59		

Abbreviations: $RMSD_{LOO}$ = The root-mean-square deviation for the leave-one-out cross validation

STUDY III

3

Supplementary material (Table S2) – All models for ^{60}Co doses

Table S2: *Final multivariable regression models for heart and lung doses for ^{60}Co plans. Model performance is given by R^2 and $RMSD_{LOO}$.*

Predictor variable	Regression coefficient (β)	95% CI	p-value
Mean heart dose (R^2 = 0.58, $RMSD_{LOO}$ = 7.6%)			
Age (y)	-1.17	(-1.82 , -0.51)	0.001
Field width (cm)	5.85	(2.54 , 9.17)	0.002
Constant	34.4		
Min. heart dose (R^2 = 0.27, $RMSD_{LOO}$ = 4.0%)			
Age (y)	-0.18	(-0.53 , 0.17)	0.29
Field width (cm)	2.05	(0.29 , 3.82)	0.03
Constant	-2.50		
Max. heart dose (R^2 = 0.05, $RMSD_{LOO}$ = 10.5%)			
Age (y)	-0.04	(-0.87 , 0.78)	0.91
Field width (cm)	-1.87	(-6.05 , 2.32)	0.36
Constant	101.6		
$V_{10\%}$ heart (R^2 = 0.57, $RMSD_{LOO}$ = 8.3%)			
Age (y)	-0.05	(-0.08 , -0.02)	0.002
Field width (cm)	0.26	(0.11 , 0.41)	0.002
Constant	2.96		
$V_{20\%}$ heart (R^2 = 0.61, $RMSD_{LOO}$ = 8.9%)			
Age (y)	-0.06	(-0.09 , -0.03)	0.001
Field width (cm)	0.32	(0.15 , 0.48)	< 0.001
Constant	2.48		
$V_{30\%}$ heart (R^2 = 0.60, $RMSD_{LOO}$ = 9.4%)			
Age (y)	-0.06	(-0.10 , -0.03)	0.001
Field width (cm)	0.34	(0.17 , 0.52)	< 0.001
Constant	2.16		
$V_{40\%}$ heart (R^2 = 0.60, $RMSD_{LOO}$ = 10.0%)			
Age (y)	-0.07	(-0.11 , -0.03)	0.001
Field width (cm)	0.37	(0.18 , 0.57)	< 0.001
Constant	1.85		
$V_{50\%}$ heart (R^2 = 0.61, $RMSD_{LOO}$ = 12.1%)			
Age (y)	-0.08	(-0.13 , -0.04)	< 0.001
Field width (cm)	0.45	(0.22 , 0.68)	< 0.001
Constant	1.36		

$V_{60\%}$ heart (R^2 = 0.61, $RMSD_{LOO}$ = 13.5%)			
Age (y)	-0.10	(-0.15 , -0.05)	< 0.001
Field width (cm)	0.47	(0.21 , 0.73)	0.001
Constant	0.79		
$V_{70\%}$ heart (R^2 = 0.48, $RMSD_{LOO}$ = 11.2%)			
Age (y)	-0.06	(-0.10 , -0.02)	0.005
Field width (cm)	0.30	(0.09 , 0.51)	0.008
Constant	0.31		
$V_{80\%}$ heart (R^2 = 0.17, $RMSD_{LOO}$ = 7.0%)			
Age (y)	-0.02	(-0.04 , 0.006)	0.13
Field width (cm)	0.08	(0.05 , 0.21)	0.20
Constant	0.19	(-0.46 , 0.84)	0.55

Predictor variable	Regression coefficient (β)	95% CI	p-value
Mean lung dose (R^2 = 0.78, $RMSD_{LOO}$ = 4.9%)			
Age (y)	-0.88	(-1.31 , -0.45)	< 0.001
Field width (cm)	7.64	(5.45 , 9.84)	< 0.001
Constant	-6.37		
Min. lung dose (R^2 = 0.37, $RMSD_{LOO}$ = 0.36%)			
Age (y)	-0.02	(-0.05 , 0.01)	0.20
Field width (cm)	0.25	(0.08 , 0.41)	0.006
Constant	0.17		
Max. lung dose (R^2 = 0.02, $RMSD_{LOO}$ = 12.6%)			
Age (y)	0.30	(-0.77 , 1.37)	0.56
Field width (cm)	0.32	(-5.11 , 5.75)	0.90
Constant	102.9		
$V_{10\%}$ lungs (R^2 = 0.84, $RMSD_{LOO}$ = 6.5%)			
Age (y)	-0.07	(-0.10 , -0.05)	< 0.001
Field width (cm)	0.49	(0.36 , 0.62)	< 0.001
Constant	0.04		
$V_{20\%}$ lungs (R^2 = 0.82, $RMSD_{LOO}$ = 6.4%)			
Age (y)	-0.07	(-0.09 , -0.04)	< 0.001
Field width (cm)	0.46	(0.33 , 0.58)	< 0.001
Constant	-0.21		
$V_{30\%}$ lungs (R^2 = 0.80, $RMSD_{LOO}$ = 6.4%)			
Age (y)	-0.06	(-0.08 , -0.03)	< 0.001
Field width (cm)	0.43	(0.31 , 0.55)	< 0.001
Constant	-0.37		

$V_{40\%}$ lungs (R^2 = 0.77, $RMSD_{LOO}$ = 7.7%)

STUDY III

2

Age (y)	-0.05	(-0.08 , -0.03)	< 0.001
Field width (cm)	0.40	(0.28 , 0.52)	< 0.001
Constant	-0.48		
$V_{50\%}$ lungs (R^2 = 0.73, $RMSD_{LOO}$ = 6.5%)			
Age (y)	-0.04	(-0.07 , -0.02)	0.001
Field width (cm)	0.37	(0.25 , 0.50)	< 0.001
Constant	-0.55		
$V_{60\%}$ lungs (R^2 = 0.65, $RMSD_{LOO}$ = 6.6%)			
Age (y)	-0.04	(-0.06 , -0.01)	0.009
Field width (cm)	0.33	(0.20 , 0.46)	< 0.001
Constant	-0.61		
$V_{70\%}$ lungs (R^2 = 0.63, $RMSD_{LOO}$ = 5.6%)			
Age (y)	-0.03	(-0.04 , -0.001)	0.04
Field width (cm)	0.27	(0.17 , 0.38)	< 0.001
Constant	-0.64		
$V_{80\%}$ lungs (R^2 = 0.63, $RMSD_{LOO}$ = 4.1%)			
Age (y)	-0.01	(-0.03 , 0.003)	0.10
Field width (cm)	0.21	(0.13 , 0.29)	< 0.001
Constant	-0.56		

Abbreviations: $RMSD_{LOO}$ = The root-mean-square deviation for the leave-one-out cross validation

3